NLO QCD Corrections to Higgs Boson Pair Production in Gluon Fusion

Zur Erlangung des akademischen Grades eines

DOKTORS DER NATURWISSENSCHAFTEN

von der KIT-Fakultät für Physik des

Karlsruher Instituts für Technologie (KIT)

genehmigte

DISSERTATION

von

Dipl. Phys. Juraj Streicher

aus Bratislava

Tag der mündlichen Prüfung: 24. Juni 2016

Referentin: Prof. Dr. Margarete Mühlleitner

Korreferent: Dr. Michael Spira

Contents

CHAPTER 1

Introduction

The properties and fundamental interactions of all known elementary particles are remarkably well described by the Standard Model (SM) of elementary particle physics. One of the cornerstones of the SM is the Higgs mechanism [1–6], which is required to explain the spontaneous breaking of the electroweak (EW) symmetry [7–9]. A consequence of the Higgs mechanism is the existence of one scalar Higgs boson as a remainder of the EW symmetry breaking and ever since the formulation of the SM in the 1960's, the search for the Higgs boson was one of the major tasks of experimental and theoretical particle physics research.
In 2012 this endeavour lead to a successful result when the LHC experiments ATLAS [10] and CMS [11] announced the discovery of a new scalar particle with mass of about 125 GeV. The combined analysis [12] of the data gathered in LHC Run 1 suggests that the couplings of the newly found particle to the massive gauge bosons, to pairs of τ leptons and of bottom quarks, as well as the loop-induced couplings to gluons and photons are in good agreement with the SM predictions for the Higgs boson couplings within the experimental uncertainties. Additionally, the experimental data also strongly suggests that the newly found boson carries zero spin and positive CP parity [13, 14], which further supports the interpretation of the particle as the long-sought SM Higgs boson. The ultimate proof of this interpretation requires the determination of the particle's trilinear and quartic self-interactions, which are accessible in multi-Higgs production processes [15–18]. The measurement of these couplings allows for the experimental reconstruction of the Higgs potential, which is required to possess a non-vanishing vacuum expectation value.

While the measurement of the quartic self-coupling is out of reach of current and planned collider experiments [16, 18–23], the determination of the trilinear self-coupling is a demanding yet promising goal [24–44] of a possible high luminosity upgrade of the LHC. The experimental determination of the Higgs pair production process at the LHC is difficult, since the production cross section is small and the main Higgs boson decay modes are plagued by large QCD backgrounds. This necessitates on the theoretical side precise predictions for the total and differential production cross sections by including higher order corrections. The dominant Higgs boson pair production process is gluon fusion [45, 46], for which the knowledge of the higher order corrections has long been based solely on the heavy top quark mass approximation [15]. The approximate corrections increase the production cross section for SM Higgs bosons at the LHC by approximately 80%. The heavy top quark mass approximation

reduces the complexity of the next-to-leading order (NLO) calculation considerably and was applied successfully in the past to single Higgs boson production in gluon fusion. For Higgs pair production, the approximation is less precise, since the leading order (LO) approximate result is known to differ from the result with full top quark mass dependence by 20%. Furthermore, the approximation fails to produce correct kinematic distributions [25, 47], which are required by experiment to extract the self-coupling.
The main project of this thesis was the calculation of the two-loop NLO QCD corrections to Higgs pair production in gluon fusion with full top quark mass dependence. This is a challenging task, since the Higgs pair production process is already loop induced at LO, making the virtual corrections a two-loop calculation of a two-to-two process with massive and massless particles running in the loops, which lead to ultraviolet (UV) and infrared (IR) divergent expressions for the NLO amplitude. While there are established procedures for the pole extraction and numerical evaluation of one-loop integrals with arbitrary masses in the loop and ongoing improvements for massless multi-loop calculations, the integrals involved in this process are still uncharted territory. The calculation is performed in dimensional regularisation and its strategy is similar to the one successfully applied in the single Higgs production case. It involves non-trivial transformations in Feynman parameter space, allowing the isolation of singularities through endpoint subtractions, as well as the treatment of additional threshold singularities by partial integration. This procedure results in numerically integrable expressions for the virtual amplitude with fully isolated UV and IR poles. The calculation of the amplitude of the virtual corrections poses the crucial step in the calculation of the NLO QCD corrections with full top quark mass dependence.

The Higgs pair production process is also of interest in the context of new physics (NP) searches, as many beyond the Standard Model (BSM) extensions contain scenarios, in which the cross section for Higgs pair production differs largely from the SM prediction, while the other observable properties of the Higgs boson are still fairly SM-like. The absence of a discovery of new physical states during LHC Run 1 suggests that the scale of NP is well separated from the EW scale. This encourages the description of NP within the framework of the Effective Field Theory (EFT), in which the NP effects are parametrised by local higher-dimensional operators of the SM fields and their derivatives. These EFT operators allow for a rather model-independent description of BSM physics. In this project we have calculated the NLO QCD corrections to Higgs pair production including dimension-6 operators in the heavy quark limit and investigated the impact of these operators on the NLO QCD corrections of the Higgs pair production cross section.
Prior to this project, the results of which were published in [48], the Higgs pair production process was already studied in the EFT framework including approximate NLO QCD corrections in [49]. The strategy to account for higher order corrections in this analysis was to calculate the LO amplitude including dimension-6 EFT operators and to multiply the resulting cross section with the overall K-factor, given by the ratio of the SM result for the NLO QCD cross section divided by the LO cross section in the heavy top quark limit [15]. We investigate the validity of this approximation by including the dimension-6 contributions directly at the NLO amplitude level in the heavy top quark limit. These two approaches lead to different results, as the individual contributions to Higgs pair production are affected differently by the NLO QCD corrections.

This thesis is organised as follows: Chapter 2 provides the theoretical basics by giving a brief introduction to the SM in section 2.1, section 2.2 describes the general techniques used for calculations of NLO QCD corrections and in section 2.3 the phenomenology of Higgs boson pair production at the LHC is discussed.
Chapter 3 presents the details on the derivation of the NLO QCD corrections to Higgs pair

production in gluon fusion with full top quark mass dependence. In section 3.1 the LO cross section is recalculated with all contributions up to $\mathcal{O}(\varepsilon^2)$ in the regulator ε explicitly kept in the amplitude, as these are required for the NLO calculation. Section 3.2 gives a detailed strategy for the technically involved calculation of the two-loop virtual amplitude and section 3.3 briefly introduces the structure of the real corrections.
Chapter 4 reports on the calculation of the dimension-6 EFT contributions to Higgs pair production at NLO. First the framework of EFT and the heavy top quark limit are introduced in section 4.1 and section 4.2, respectively, before the actual calculation is presented in section 4.3. The results of our analysis are summarised in section 4.4.
Chapter 5 serves as a brief conclusion of the results and gives an outlook on the next steps of the main project of chapter 3.

CHAPTER 2

Theoretical Foundations

2.1. The Standard Model

The SM of particle physics is the result of an ambitious pursuit to explain all data gathered by collider experiments in a coherent relativistic quantum field theory framework. Ever since its formulation in the 1960's it has provided the theoretical basis for the description of the interactions between elementary particles. The following chapter presents a brief introduction to the formulation of the SM as a renormalisable gauge theory.

2.1.1. The Standard Model Gauge Group

The Standard Model successfully combines all known elementary particles and three of the four observed forces of nature into a spontaneously broken gauge theory. The Lagrangian of this quantum field theory is symmetric under transformations of a non-abelian group represented by the tensor product

$$\mathrm{SU}(3)_C \otimes \mathrm{SU}(2)_L \otimes \mathrm{U}(1)_Y \ . \tag{2.1}$$

The $\mathrm{SU}(3)_C$ is the symmetry group of the strong interaction between quarks and gluons, the latter being the interaction mediators, and associated conservation of the colour charge. The phenomenology of strongly interacting particles is described by quantum chromodynamics (QCD) [50–53]. The EW gauge group $\mathrm{SU}(2)_L \otimes \mathrm{U}(1)_Y$ is associated with the conservation of the weak isospin I and hypercharge[1] Y and it describes the electromagnetic and weak interactions unified within the Glashow-Weinberg-Salam theory [7, 8, 54]. All heretofore observed elementary fermionic particles can be classified within the Standard Model into chiral right-handed singlets and left-handed doublets according to their transformation behaviour under the symmetry group eq. (2.1) as stated in table 2.1. Right-handed neutrinos, while not forbidden by theoretical arguments, are not included in the Standard Model, as they transform as singlets under the gauge group eq. (2.1) and therefore couple to none of the force mediators.
In addition to the matter fields, one gauge field for every generator of the symmetry group

[1] In the process of electroweak symmetry breaking these quantities lead to the conservation of electric charge Q given by the Gell-Mann-Nishijima formula: $Q = I_3 + Y$, where I_3 is the third component of the weak isospin.

Field				SU(3)	SU(2)	U(1)
Q_L^i	$(u_L,\, d_L)^{\mathrm{T}}$	$(c_L,\, s_L)^{\mathrm{T}}$	$(t_L,\, b_L)^{\mathrm{T}}$	3	2	1/6
u_R^i	u_R	c_R	t_R	3	1	2/3
d_R^i	d_R	s_R	b_R	3	1	$-1/3$
L_L^i	$(\nu_{e,L},\, e_L)^{\mathrm{T}}$	$(\nu_{\mu,L},\, \mu_L)^{\mathrm{T}}$	$(\nu_{\tau,L},\, \tau_L)^{\mathrm{T}}$	1	2	$-1/2$
l_R^i	e_R	μ_R	τ_R	1	1	-1

Table 2.1: Matter field content of the Standard Model with corresponding gauge quantum numbers. The fermionic quark and lepton fields Q_L^i, L_L^i, u_R^i, d_R^i, l_r^i exist in three generations $i = 1, 2, 3$ distinguished solely by the mass of the particles.

has to be included in the theory. These are the 8 gluon fields G_μ^a for the strongly interacting sector and 4 fields W_μ^1, W_μ^2, W_μ^3, B_μ for the electroweak sector, so that the kinetic part of the Lagrangian $\mathcal{L}$ for the fermions,

$$\begin{aligned} \mathcal{L}_{\mathrm{kin}}^{\mathrm{F}} &= \mathrm{i}\,\overline{\psi}\not{\mathcal{D}}\psi\,, \quad \text{with} \quad \psi = Q_L^i, u_R^i, d_R^i, L_L^i, l_R^i \quad \text{and} \\ \mathcal{D}_\mu &= \partial_\mu - \mathrm{i}g_s\frac{t_a}{2}G_\mu^a - \mathrm{i}g_2\frac{\sigma_k}{2}W_\mu^k - \mathrm{i}g_1 Y B_\mu \quad a \in \{1,\dots 8\},\ k \in \{1,2,3\} \end{aligned} \tag{2.2}$$

remains invariant under gauge transformations. These fields are the mediator fields of the interactions and the parameters g_i, $i \in \{s, 1, 2\}$ the corresponding couplings. Gauge invariant couplings between matter and mediator fields are generated dynamically from the kinetic term, whereas self-interactions among the gauge fields result from the gauge-kinetic part of $\mathcal{L}$

$$\mathcal{L}_{\mathrm{kin}}^{\mathrm{G}} = -\frac{1}{4}\left(G_{\mu\nu}^a G^{a\mu\nu} + W_{\mu\nu}^a W^{a\mu\nu} + B_{\mu\nu}B^{\mu\nu}\right). \tag{2.3}$$

With the field strength tensors $G_{\mu\nu}^a$, $W_{\mu\nu}^i$, and $B_{\mu\nu}$ defined by,

$$G_{\mu\nu}^a = \partial_\mu G_\nu^a - \partial_\nu G_\mu^a - g_s\, f_{abc} G_\mu^b G_\nu^c\,, \tag{2.4}$$

$$W_{\mu\nu}^i = \partial_\mu W_\nu^i - \partial_\nu W_\mu^i - g_2\, \epsilon_{ijk} W_\mu^j W_\nu^k\,, \tag{2.5}$$

$$B_{\mu\nu} = \partial_\mu B_\nu - \partial_\nu B_\mu\,, \tag{2.6}$$

where f_{abc} $(a, b, c \in \{1, \dots, 8\})$ and ϵ_{ijk} $(i, j, k \in \{1, 2, 3\})$ are the structure constants of the SU(3) and SU(2), respectively.

2.1.2. The Higgs Mechanism

Complications arise when gauge theories are to contain massive gauge bosons, as the usual Lorentz-invariant mass terms quadratic in the fields break gauge invariance. In the Standard Model this problem is solved by the Higgs mechanism [1–6] by adding a complex isospin doublet scalar field $\Phi = (\phi^+, \phi^0)^{\mathrm{T}}$ with hypercharge $Y = 1/2$. When the Higgs field potential is constructed as

$$V_{\mathrm{Higgs}} = \mu^2 \Phi^\dagger\Phi + \frac{\lambda}{2}\left|\Phi^\dagger\Phi\right|^2 \tag{2.7}$$

with $\mu^2 < 0$ and $\lambda > 0$, it possesses a non-vanishing vacuum expectation value

$$\langle\Phi\rangle = (0, v/\sqrt{2})^{\mathrm{T}}\,, \quad \text{with} \quad v = \sqrt{-2\mu^2/\lambda}\,. \tag{2.8}$$

The vacuum expectation value v is related to the Fermi constant G_F as $v = (\sqrt{2}\,G_F)^{-1/2}$ and thereby experimentally determined to be $v \simeq 246\,\text{GeV}$. The shift of the Higgs field ground state in the kinetic part of the Higgs Lagrangian,

$$\mathcal{L}^{\text{H}}_{\text{kin}} = (\mathcal{D}_\mu\Phi)^\dagger\,(\mathcal{D}^\mu\Phi) \xrightarrow{\Phi\to\langle\Phi\rangle} \frac{v^2}{8}\big[g_2^2\,\big(W^1_\mu{+}\text{i}W^2_\mu\big)\,\big(W^1_\mu{-}\text{i}W^2_\mu\big){+}\big(g_2W^3_\mu{-}g_1B_\mu\big)^2\big], \tag{2.9}$$

yields mass terms for physical combinations of the gauge fields. These are the massless neutral photon A^0_μ, the massive neutral Z-boson Z^0_μ and the charged W-bosons $W^\pm_\mu$. With the Weinberg angle θ_W defined by $\cos\theta_W = g_2/\sqrt{g_1^2{+}g_2^2}$, these can be written in terms of the gauge $\text{SU}(2)_L{\otimes}\text{U}(1)_Y$ fields as

$$W^\pm_\mu = \frac{1}{\sqrt{2}}\left(W^1_\mu \mp \text{i}W^2_\mu\right), \qquad \text{with } m_W = \frac{g_2 v}{2}, \tag{2.10}$$

$$Z^0_\mu = \cos\theta_W W^3_\mu - \sin\theta_W B_\mu, \qquad \text{with } m_Z = \frac{v}{2}\sqrt{g_1^2{+}g_2^2}, \tag{2.11}$$

$$A^0_\mu = \sin\theta_W W^3_\mu + \cos\theta_W B_\mu, \qquad \text{with } m_A = 0. \tag{2.12}$$

Gauge invariant fermion mass terms can also be included in the Lagrangian by introducing the Yukawa couplings between the fermion fields and the Higgs doublet field[2],

$$\begin{aligned}
\mathcal{L}^{\text{F}}_{\text{mass}} &= \mathcal{L}^{\text{F}}_y + h.c., \quad \text{with}\\
-\mathcal{L}^{\text{F}}_y &= Y^e_{ij}\,\overline{L}^i_L\Phi\,l^j_R + Y^u_{ij}\,\overline{Q}^i_L\Phi^c\,u^j_R + Y^d_{ij}\,\overline{Q}^i_L\Phi\,d^j_R\\
&\xrightarrow{\Phi\to\langle\Phi\rangle} \frac{v}{\sqrt{2}}\left(Y^e_{ij}\,\overline{l}^i_L l^j_R + Y^u_{ij}\,\overline{u}^i_L u^j_R + Y^d_{ij}\,\overline{d}^i_L d^j_R\right)
\end{aligned} \tag{2.13}$$

where the Yukawa matrices Y^e, Y^u, Y^d are diagonal in the unitary gauge and fermion masses are proportional to the corresponding diagonal element. Yukawa couplings for the neutrino fields are not included in $\mathcal{L}^{\text{F}}_y$ as in the usual formulation of the SM neutrinos are considered to be massless and the right-handed neutrino fields are singlets of the SM gauge group eq. (2.1). This brief introduction of the SM can therefore be summarised using eq. (2.2)-(2.13) by recapitulating the SM Lagrangian, apart from gauge fixing and ghost contributions of the strong sector, as

$$\mathcal{L}_{\text{SM}} = \mathcal{L}^{\text{F}}_{\text{kin}} + \mathcal{L}^{\text{G}}_{\text{kin}} + \mathcal{L}^{\text{H}}_{\text{kin}} + \mathcal{L}^{\text{F}}_{\text{mass}} - V_{\text{Higgs}}\,. \tag{2.14}$$

2.2. Next-to-Leading Order Corrections

2.2.1. Hadronic Cross Sections

According to the factorisation theorem [55], high energy collisions of hadrons can be described by interactions of individual constituents of the hadronic bound states called partons. Theoretical perturbative predictions for cross sections measured at hadron collider experiments are calculated within this parton model as a scattering of quarks and gluons, which carry a fraction x_i of the hadron momenta P_i. Since the subject of this thesis is the calculation of the NLO corrections for the hadronic cross section of Higgs boson pair production in gluon fusion, let us discuss the general features of hadronic NLO calculations on this example. At LO of the perturbative expansion in the strong coupling $\alpha_{\text{s}} = g_s^2/(4\pi)$, the hadronic cross section of this subprocess is given by

$$\sigma(pp \to gg \to hh) = \int_0^1 \text{d}x_1 \int_0^1 \text{d}x_2\, f_g(x_1,\mu_F)\, f_g(x_2,\mu_F)\, \hat{\sigma}(g(p_1)\,g(p_2) \to hh)\,, \tag{2.15}$$

[2] Φ^c denotes the charge conjugated Higgs doublet field given as $\Phi^c = \text{i}\sigma_2\,\Phi^* = ((v{+}h^*(x))/\sqrt{2},\,0)^{\text{T}}$ in the unitary gauge.

where μ_F denotes the factorisation scale and $\hat{\sigma}(g(p_1)\,g(p_2) \to hh)$ is the partonic LO cross section of Higgs boson pair production in the collision of two gluons g which carry fractions of the proton momenta $p_i = x_i P_i$ ($i \in 1, 2$). The SM Lagrangian eq. (2.14) does not contain direct couplings of gluons and Higgs fields, as the gluons are massless. This means that in the Feynman diagrammatic approach [56] the gluon fusion process is mediated by quark loops already at LO [45, 57] and the LO cross section is of $\mathcal{O}(\alpha_s^2)$.
The process-independent parton distribution functions (PDFs) $f_g(x_i, \mu_F)$ are non-perturbative quantities which are determined by fits to experimental data obtained in deep inelastic scattering experiments. They can be interpreted as the probability densities for finding a gluon with momentum fraction x_i in the proton. Since the collisions at the LHC occur in the centre-of-mass frame of the protons with the hadronic centre-of-mass energy $\sqrt{s}$ and the production cross section is non-zero only for partonic energies $\sqrt{\hat{s}}$ above the Higgs pair production threshold given by the Higgs boson mass m_h as $\hat{s} > 4m_h^2$, the PDF integrations can be rewritten in terms of the fraction $\tau = \hat{s}/s$ of the squared hadronic and partonic centre-of-mass energies and the gluon luminosity $d\mathcal{L}^{gg}/d\tau$ as,

$$\begin{aligned} \sigma(pp \to gg \to hh) &= \int_{\tau_0}^{1} \mathrm{d}\tau \, \frac{d\mathcal{L}^{gg}}{d\tau} \, \hat{\sigma}(\hat{s} = \tau s) \,, \quad \text{with} \quad \tau_0 = 4m_h^2/s \quad \text{and} \\ \frac{d\mathcal{L}^{gg}}{d\tau} &= \int_{\tau}^{1} \frac{\mathrm{d}x}{x} \, f_g(x, \mu_F) \, f_g(\tau/x, \mu_F) \,. \end{aligned} \tag{2.16}$$

The calculation of NLO corrections requires the computation of all $\mathcal{O}(\alpha_s^3)$ contributions to the hadronic cross section. These can be expressed as,

$$\Delta\sigma_{\mathrm{NLO}} = \Delta\sigma_{\mathrm{virt}} + \Delta\sigma_{gg} + \Delta\sigma_{qg} + \Delta\sigma_{q\bar{q}} \,, \tag{2.17}$$

where the virtual corrections $\Delta\sigma_{\mathrm{virt}}$ are proportional to the interference term of the LO amplitude with the two-loop amplitude, which involves the exchange of a virtual gluon, and the real corrections $\Delta\sigma_{ij}$ are proportional to the matrix element squared of the corrections to the LO process with an additional massless parton in the final state. The additional final state parton can be a gluon emitted off the quark loop, or due to an initial state splitting, which gives rise to additional contributions to the gluon fusion process at NLO with quark-gluon ($\Delta\sigma_{qg}$) and quark-antiquark ($\Delta\sigma_{q\bar{q}}$) initial states. The reason why real corrections need to be included to the process will be explained in section 2.2.4.

2.2.2. Regularisation of Divergences

A consequence of the perturbative description in quantum field theories is the appearance of divergences in higher order calculations. In virtual corrections these divergences originate from the enclosed propagator loops of the Feynman diagrams. Even when momentum conservation at each vertex of the amplitude is utilised, the momentum k^μ of one propagator within the loop can always acquire an arbitrary value. In the spirit of quantum field theory, all possible values of this indeterminate momentum contribute to the amplitude, which is mathematically expressed by an indefinite integration over the loop momentum. The momentum integration can lead to UV and IR divergences of the amplitude. UV singularities occur in the limit $|k^\mu| \to \infty$ and IR singularities are present when a massless loop propagator connecting external particles has vanishing momentum, or when the momenta of two massless loop propagators attached to an external massless particle are collinear to the external particles momentum – these momentum constellations correspond to the soft and collinear limits [58, 59].
In order to perform numerical NLO calculations, the UV and IR divergences of the amplitudes need to be isolated and cancelled in an unambiguous way. The first step is achieved by defining a regularisation scheme. A regularisation method suitable for SM calculations which

preserves gauge and Lorentz invariance called dimensional regularisation was introduced by 't Hooft and Veltman [60]. Both UV and IR divergences are isolated by calculating amplitudes as analytic functions of the space-time dimensionality $D = 4-2\varepsilon$. Mathematically this corresponds to the replacement of the loop momentum integration as,

$$\int \frac{\mathrm{d}^4 k}{(2\pi)^4} \to \mu^{4-D} \int \frac{\mathrm{d}^D k}{(2\pi)^D} \,, \tag{2.18}$$

where μ denotes the arbitrary 't Hooft scale, which is introduced in order to preserve the dimensionality of the amplitude. For one-loop amplitudes the isolation of the UV and IR divergences is achieved in a straightforward way by reducing the loop momentum integrals to a set of scalar one-loop master integrals according to the Passarino-Veltman reduction [61]. The UV and IR divergences manifest as ε^{-1} and ε^{-2} poles in the physical limit $\varepsilon \to 0$ with intgrable coefficients and the remaining finite parts parts of the loop integrals can be evaluated. This calculational strategy is used in section 3.1.3 in order to obtain the LO amplitude[3]. The calculation of the NLO amplitude is more involved, since arbitrary two-loop amplitudes cannot be reduced to a finite set of master integrals. The isolation of the UV and IR poles and the numerical calculational strategy will be presented in detail in section 3.2.1.

2.2.3. Renormalisation and Counterterms

Once the UV and IR poles have been isolated, they still need to be cancelled in order to obtain non-divergent results. For the UV divergences this is achieved through renormalisation. This procedure is based on the interpretation of the fields, couplings and masses in the SM Lagrangian eq. (2.14) as bare parameters which develop divergences in higher order calculations and need to be expressed in terms of the corresponding physical parameters and divergent renormalisation constants. For the calculation of the NLO QCD corrections to Higgs boson pair production, the bare parameters involved in the LO amplitude are the strong coupling constant $\alpha_{s,0}$ and the top quark mass $m_{t,0}$. These need to be replaced by the physical parameters α_s and m_t and the counterterms $\delta\alpha_\mathrm{s}$ and δm_t connected via,

$$\alpha_{s,0} = \alpha_\mathrm{s} + \delta\alpha_\mathrm{s} \,, \tag{2.19}$$

$$m_{t,0} = m_t + \delta m_t \,. \tag{2.20}$$

The counterterms $\delta\alpha_\mathrm{s}$ and δm_t are determined solely by the requirement that the counterterm exactly cancels the divergent behaviour of the bare parameter. They can also contain a finite part, which is determined by the renormalisation condition. The choice of renormalisation conditions does not effect the results of physical observables calculated to all orders of perturbation theory, however the truncation of the perturbative expansion at a finite order leads to a dependence of the result on the renormalisation conditions. The two most frequently used renormalisation conditions are the on-shell and $\overline{\mathrm{MS}}$ conditions.

The $\overline{\mathrm{MS}}$ scheme is defined by the modified minimal subtraction condition according to which the counterterm absorbs only the UV pole and a universal constant. This renormalisation condition is usually applied for parameters which are not directly accessible in experiments. The strong coupling is a parameter which is commonly renormalised in the $\overline{\mathrm{MS}}$ scheme and the NLO counterterm $\delta\alpha_\mathrm{s}^{\overline{\mathrm{MS}}}$ is given by

$$\delta\alpha_\mathrm{s}^{\overline{\mathrm{MS}}} = \frac{\alpha_\mathrm{s}^2}{4\pi}\beta_0(-\Delta + \log\frac{\mu_R^2}{\mu^2}) \,, \tag{2.21}$$

[3]Even though the gluon fusion process is loop induced already at LO, the amplitude is UV and IR finite.

where μ is the 't Hooft scale, μ_R the renormalisation scale and the modified minimal subtraction scheme pole $\Delta = \varepsilon^{-1} - \gamma_E + \log 4\pi$ includes universal finite contributions of $\log 4\pi$ and the Euler-Mascheroni constant γ_E. The one-loop coefficient of the β-function reads

$$\beta_0 = \left[11 - \frac{2}{3} N_F\right] - \frac{2}{3}\,, \tag{2.22}$$

where the term in the bracket in eq. (2.22) contains the contribution of the gluon and of the $N_F = 5$ light quark flavours to the running of α_s, and the last term gives the additional contribution of the heavy top quark. As can be inferred from eqs. (2.21) and (2.22), the μ_R dependence of the strong coupling constant in the $\overline{\text{MS}}$ scheme is given by both the light and the heavy quark flavours, but it only depends on the number of the particles and not their mass. Thus, the heavy top quark does not decouple automatically, which may lead to large logarithms, if the scale of the process and the top quark mass are widely separated. These large logarithms can be avoided by explicitly decoupling the top quark from the running of $\alpha_s^{\overline{\text{MS}}}$ [62–64]. At NLO this is achieved by the replacement,

$$\alpha_s^{(5)\overline{\text{MS}}}(\mu_R) = \alpha_s^{\overline{\text{MS}}}(\mu_R)\left[1 + \frac{\alpha_s^{\overline{\text{MS}}}(\mu_R)}{4\pi}\frac{2}{3}\log\frac{m_t^2}{\mu_R^2}\right], \tag{2.23}$$

which can be introduced into the calculation by modifying the counterterm $\delta\alpha_s^{\overline{\text{MS}}}$ as,

$$\delta\alpha_s^{\overline{\text{MS}}} \to \delta\alpha_s^{(5),\overline{\text{MS}}} = \delta\alpha_s^{\overline{\text{MS}}} - \frac{\alpha_s^{(5)\overline{\text{MS}}}}{4\pi}\frac{2}{3}\log\frac{m_t^2}{\mu_R^2}\,. \tag{2.24}$$

With this replacement, the evolution of the strong coupling is correctly described by the light contributions,

$$\frac{\partial\alpha_s^2(\mu_R^2)}{\partial\log\mu_R^2} = -\frac{\alpha_s^2(\mu_R^2)}{4\pi}\left[\beta_0 + \frac{2}{3}\right] \tag{2.25}$$

so that only the gluon and the five light quark flavours contribute to the running of α_s.

In contrast to the $\overline{\text{MS}}$ scheme, the counterterms of the on-shell scheme contain more involved finite parts. These are defined in such a way that the counterterm not only cancels the divergent behaviour but also any finite shifts which the bare parameter acquires in higher orders, so that the physical parameter retains the same numerical value in higher orders. For the top mass counterterm δm_t the on-shell renormalisation condition requires the real part of the pole of the renormalised top quark propagator to be located at $k^2 = m_t^2$. The counterterm is obtained from the renormalised one-particle-irreducible two-point function $\hat{\Gamma}_t(k)$ of the top quark field, which can be expressed in terms of scalar form factors $\hat{\Sigma}_t^V(k^2)$ and $\hat{\Sigma}_t^S(k^2)$ defined according to the conventions[4] of [65],

$$\hat{\Gamma}_t(k) = \mathrm{i}(\not{k} - m_t) + \mathrm{i}\left[\not{k}\,\hat{\Sigma}_t^V(k^2) + m_t\,\hat{\Sigma}_t^S(k^2)\right]. \tag{2.26}$$

The on-shell renormalisation condition can be expressed as,

$$\mathrm{Re}\big[\hat{\Gamma}_t(k)\,u(k)\big]_{k^2=m_t^2} = 0 \quad \Rightarrow \quad \mathrm{Re}\big[\hat{\Sigma}_t^V(m_t^2) + \hat{\Sigma}_t^S(m_t^2)\big] = 0\,, \tag{2.27}$$

where $u(k)$ is the top quark spinor. The top mass counterterm is thus given in terms of the components of the unrenormalised one-particle-irreducible two-point function of the top quark field,

$$\delta m_t = m_t\,\mathrm{Re}\big[\Sigma_t^V(m_t^2) + \Sigma_t^S(m_t^2)\big]\,. \tag{2.28}$$

[4] The calculation is in this case even simpler, as, unlike for the EW corrections, no flavour mixing is induced by the QCD NLO corrections.

2.2.4. Cancellation of Infrared Singularities

The inclusion of the counterterms to the NLO amplitude of the process renders the virtual corrections UV finite, however they still contain IR divergences. These divergences are resolved by a reinterpretation of the process itself. According to the Kinoshita-Lee-Nauenberg theorem [58, 59], IR divergences do not occur in sufficiently inclusive observables due to a cancellation between the IR poles of the virtual corrections $\Delta\sigma_{\text{virt}}$ and the real emission contributions $\Delta\sigma_{ij}$. The formulation "sufficiently inclusive" refers to the existence of a finite cutoff of the energy and angular resolution of any physical measurement, which implies that signal events are indistinguishable from events with additional soft and/or collinear particles in the final state and thus the calculation of a sufficiently inclusive observables must take both contributions into account. While the sum of the separately IR divergent real and virtual corrections is finite for any process, the numerical evaluation is technically involved, as the IR cancellation takes place between terms which are integrated over the D dimensional phase space dPS with different final-state multiplicities,

$$\underbrace{\sigma_{\text{NLO}}}_{\text{IR finite}} = \underbrace{\int \text{dPS}_n \, d\sigma_{\text{LO}} + d\sigma_{\text{virt}}}_{\text{IR divergent}} + \underbrace{\int \text{dPS}_n \text{dPS}_1 \, [d\sigma_{gg} + d\sigma_{qg} + d\sigma_{q\bar{q}}]}_{\text{IR divergent}} . \tag{2.29}$$

A solution to this issue is provided by subtraction techniques such as the Catani-Seymour- [66–68], FKS- [69] or antenna-subtraction [70, 71]. The subtraction techniques define an auxiliary cross section σ^A, which has the same pointwise IR singular behaviour as the real corrections and can be integrated analytically over the 1-particle phase space of the additional real emission. Subtracting σ^A in the real corrections and readding the integrated form $\int \text{dPS}\, \sigma^A$ in the virtual corrections renders both contributions separately IR finite,

$$\underbrace{\sigma_{\text{NLO}}}_{\text{IR finite}} = \underbrace{\int \text{dPS}_n \left[d\sigma_{\text{LO}} + d\sigma_{\text{virt}} + \int \text{dPS}_1 \, d\sigma_A \right]}_{\text{IR finite}} + \underbrace{\int \text{dPS}_n \text{dPS}_1 \, [d\sigma_{gg} + d\sigma_{qg} + d\sigma_{q\bar{q}} - d\sigma_A]}_{\text{IR finite}} . \tag{2.30}$$

Due to the factorisation of QCD, the auxiliary cross section σ^A can be unambiguously constructed from the LO cross section and process independent dipole operators.

The cancellation of the IR singularities in this project follows a similar strategy as the subtraction techniques, but is performed in a more process specific way based on the knowledge of the NLO corrections to Higgs boson pair production in the heavy quark mass limit [15]. While this process specific subtraction technique yields IR finite expressions for the virtual corrections already on the amplitude level, the real corrections still contain initial state collinear divergences, which are cancelled by PDF renormalisation. The cancellation of the IR divergences will be discussed in detail in section 3.3.

2.3. Higgs Boson Phenomenology at the LHC

2.3.1. The Higgs Boson discovery

With the discovery of the Higgs boson [1–6] by the LHC experiments ATLAS [10] and CMS [11] in 2012, the last free parameter of the SM, the Higgs boson mass, has been pinned down to the value [72]

$$m_h = 125.09 \pm 0.24 \, \text{GeV} . \tag{2.31}$$

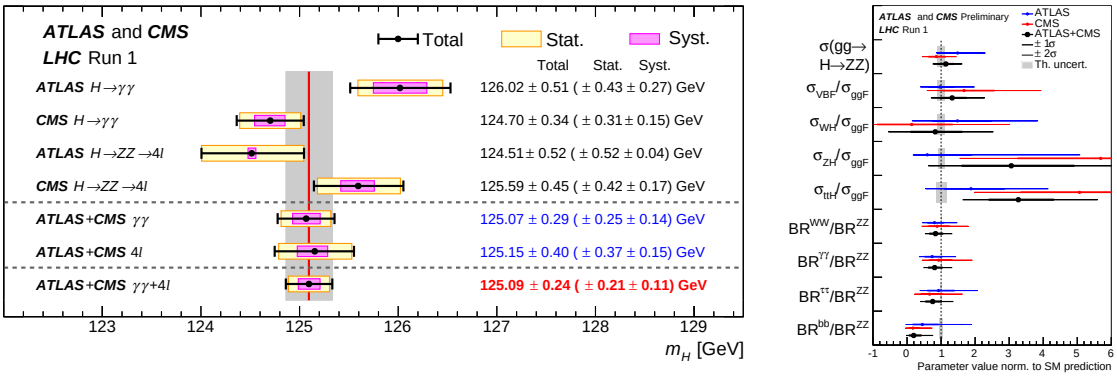

Figure 2.1: Combined results of the ATLAS and CMS experiments for LHC Run 1. Left: Higgs boson mass determination. [72] Right: Best fits for the signal of Higgs boson production in gluon fusion with subsequent decay into a Z boson pair and ratios of the production cross sections and branching ratios in comparison with the SM prediction. [12]

By determining the Higgs boson mass, all its properties, such as the production cross section and partial decay widths in the individual channels, can be uniquely predicted by theory and compared with experimental findings, ushering in a new era of LHC phenomenology. The role of the Higgs boson has thus developed from the long-sought missing piece of the SM to a tool for probing the validity of the SM as the complete theory of elementary particle physics on the TeV scale.
During LHC Run 1 both experiments recorded datasets each corresponding to approximately $5\,\text{fb}^{-1}$ at $\sqrt{s} = 7\,\text{TeV}$ and $20\,\text{fb}^{-1}$ at $\sqrt{s} = 8\,\text{TeV}$ centre-of-mass energy which were recently used for elaborate combined data analyses. For the determination of the Higgs boson mass the combined analysis [72] is based on the data obtained in the $H \to \gamma\gamma$ and $H \to ZZ \to 4l$ channels, yielding results which are remarkably complementary for the individual channels and experiments, as shown in the left summary plot of fig. 2.1. The results of the detailed analysis for the Higgs boson production and decay rates performed in [12] are exemplary shown in the right plot of fig. 2.1. The best fit values for the production cross sections in vector boson fusion (σ_{VBF}), and in associated production with vector bosons (σ_{WH}, σ_{ZH}) or top quark pairs (σ_{ttH}) normalised to the gluon fusion cross section (σ_{ggH}), as well as the branching ratios of the Higgs boson decays into W bosons (BR^{WW}), photons ($\text{BR}^{\gamma\gamma}$), tau leptons ($\text{BR}^{\tau\tau}$) and bottom quarks (BR^{bb}) normalised to the branching ratio of the decay into Z bosons (BR^{ZZ}) are compared to the corresponding SM values, yielding results consistent with the SM predictions. The experimental data also strongly favours the newly found boson to carry zero spin and positive CP parity [13, 14]. This favours the SM hypothesis, even though there is still room left for more exotic interpretations.

2.3.2. Higgs Boson Pair Production

Even though the so far gathered data supports the interpretation of the newly found bosonic particle as the SM Higgs boson, the final proof of this assumption requires comprehensive studies of the particles properties. In addition to the gauge boson and fermion couplings, the Higgs boson self-interactions also need to be examined, which are accessible in multi-Higgs production processes [15–18]. The Higgs boson self-couplings follow from the SM Lagrangian by rewriting the Higgs potential eq. (2.7) in terms of the physical Higgs field in the unitary gauge

$$\Phi(x) = \frac{1}{\sqrt{2}} \begin{pmatrix} 0 \\ v+h(x) \end{pmatrix} \quad \Rightarrow \quad V_{\text{Higgs}} = -\frac{m_h^2 v^2}{8} + \frac{m_h^2}{2} h(x)^2 + \frac{\lambda_{hhh}}{3!} h(x)^3 + \frac{\lambda_{4h}}{4!} h(x)^4 \,, \tag{2.32}$$
$$\text{with} \quad m_h^2 = -2\mu^2 \,, \quad \lambda_{hhh} = 3m_h^2/v \quad \text{and} \quad \lambda_{4h} = 3m_h^2/v^2 \,.$$

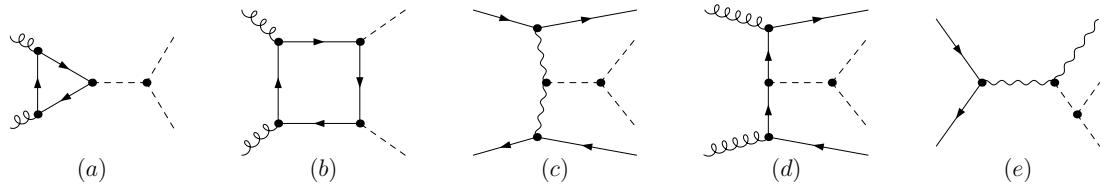

Figure 2.2: Sample diagrams for the Higgs boson pair production in gluon fusion which are sensitive (a) and non-sensitive (b) to the trilinear Higgs self-coupling. For the vector boson fusion (c), associated production with top quarks (d) and Higgs radiation (e) only the sensitive diagrams are shown.

The determination of the trilinear and quartic couplings λ_{hhh} and λ_{4h} allows to probe the shape of the Higgs potential with a non-vanishing vacuum expectation value, which is required by the Higgs mechanism. While the measurement of the quartic Higgs coupling seems to be out of reach of current and planned collider experiments as it suffers from low production rates and large backgrounds [16, 18–23], the determination of the trilinear coupling is challenging, yet more promising [24–44] and presents an important first step towards the reconstruction of the Higgs potential.
The main production channels for Higgs pairs at the LHC are similar to the single Higgs production. Sample LO Feynman diagrams for the production in gluon fusion [45, 46, 73, 74], vector boson fusion [73,75–79] and associated production with top quarks [80,81] and in Higgs radiation [30,73,82] are shown in fig. 2.2 (a), (c), (d) and (e) respectively. The diagrams giving access to the trilinear Higgs self-coupling involve the production of a single off-shell Higgs boson decaying into a pair of real Higgs bosons. However, all production mechanisms also contain diagrams in which the Higgs bosons are produced separately, as shown for the gluon fusion production in fig. 2.2 (b). These pose an irreducible background for the determination of the trilinear Higgs self-coupling. In comparison to single Higgs production, the processes have much lower production cross sections due to being of higher order in the electroweak coupling and due to phase space suppression because of the additional heavy particle in the final state. The cross sections for the Higgs pair production processes and the prospects for the determination of the trilinear Higgs self-coupling in hadron collisions have been investigated in many analyses throughout the years [15,17,18,24–44], yielding predictions for the production cross sections in the main channels including higher order corrections, which were summarised in [83] and are shown in fig. 2.3 left. The hierarchy of the cross sections is similar to single Higgs production, with the main channel being gluon fusion and the other production channels suppressed by factors of $10-30$.

2.3.3. Measurement Prospects

The cross sections for Higgs boson pair production are approximately three orders of magnitude smaller compared to the single Higgs production. Furthermore, the SM Higgs boson with $m_h = 125\,\text{GeV}$ decays predominantly into bottom quark pairs, as can be inferred from fig. 2.3 right, which is a final state plagued by the large QCD background in proton collisions, making the signal extraction a demanding task. A solution to this issue was proposed in [24–27] by considering the rare decay channels $b\bar{b}\gamma\gamma$ and $b\bar{b}\tau\bar{\tau}$, which pose a compromise between the requirements of statistics and significance.
An updated analysis of the $b\bar{b}\tau\tau$ channel presented in [30] for the proposed high-luminosity upgrade of the LHC with an integrated luminosity of $\int \mathcal{L} = 3\,\text{ab}^{-1}$ yielded a significance of $S/\sqrt{B} = 9.36$ with 330 signal events after cuts. A major improvement of the sensitivity in this channel is given by making use of jet substructure analysis [85]. This technique was applied in [28] and found to improve the signal-to-background ratio significantly, yielding values of $S/B \simeq 0.5$ with 95 signal events, which corresponds to a significance of $S/\sqrt{B} = 6.89$, already

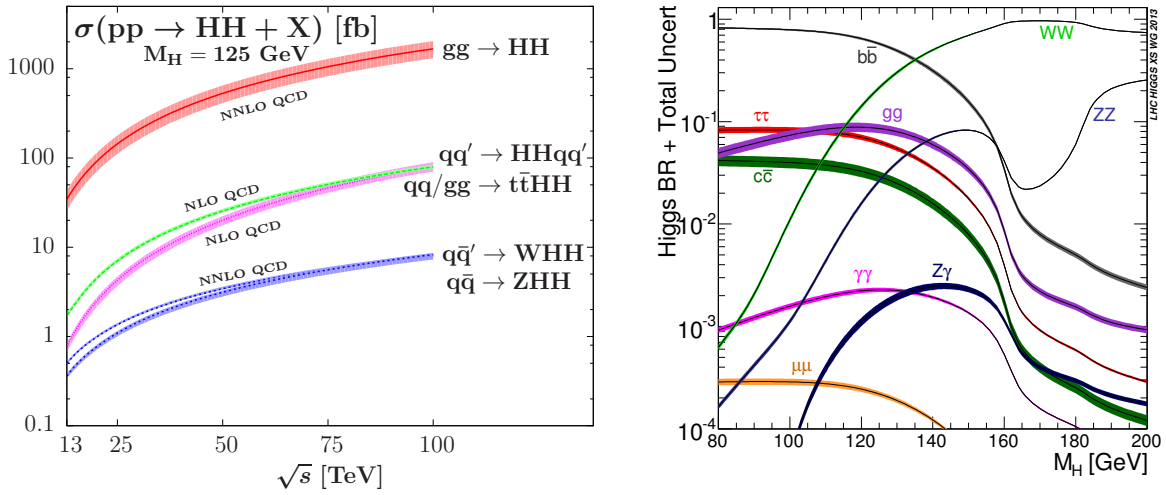

Figure 2.3: Left: Total hadronic cross section for the production of pairs of Higgs bosons with $m_h = 125\,\text{GeV}$ in the main production channels [83](updated version). Right: Branching ratios and their uncertainties for the SM Higgs boson decays in the low Higgs mass range [84].

for an integrated luminosity of $1\,\text{ab}^{-1}$. The addition of a jet to the final state was analysed in [33] and found to further improve the signal-to-background ratio up to $S/B = 1.5$. A combination of these techniques together with further feasible improvements can allow for a 60% accuracy on the determination of the trilinear Higgs coupling in the $b\bar{b}\tau\tau$ channel with $3\,\text{ab}^{-1}$ [33].
The $b\bar{b}\gamma\gamma$ channel produces a small yet pure signal, which was also analysed in [30], yielding a significance of $S/\sqrt{B} = 6.46$ with 47 signal events at $3\,\text{ab}^{-1}$ after detector level cuts due to diphoton fake rate simulation being taken into account. The authors of [35] have shown that the results of this channel can further be improved by a multivariate analysis, which increases the significance and could allow for a 40% uncertainty determination of the triple Higgs coupling with $\int \mathcal{L} = 3\,\text{ab}^{-1}$.
The ongoing development of analysis techniques can lead to further improvements of the measurement prospects. The $b\bar{b}WW$ channel was long considered less promising due to the large $t\bar{t}$ background, however by making use of multivariate and jet substructure techniques, the analysis performed in [29] yields a significance of $S/\sqrt{S+B} = 2.4$ with 9 signal events already at $0.6\,\text{ab}^{-1}$. Similarly, the background plagued $b\bar{b}b\bar{b}$ channel has been reanalysed in [36] using jet substructure and side-band techniques and was found to have the potential to constrain the trilinear coupling to $\lambda < 1.2\times\lambda_{\text{SM}}$ at 95% confidence level. This indicates that the measurement of the Higgs pair production process is a challenging long-term goal of the LHC project requiring precise theoretical predictions for the inclusive cross section as well as differential distributions.

2.3.4. Gluon Fusion Beyond Leading Order

The gluon fusion is the dominant production mechanism for Higgs boson pairs. As gluons do not directly couple to Higgs bosons, the process is already at LO mediated by quark loops with the typical LO contributions depicted in fig. 2.2 (a) and (b). The Yukawa couplings between quarks and Higgs bosons are proportional to the quark mass, which is why the main contributions to the production cross section originate from top quark loops and the remaining light quark flavours, including the bottom quark, contribute with less than 1% [15, 30]. The LO cross section was first calculated in [45] and revisited in [46]. For a long time the knowledge of higher order QCD corrections was limited to the NLO corrections in the heavy quark mass limit [15], in which the quark loops are reduced to effective contact interactions

of the gluons with the Higgs fields, thereby reducing the NLO amplitude to a one-loop calculation. Similarly to single Higgs production, the NLO corrections for Higgs pair production obtained in this approximation are large, yielding K-factors[5] of the order of 2. New interest in the theoretical community for the higher order corrections was triggered by the discovery of the Higgs boson. The next-to-next-to-leading order (NNLO) corrections were obtained in the heavy quark mass limit in [86–88]. These corrections increase the production cross section for SM Higgs pairs at the LHC by additional 20% atop of the NLO calculation and further reduce the scale uncertainty due to the variation of the renormalisation scale μ_R and the factorisation scale μ_F. Threshold resummation in the soft-collinear effective theory of soft gluons in the initial state were calculated in [89] at next-to-leading logarithmic level and further extended to the next-to-next-to-leading logarithmic order by [90] within the conventional QCD approach.

All the previously presented higher order calculations rely on the LO-improved heavy quark mass limit, in which the higher order corrections are calculated in the $m_t \to \infty$ limit and the top quark mass dependence is kept explicitly in the LO form factors. This improves the estimates for the inclusive K-factor due to the fact that the LO cross section can be factored out of the soft and collinear corrections, which provide the dominant higher order contributions. The validity of the LO-improved heavy quark mass limit was investigated in [88, 91, 92] by calculating additional terms in the inverse top mass expansion of the higher order corrections, estimating the finite quark mass effects to be of the order of 10% at NLO and 5% at NNLO. While this analysis suggests that the calculation of the NLO corrections with full mass dependence can reduce the uncertainties of the inclusive K-factor by $\mathcal{O}(10\%)$, the calculation is expected to have a much larger effect in differential distributions. This assumption is based on a corresponding LO analysis [25], in which the heavy quark mass approximation leads to uncertainties of order 20% on the inclusive cross section at centre-of-mass energy $\sqrt{s} = 14\,\text{TeV}$, but completely fails to reproduce correct differential distributions. Since precise predictions for differential distributions are essential to improve the signal-to-background ratios, the calculation of the finite NLO mass effects is crucial for the determination of the trilinear Higgs self-coupling at the LHC.

First steps towards the fully differential NLO calculation were already presented in [44, 81] by calculating the real NLO corrections with full top mass dependence. The main project of this thesis was the calculation of the virtual NLO corrections, which were the missing piece of the NLO calculation with full top mass dependence. While all the major aspects of this challenging calculation have already been addressed as will be described in chapter 3, the final results are still in preparation. In the recently published work of [93] the authors have managed to perform the calculation aimed by this project within the `GoSam` [94] and `SecDec` [95] framework. This gives the opportunity for a completely independent cross check of the results obtained by both collaborations, which is beneficial for future analyses based on this involved calculation.

[5] The K-factor is defined as the ratio of the NLO and LO cross section, $K = \sigma_{\text{NLO}}/\sigma_{\text{LO}}$ with α_s and PDF effects taken at consistent orders.

CHAPTER 3

NLO Corrections with Full Mass Dependence

The dominant NLO contributions to Higgs boson pair production in gluon fusion are the QCD corrections. In the limit of large quark masses, these corrections are known to increase the production cross section for pairs of Standard Model Higgs bosons at the LHC by approximately 80% [15]. However, while the heavy quark mass limit provides reliable results for single Higgs boson production, the uncertainties of this approximation are larger in Higgs pair production. At LO, the heavy quark mass result differs from the calculation with full quark mass dependence by 20% [45,46] and it fails to produce correct kinematic distributions required by experiment [25,47].
Improving these results, by taking into account the full quark mass dependence, increases the complexity of the NLO calculation significantly, since the LO process is already loop induced as shown in fig. 3.1 $(1a, b)$. In addition to the diagrams involving the trilinear Higgs coupling shown in the first line of fig. 3.1, each of the subprocesses also receives contributions from the continuum pair production depicted in the second line of fig. 3.1, which are the most challenging diagrams of the calculation. The NLO amplitude involves virtual two-loop diagrams of the two-to-two process, such as the diagrams in fig. 3.1 $(2a, b)$, and real corrections, which are one-loop diagrams with an additional massless parton in the final state. The real corrections can be classified according to their initial state partons into the gg channel, fig. 3.1 $(3a, b)$ and $(4a, b)$, the qg channel, fig. 3.1 $(5a, b)$, and the $q\bar{q}$ channel of fig. 3.1 $(6a, b)$.

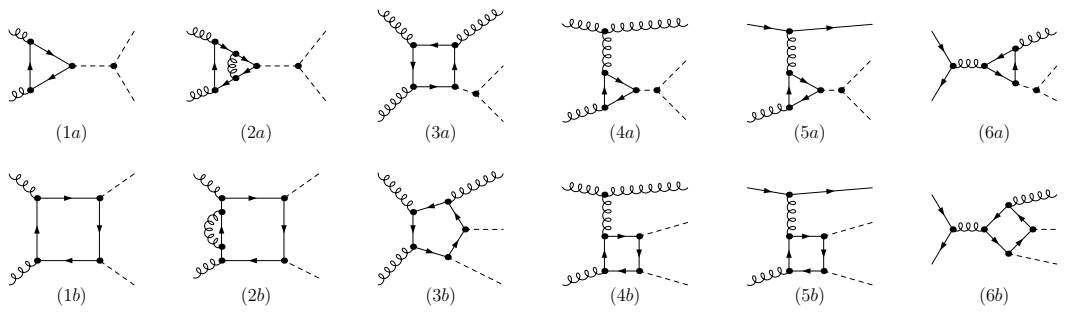

Figure 3.1: Sample diagrams contributing to Higgs boson pair production at LO and NLO.

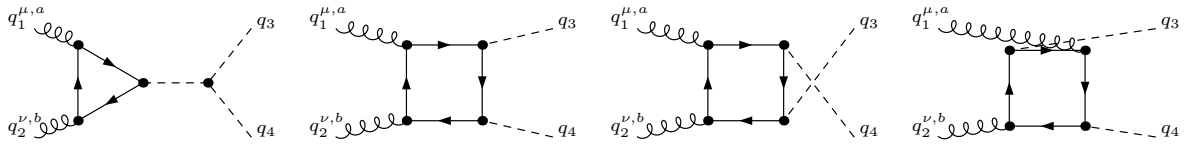

Figure 3.2: Feynman diagrams contributing to Higgs boson pair production in gluon fusion at leading order. Not shown are additional four diagrams with opposite fermion flow.

A common feature of NLO QCD amplitudes is the presence of infrared (IR) and ultraviolet (UV) singularities, which need to be regularised before numerical calculations can be performed. Within the framework of dimensional regularisation [60], the singularities are isolated by calculating amplitudes as analytic functions of the dimensionality of space-time, $D = 4-2\varepsilon$. In the physical limit $D \to 4$, the singularities manifest as ε^{-1} and ε^{-2} poles. The UV singularities of the virtual diagrams are cancelled through renormalisation of the physical parameters, specifically the strong coupling α_s and the top quark mass m_t. While the gluon fusion process also receives contributions from the other flavours running within the quark loop, due to the smallness of the corresponding Yukawa couplings, these contribute with less than 1% and can thus be neglected [15,30]. Both the real and virtual corrections contain IR singularities, which cancel exactly according to the Kinoshita-Lee-Nauenberg theorem [58,59]. Remaining initial state singularities are absorbed into the NLO parton densities, leading to a finite hadronic NLO cross section of the form,

$$\sigma_\mathrm{NLO} = \sigma_\mathrm{LO} + \Delta\sigma_\mathrm{virt} + \Delta\sigma_{gg} + \Delta\sigma_{qg} + \Delta\sigma_{q\bar{q}}\,. \tag{3.1}$$

The LO cross section σ_LO and the real corrections $\Delta\sigma_{gg}$, $\Delta\sigma_{qg}$, $\Delta\sigma_{q\bar{q}}$ are obtained from the matrix element squared of the contributing diagrams, while the virtual corrections $\Delta\sigma_\mathrm{virt}$ consist of the interference between the LO matrix element with the matrix element of the two-loop diagrams. The calculation of these contributions is presented in this chapter.

3.1. Leading Order Calculation

The LO matrix element, $\mathcal{M}_\mathrm{LO}$, for Higgs boson pair production was first calculated almost thirty years ago in [45]. However, in order to consistently determine the NLO corrections, the LO amplitude has to be recalculated including terms up to $\mathcal{O}(\varepsilon^2)$ in the regulator. This is required, because the virtual corrections $\Delta\sigma_\mathrm{virt}$ in eq. (3.1) are proportional to the interference term of the LO matrix element with the two-loop matrix element $\mathcal{M}_\mathrm{virt}$. The quadratically divergent parts of $\mathcal{M}_\mathrm{virt}$ thus produce finite contributions to the virtual corrections when multiplied with the $\mathcal{O}(\varepsilon^2)$ part of $\mathcal{M}_\mathrm{LO}$.

3.1.1. Process Definitions

For the derivation of $\mathcal{M}_\mathrm{LO}$ we follow the calculation strategy of [45, 46] and point out where differences arise due to retaining all terms of up to $\mathcal{O}(\varepsilon^2)$. Due to their distinct topologies, the contributions originating from the first diagram of fig. 3.2 are referred to as triangle contributions, while the latter three diagrams give rise to the box contributions. The matrix element for the gluon polarisations ϵ_μ, ϵ_ν yields,

$$\mathcal{M}_\mathrm{LO}^{ab} = 2\,F_c\,(-1)\,\mathrm{i}\,\frac{(2\pi\mu)^{4-D}}{16\pi^2}\int\frac{\mathrm{d}^D q}{\mathrm{i}\pi^2}\left[\mathcal{M}_\triangle^{\mu\nu}+\mathcal{M}_\square^{\mu\nu}\right]\epsilon_\mu(q_1)\,\epsilon_\nu(q_2)\,, \tag{3.2}$$

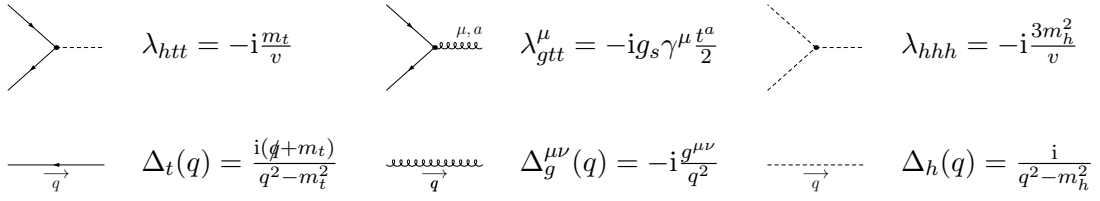

Figure 3.3: Feynman rules of the couplings λ_i and the propagators Δ_i required for the calculation with the gluon propagator defined in the Feynman gauge.

where the symmetry factor 2 is due to the not depicted diagrams with reversed fermion flow, the factor $F_c = \frac{1}{2}\delta_{ab}$ originates from the color structure with the color indices $a, b \in \{1, \ldots, 8\}$ and μ is an arbitrary renormalisation scale required to keep the dimensionality of the matrix element fixed. The integrands of the loop momentum q integral $\mathcal{M}_{\Delta}^{\mu\nu}$ and $\mathcal{M}_{\Box}^{\mu\nu}$ with the external momenta q_i assigned according to fig. 3.2 read explicitly,

$$\mathcal{M}_{\Delta}^{\mu\nu} = \lambda_{htt}\,\Delta_h(q_1{+}q_2)\,\lambda_{hhh}\,\mathrm{Tr}\left[\Delta_t(q)\,\lambda^{\mu}_{gtt}\,\Delta_t(q{+}q_1)\,\lambda^{\nu}_{gtt}\,\Delta_t(q{+}q_1{+}q_2)\right]\,, \tag{3.3}$$

$$\begin{aligned}\mathcal{M}_{\Box}^{\mu\nu} = {}& \mathrm{Tr}\left[\Delta_t(q)\,\lambda^{\mu}_{gtt}\,\Delta_t(q{+}q_1)\,\lambda^{\nu}_{gtt}\,\Delta_t(q{+}q_1{+}q_2)\,\lambda_{htt}\,\Delta_t(q{-}q_3)\,\lambda_{htt}\right] \\ & + \mathrm{Tr}\left[\Delta_t(q)\,\lambda^{\mu}_{gtt}\,\Delta_t(q{+}q_1)\,\lambda^{\nu}_{gtt}\,\Delta_t(q{+}q_1{+}q_2)\,\lambda_{htt}\,\Delta_t(q{+}q_1{+}q_2{+}q_3)\,\lambda_{htt}\right] \\ & + \mathrm{Tr}\left[\Delta_t(q)\,\lambda^{\mu}_{gtt}\,\Delta_t(q{+}q_1)\,\lambda_{htt}\,\Delta_t(q{+}q_1{+}q_3)\,\lambda^{\nu}_{gtt}\,\Delta_t(q{+}q_1{+}q_2{+}q_3)\,\lambda_{htt}\right],\end{aligned} \tag{3.4}$$

with the Feynman rules for the couplings λ_i and for the propagators Δ_i summarised in fig. 3.3, where m_h and m_t are the Higgs boson and top quark mass, respectively, v is the vacuum expectation value of the Higgs doublet field, g_s is connected to the strong coupling constant $\alpha_\mathrm{s} = g_s^2/(4\pi)$ and t^a are the Gell-Mann matrices. The external momenta are all defined as incoming, so that the Mandelstam variables of the partonic process are,

$$\begin{aligned}\hat{s} &= (q_1{+}q_2)^2 = (q_3{+}q_4)^2\,, \\ \hat{t} &= (q_1{+}q_3)^2 = (q_2{+}q_4)^2\,, \\ \hat{u} &= (q_2{+}q_3)^2 = (q_1{+}q_4)^2\,.\end{aligned} \tag{3.5}$$

For future reference, we also define the variables ρ_i, which are particularly convenient for this process,

$$\begin{aligned}\rho_1 \equiv \rho_s &= \frac{2\,q_1{\cdot}q_2}{m_t^2}\,, \qquad & \rho_2 \equiv \rho_t &= \frac{2\,q_1{\cdot}q_3}{m_t^2}\,, \\ \rho_3 \equiv \rho_u &= \frac{2\,q_2{\cdot}q_3}{m_t^2}\,, \qquad & \rho_4 \equiv \rho_h &= \frac{q_3{\cdot}q_3}{m_t^2}\,.\end{aligned} \tag{3.6}$$

3.1.2. Lorentz Structure Projectors

The matrix element of a process involving two massless vector bosons and two massive scalars can be expressed in terms of two process independent Lorentz tensors $T_i^{\mu\nu}$ weighted with Lorentz- and gauge-invariant form factors. The Lorenz tensors $T_i^{\mu\nu}$ follow from the most general structure of the matrix element given as $\mathcal{M} = T^{\mu\nu}\,\epsilon_\mu(q_1)\,\epsilon_\nu(q_2)$, with

$$T^{\mu\nu} = f_{00}\,g^{\mu\nu} + \sum_{i,j=1}^{3} f_{ij}\,q_i^{\mu}\,q_j^{\nu}\,. \tag{3.7}$$

The coefficients f_{00}, f_{ij} can be set into relation by applying the on-shell properties and the Ward identities for the gluons

$$q_1^{\mu}\,\epsilon_\mu(q_1) = q_2^{\nu}\,\epsilon_\nu(q_2) = 0\,, \tag{3.8}$$

$$q_1^{\mu}\,T_{\mu\nu} = q_2^{\nu}\,T_{\mu\nu} = 0\,, \tag{3.9}$$

yielding only two linear independent coefficients. The basis of these coefficients can be chosen such that the corresponding Lorentz tensors,

$$\begin{aligned} T_1^{\mu\nu} &= g^{\mu\nu} - \frac{q_2^\mu q_1^\nu}{q_1\cdot q_2}\,, \\ T_2^{\mu\nu} &= g^{\mu\nu} + \frac{(q_3\cdot q_3)q_2^\mu q_1^\nu - 2(q_2\cdot q_3)q_3^\mu q_1^\nu - 2(q_1\cdot q_3)q_2^\mu q_3^\nu + 2(q_1\cdot q_2)q_3^\mu q_3^\nu}{(q_1\cdot q_2)p_T^2}\,, \quad \text{with} \\ p_T^2 &= 2\frac{(q_2\cdot q_3)(q_1\cdot q_3)}{q_1\cdot q_2} - q_3\cdot q_3 \end{aligned} \tag{3.10}$$

are orthogonal in four dimensions. However, in $D = 4-2\varepsilon$ we find,

$$T_1^{\mu\nu}\cdot T_{1,\mu\nu} = T_2^{\mu\nu}\cdot T_{2,\mu\nu} = (D-2)\,, \qquad T_1^{\mu\nu}\cdot T_{2,\mu\nu} = (D-4), \tag{3.11}$$

which means that new projectors $P_i^{\mu\nu}$ need to be redefined in order to extract the form factors for eq. (3.2) in D dimensions. With the Ansatz $P_i^{\mu\nu} = a_i T_1^{\mu\nu} + b_i T_2^{\mu\nu}$ and the defining property

$$P_i^{\mu\nu}\cdot T_{j,\mu\nu} = \delta_{ij}\,, \quad i,j \in 1,2\,, \tag{3.12}$$

the projectors follow as,

$$\begin{aligned} P_1^{\mu\nu} &= \frac{(D-2)T_1^{\mu\nu} - (D-4)T_2^{\mu\nu}}{4(D-3)}\,, \\ P_2^{\mu\nu} &= \frac{(D-2)T_2^{\mu\nu} - (D-4)T_1^{\mu\nu}}{4(D-3)}\,. \end{aligned} \tag{3.13}$$

As this form factor decomposition is independent of the internal structure of the process, it can also be applied to the two-loop matrix element of the virtual corrections discussed in section 3.2.
Using these definitions, the matrix element $\mathcal{M}_{\text{LO}}^{ab}$ of eq. (3.2) can be rewritten as,

$$\mathcal{M}_{\text{LO}}^{ab} = \frac{\alpha_\text{s}}{\pi}\left[(\mathcal{A}_\Delta + \mathcal{A}_1)T_1^{\mu\nu} + \mathcal{A}_2 T_2^{\mu\nu}\right]\delta_{ab}\,\epsilon_\mu(q_1)\,\epsilon_\nu(q_2)\,, \tag{3.14}$$

with the scalar form factors $\mathcal{A}_\Delta$, $\mathcal{A}_1$ and $\mathcal{A}_2$ given by

$$\frac{\alpha_\text{s}}{\pi}\mathcal{A}_\Delta = (-1)\,\text{i}\,\frac{(2\pi\mu)^{4-D}}{16\pi^2}\int\frac{\text{d}^D q}{\text{i}\pi^2}\,\mathcal{M}_\Delta^{\mu\nu}\cdot P_{1,\mu\nu}\,, \tag{3.15}$$

$$\frac{\alpha_\text{s}}{\pi}\mathcal{A}_1 = (-1)\,\text{i}\,\frac{(2\pi\mu)^{4-D}}{16\pi^2}\int\frac{\text{d}^D q}{\text{i}\pi^2}\,\mathcal{M}_\Box^{\mu\nu}\cdot P_{1,\mu\nu}\,, \tag{3.16}$$

$$\frac{\alpha_\text{s}}{\pi}\mathcal{A}_2 = (-1)\,\text{i}\,\frac{(2\pi\mu)^{4-D}}{16\pi^2}\int\frac{\text{d}^D q}{\text{i}\pi^2}\,\mathcal{M}_\Box^{\mu\nu}\cdot P_{2,\mu\nu}\,. \tag{3.17}$$

Due to the definition of the projectors $P_i^{\mu\nu}$ in D dimensions, the second form factor of the triangle contributions vanishes exactly, as $\mathcal{M}_\Delta^{\mu\nu}\cdot P_{2,\mu\nu} = 0$ similarly to the four dimensional LO calculation. The explicit expressions for the triangle and box form factors are derived in the following subsection.

3.1.3. Leading Order Form Factors

The triangle form factor $\mathcal{A}_\Delta$ involves three-point one-loop functions with up to the power two of the loop momentum q in the numerator, which in the notation of [65] are defined as,

$$C_{\{0,\mu,\mu\nu\}}(p_1,p_2) = (2\pi\mu)^{4-D}\int\frac{\text{d}^D q}{\text{i}\pi^2}\,\frac{\{1, q_\mu, q_\mu q_\nu\}}{[q^2-m_t^2][(q+p_1)^2-m_t^2][(q+p_2)^2-m_t^2]}\,. \tag{3.18}$$

The coefficients of the rank 1 and 2 tensor one-loop functions C_μ and $C_{\mu\nu}$ first have to be reduced to scalar one-loop integrals B_0 and C_0 by using reduction properties of one-loop integrals [61]. This is done according to the formulae summarised in appendix A.1.1, which were derived from [96] with modifications to retain the full dimensional dependence and simplifications for the special case of equal masses in the loop propagators. The form factor eventually reads,

$$\mathcal{A}_\Delta = -\frac{\lambda_{hhh}\lambda_{htt}m_t}{2(\hat{s}-m_h^2)}\Big[2\varepsilon(1+\varepsilon)B_0(q_1+q_2)+\big(4(1+\varepsilon+\varepsilon^2)m_t^2-\hat{s}\big)\,C_0(q_1,q_1+q_2)\Big] \tag{3.19}$$

which agrees with the results of [45, 46] in the limit $\varepsilon \to 0$.

The form factor contributions of the box diagrams are more involved due to the additional fermion propagator. Formally, we encounter four-point tensor integrals of up to rank four. While the reduction procedure of [96] can also be implemented for these integrals, it is computationally much simpler to first reduce the four-point tensor integrals to three-point integrals. This can be achieved by expanding the numerators according to,

$$q\cdot p_i = \frac{1}{2}\Big\{[(q+p_i)^2-m_t^2]-[q^2-m_t^2]-p_i^2\Big\}, \tag{3.20}$$

$$q^2 = [q^2-m_t^2]+m_t^2, \tag{3.21}$$

so that the terms of the numerator cancel against appropriate factors in the denominator. All structures occurring in the box form factors $\mathcal{A}_1$ and $\mathcal{A}_2$ can be reduced to scalar two-, three- and four-point one-loop integrals B_0, C_0, D_0 by the identities listed in appendix A.1.2, yielding,

$$\begin{aligned}
\mathcal{A}_1 = \frac{\lambda_{htt}^2}{4(m_h^4-\hat{t}\hat{u})}\Big\{&B_0(q_1+q_2)(m_h^4-\hat{t}\hat{u})(4\varepsilon(1+\varepsilon))\\
&+C_0(q_1,q_1+q_2)\big[8m_t^2(1+\varepsilon+\varepsilon^2)(m_h^4-\hat{t}\hat{u})+\varepsilon(1+2\varepsilon)(\hat{t}+\hat{u})[16m_h^2m_t^2-(\hat{t}+\hat{u})(8m_t^2+\hat{s})]\big]\\
&+C_0(q_1,q_1+q_3)\frac{2}{\hat{s}}(\hat{t}-m_h^2)\big[2(m_h^2-4m_t^2)(m_h^4-\hat{t}\hat{u})+\varepsilon(1+2\varepsilon)(m_h^2-\hat{t})^2(\hat{t}+\hat{u}-8m_t^2)\big]\\
&+C_0(q_2,q_2+q_3)\frac{2}{\hat{s}}(\hat{u}-m_h^2)\big[2(m_h^2-4m_t^2)(m_h^4-\hat{t}\hat{u})+\varepsilon(1+2\varepsilon)(m_h^2-\hat{u})^2(\hat{t}+\hat{u}-8m_t^2)\big]\\
&+C_0(q_3,q_3+q_4)\hat{s}(\hat{s}-4m_h^2)\big[\varepsilon(1+2\varepsilon)(\hat{t}+\hat{u}-8m_t^2)\big]\\
&+D_0(q_1,q_1+q_2,q_1+q_2+q_3)\big\{2m_t^2(8m_t^2-\hat{s}-2m_h^2)(m_h^4-\hat{t}\hat{u})\\
&\quad+4\varepsilon(1+2\varepsilon)[m_h^4m_t^2(8m_t^2-\hat{t}-\hat{u})+\hat{u}(m_t^2((\hat{t}+\hat{u})(\hat{t}+2\hat{u})-(m_h^2\hat{u}+2m_t^2\hat{t}))+\frac{\hat{s}\hat{u}}{4}(\hat{t}+\hat{u}))]\big\}\\
&+D_0(q_2,q_1+q_2,q_1+q_2+q_3)\big\{2m_t^2(8m_t^2-\hat{s}-2m_h^2)(m_h^4-\hat{t}\hat{u})\\
&\quad+4\varepsilon(1+2\varepsilon)[m_h^4m_t^2(8m_t^2-\hat{t}-\hat{u})+\hat{t}(m_t^2((\hat{t}+\hat{u})(\hat{u}+2\hat{t})-(m_h^2\hat{t}+2m_t^2\hat{u}))+\frac{\hat{s}\hat{t}}{4}(\hat{t}+\hat{u}))]\big\}\\
&+D_0(q_1,q_1+q_3,q_1+q_2+q_2)\frac{2}{\hat{s}}(m_h^4-\hat{t}\hat{u})\big\{\hat{s}m_t^2(8m_t^2-\hat{s}-2m_h^2)+(m_h^4-\hat{t}\hat{u})(m_h^2-4m_t^2)\\
&\quad-\varepsilon(1+2\varepsilon)[m_h^4(8m_t^2-\hat{t}-\hat{u})+4m_t^2(2m_h^2(\hat{t}+\hat{u})-8m_t^2\hat{s}-(\hat{t}+\hat{u})^2-2\hat{t}\hat{u})+\hat{t}\hat{u}(\hat{t}+\hat{u})]\big\}\Big\}
\end{aligned} \tag{3.22}$$

and

$$
\begin{aligned}
\mathcal{A}_2 = \frac{\lambda_{htt}^2}{4(m_h^4-\hat{t}\hat{u})}\Big\{ & \\
&+C_0(q_1,q_1{+}q_2)\big[\hat{s}(8m_t^2(\hat{t}{+}u){-}2m_h^4{-}t^2{-}u^2){+}e(1{+}2e)\hat{s}(8m_t^2{-}\hat{t}{-}u)(\hat{t}{+}u)\big] \\
&+C_0(q_1,q_1{+}q_3)\big[2(m_h^2{-}t)(m_h^4{-}\hat{t}(8m_t^2{-}t)){+}\frac{2}{s}e(1{+}2e)(m_h^2{-}t)^3(8m_t^2{-}\hat{t}{-}u)\big] \\
&+C_0(q_2,q_2{+}q_3)\big[2(m_h^2{-}u)(m_h^4{-}\hat{u}(8m_t^2{-}u)){+}\frac{2}{s}e(1{+}2e)(m_h^2{-}t)^3(8m_t^2{-}\hat{t}{-}u)\big] \\
&+C_0(q_3,q_3{+}q_4)\big[(8m_t^2{-}\hat{t}{-}u)(2m_h^4{-}t^2{-}u^2){+}e(1{+}e)(4m_h^2{-}s)\hat{s}(8m_t^2{-}\hat{t}{-}u)\big] \\
&+D_0(q_1,q_1{+}q_2,q_1{+}q_2{+}q_3)\big\{2m_t^2(8m_t^2{+}\hat{s}{-}2m_h^2)(\hat{u}\hat{t}{-}m_h^2){-}\hat{s}\hat{u}(8\hat{u}m_t^2{-}u^2{-}m_h^4) \\
&\quad{+}4\varepsilon(1{+}2\varepsilon)[m_h^4m_t^2(8m_t^2{-}\hat{t}{-}u){+}\hat{u}(m_t^2((\hat{t}{+}u)(\hat{t}{+}2u){-}4(m_h^2\hat{u}{+}2m_t^2t)){+}\frac{\hat{s}\hat{u}}{4}(\hat{t}{+}u))]\big\} \\
&+D_0(q_2,q_1{+}q_2,q_1{+}q_2{+}q_3)\big\{2m_t^2(8m_t^2{+}\hat{s}{-}2m_h^2)(\hat{u}\hat{t}{-}m_h^2){-}\hat{s}\hat{t}(8\hat{t}m_t^2{-}t^2{-}m_h^4) \\
&\quad{+}4\varepsilon(1{+}2\varepsilon)[m_h^4m_t^2(8m_t^2{-}\hat{t}{-}u){+}\hat{u}(m_t^2((\hat{t}{+}u)(\hat{u}{+}2t){-}4(m_h^2\hat{t}{+}2m_t^2u)){+}\frac{\hat{s}\hat{t}}{4}(\hat{t}{+}u))]\big\} \\
&+D_0(q_1,q_1{+}q_3,q_1{+}q_2{+}q_2)\big\{2m_t^2(8m_t^2{-}\hat{t}{-}u)(m_h^4{-}\hat{t}\hat{u}) \\
&\quad{-}\varepsilon(1{+}2\varepsilon)[m_h^4(8m_t^2{-}\hat{t}{-}u){+}4m_t^2(2m_h^2(\hat{t}{+}u){-}8m_t^2\hat{s}{-}(\hat{t}{+}u)^2{-}2\hat{t}u){+}\hat{t}\hat{u}(\hat{t}{+}u)]\big\}\Big\}\,,
\end{aligned}
\tag{3.23}
$$

which also agree with the results of [45, 46] in the limit $\varepsilon \to 0$. While eqs. (3.19), (3.22) and (3.23) contain the complete dimensional dependence of the amplitude up to $\mathcal{O}(\varepsilon^2)$ due to the tensorial reduction, the scalar one-loop integrals B_0, C_0 and D_0 themselves possess higher order terms in the ε expansion. These contributions are computed numerically.

3.1.4. Leading Order Cross Section

While the $\mathcal{O}(\varepsilon^2)$ terms of the LO amplitude are crucial for the calculation of the NLO corrections, the LO hadronic cross section σ_{LO} contributing to eq. (3.1) can be evaluated in the physical $\varepsilon \to 0$ limit. The total LO hadronic cross section follows by integrating the partonic cross section $\hat{\sigma}_{\text{LO}}$ over the gluon luminosity $d\mathcal{L}^{gg}/d\tau$,

$$
\sigma_{\text{LO}}(pp \to gg \to hh) = \int_{\tau_0}^1 \mathrm{d}\tau \frac{d\mathcal{L}^{gg}}{d\tau}\, \hat{\sigma}_{\text{LO}}(\hat{s}=\tau s)\,, \quad \text{with } \tau_0 = \frac{4m_h^2}{s} \quad \text{and} \tag{3.24}
$$

$$
\frac{d\mathcal{L}^{gg}}{d\tau} = \int_\tau^1 \frac{\mathrm{d}x}{x} f_g(x,\mu_F)\, f_g(\tau/x,\mu_F)\,, \tag{3.25}
$$

where $\sqrt{s}$ is the hadronic centre-of-mass energy, $f_g(x,\mu_F)$ denotes the parton distribution functions of the gluon in the proton and μ_F is the factorisation scale. The partonic LO cross section,

$$
\hat{\sigma}_{\text{LO}}(\hat{s}) = C_{\text{flux}} C_{\text{sym}} \int \mathrm{dPS}_2\, \overline{|\mathcal{M}_{\text{LO}}|}^2\,, \tag{3.26}
$$

can be written in terms of the form factors of eqs. (3.19), (3.22) and (3.23) as

$$
\hat{\sigma}_{\text{LO}}(\hat{s}) = \frac{\alpha_s^2(\mu_R^2)}{1024\,\pi^3\,\hat{s}^2} \int_{\hat{t}_-}^{\hat{t}_+} \mathrm{d}\hat{t}\, \left(|\mathcal{A}_\Delta{+}\mathcal{A}_1|^2{+}|\mathcal{A}_2|^2\right), \tag{3.27}
$$

with $C_{\text{sym}} = \frac{1}{2}$ being the symmetry factor due to the identical final state particles, the flux factor $C_{\text{flux}} = (2\hat{s})^{-1}$ and the renormalisation scale μ_R. The phase space integration dPS_2

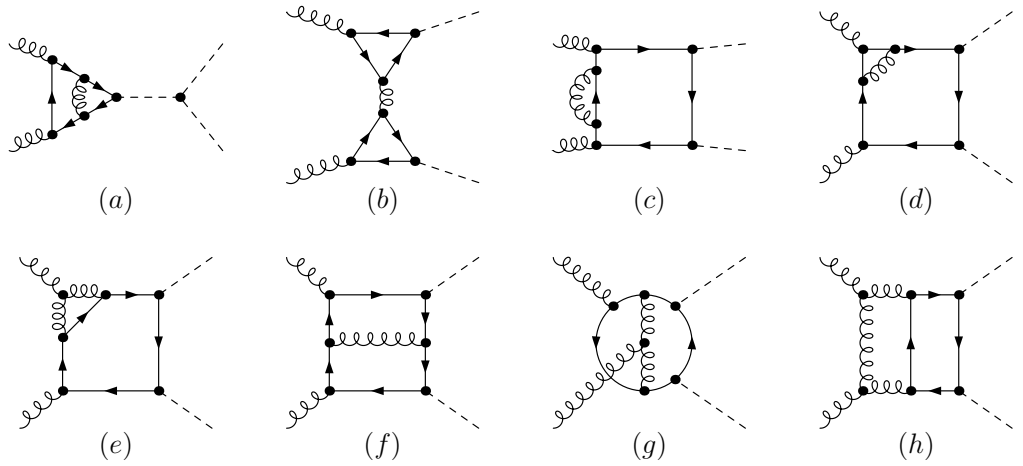

Figure 3.4: Sample diagrams contributing to the virtual QCD corrections to Higgs boson pair production with full mass dependence.

can be expressed in terms of the integration over the momentum transfer $\hat{t}$ according to

$$\hat{s} = \tau s\,, \quad \hat{t} = m_h^2 - \frac{\hat{s}(1-\beta\cos\theta)}{2}\,, \quad \hat{u} = 2m_h^2 - \hat{s} - \hat{t}\,, \quad \text{with} \quad \beta = \sqrt{1-4m_h^2/\hat{s}}\,, \tag{3.28}$$

$$\Rightarrow \mathrm{dPS}_2 = \frac{\beta}{16\pi}\mathrm{d}\cos\theta \equiv \frac{\mathrm{d}\hat{t}}{32\pi\hat{s}} \tag{3.29}$$

so that the integration region is defined by

$$\hat{t}_\pm = m_h^2 - \frac{\hat{s}(1\mp\beta)}{2}\,. \tag{3.30}$$

3.2. Virtual Corrections

The amplitude for the virtual corrections $\mathcal{M}_{\mathrm{virt}}$ involves loop corrections to the LO diagrams of fig. 3.2 with an additional gluon propagator within the loop. The complete set of two-loop diagrams obtained by `FeynArts` [97] can be organised in 8 distinct categories with sample diagrams shown in fig. 3.4.

The triangle contributions of fig. 3.4 (a) consist of 12 generic diagrams. In analogy to the following classification of the box diagrams, the triangle contributions consist explicitly of 3 self-energy corrections of the top-quark propagator, 3 abelian and 2 non-abelian vertex corrections, 2 non-planar diagrams and 2 genuine IR-divergent diagrams. They can be obtained from the already known NLO corrections to single Higgs boson production [98], since the contributions in Higgs pair production only differ by a scalar factor given by the Higgs propagator and the trilinear Higgs self-coupling. In the calculation of the virtual corrections $\Delta\sigma_{\mathrm{virt}}$ we follow a similar strategy as applied in [98], allowing the re-use of the NLO results for single Higgs production implemented in `HIGLU` [99] and providing a cross check for the routines developed for the remaining diagrams.

The amplitude of the 2 generic reducible double-triangle diagrams represented by fig. 3.4 (b) can also be obtained from single Higgs production. It is constructed from the contribution to the real corrections $\Delta\sigma_{gg}$ of [98] which involves single Higgs production with one off-shell gluon, corresponding to the real corrections of fig. 3.1 ($4a$) and ($5a$) apart from the subsequent Higgs-to-Higgs decay. The amplitude is obtained by taking off the external parton line and self-contracting the remaining expression. The explicit results for the form factors have been

Figure 3.5: Process definitions for the discussed example. Left: momentum assignment of the propagators. Right: Denominator assignment for the Feynman parametrisation of eq. (3.34).

derived in [100].

The corrections to the box diagrams are organised in 6 topologies with corresponding sample diagrams shown in fig. 3.4 $(c)-(h)$. The diagrams of topology 1 are self-energy corrections to the top quark propagator, topology 2 and 3 consist of abelian and non-abelian vertex corrections, topology 4 describes the double-box and topology 5 the non-planar diagrams, while the genuine IR divergent diagrams are collected in topology 6. The classification of all 47 generic[1] diagrams contributing to the 6 topologies is summarised in appendix B. Due to their distinct propagator structure, the topologies need to be treated individually for numerical evaluation, the treatment is however universal for diagrams of the same topology.
The calculation of these corrections is the most challenging task of the project, as there is no complete basis of master integrals for arbitrary two-loop amplitudes. Additionally, the amplitudes involve products of up to 6 fermion propagators within the loop, leading to lengthy algebraic expressions, which require proper book keeping.

3.2.1. Calculational Strategy

This section describes the calculational strategy we pursue in order to obtain numerically integrable expressions for the divergent two-loop integrals. The techniques described here were used to set up a flexible framework in the symbolic manipulation system `FORM` [101], supplemented with `Mathematica` [102] routines for the derivation of the loop mass terms and the Laurent series expansion. In the following the reduction procedure of the two-loop integrals is discussed for the example of box 13 depicted in the left diagram of fig. 3.5. Taking the direction of the external momenta as entering the loop and denoting the momenta of the two loops by k and q, respectively, the corresponding amplitude reads,

$$\mathcal{M}^{ab}_{\text{virt}} = (-1)F_c\,\epsilon_\mu(q_1)\,\epsilon_\nu(q_2)\,\mu_R^{2(4-D)}\int\frac{\mathrm{d}^D q}{(2\pi)^D}\int\frac{\mathrm{d}^D k}{(2\pi)^D}\mathcal{M}^{\mu\nu}\,,\quad\text{with}\quad F_c=-\frac{\delta_{ab}}{12} \tag{3.31}$$

$$\begin{aligned}\mathcal{M}^{\mu\nu} = \mathrm{Tr}\,\big[&\lambda^\mu_{gtt}\Delta_t(k)\lambda^\rho_{gtt}\Delta_t(k+q)\lambda^\nu_{gtt}\Delta_t(k+q+q_2)\lambda^\sigma_{gtt}\Delta_t(k+q_2)\\ &\lambda_{htt}\Delta_t(k-q_1-q_3)\lambda_{htt}\Delta_t(k-q_1)\Delta_g^{\rho\sigma}(q)\big]\end{aligned} \tag{3.32}$$

In analogy to the LO matrix element, $\mathcal{M}^{ab}_{\text{virt}}$ can be expressed in terms of Lorentz- and gauge-invariant form factors,

$$\mathcal{M}^{ab}_{\text{virt}} = \frac{\alpha_s^2}{\pi^2}\left[\mathcal{B}_1 T_1^{\mu\nu}+\mathcal{B}_2 T_2^{\mu\nu}\right]\delta_{ab}\,\epsilon_\mu(q_1)\,\epsilon_\nu(q_2)\,, \tag{3.33}$$

with the scalar form factors $\mathcal{B}_i$ obtained by contracting the amplitude with the projectors $P_i^{\mu\nu}$ defined in eq. (3.13). The form factors are tensor integrals of up to rank 6 in the loop

[1] In this context 'generic' refers to the `PaintLevel` of the program package `FeynArts`, thus the generic set includes diagrams obtained by exchange of the Higgs boson momenta, in analogy to the second and third diagram of the LO amplitude fig. 3.2.

momenta k and q, which need to be reduced to scalar integrals for numerical integration. This is achieved by the following Feynman parametrisation of the integrand,

$$\begin{aligned}\frac{1}{a_1^{\omega_1}a_2^{\omega_2}\dots a_n^{\omega_n}} &= \int \mathrm{d}\vec{x}_{n-1}\,\frac{\mathcal{N}_n\,(1-x_1-\dots-x_{n-1})^{\omega_1-1}x_1^{\omega_2-1}\dots x_{n-1}^{\omega_n-1}}{[a_1(1-x_1-\dots-x_{n-1})+a_2x_1+\dots+a_nx_{n-1}]^{\Sigma\omega_i}}\,, \quad \text{with}\\ \int \mathrm{d}\vec{x}_{n-1} &= \int_0^1 \mathrm{d}x_1 \int_0^{1-x_1}\mathrm{d}x_2\dots\int_0^{1-x_1-\dots-x_{n-2}}\mathrm{d}x_{n-1} \quad \text{and } \mathcal{N}_n = \frac{\Gamma(\omega_1+\dots+\omega_n)}{\Gamma(\omega_1)\dots\Gamma(\omega_n)}\,,\end{aligned} \tag{3.34}$$

where a_i are the denominators of the propagators assigned according to the right diagram of fig. 3.5. Subsequently, a Wick rotation and momentum integrations in D dimensional spherical coordinates can be performed,

$$\begin{aligned}\int\frac{\mathrm{d}^Dk}{(2\pi)^D}\frac{(k^2)^\alpha}{(k^2-M^2+\mathrm{i}\epsilon)^r} &= \frac{\mathcal{G}_r^\alpha}{(M^2-\mathrm{i}\epsilon)^{r-\alpha-D/2}}, \quad \alpha=0,1,\dots\,, \quad \text{with}\\ \mathcal{G}_r^\alpha &= \mathrm{i}\frac{(-1)^{r-\alpha}}{(4\pi)^{D/2}}\frac{\Gamma(r-\alpha-D/2)\Gamma(\alpha+D/2)}{\Gamma(D/2)\Gamma(r)}\,.\end{aligned} \tag{3.35}$$

The infinitesimal imaginary part $\mathrm{i}\epsilon$ of the loop mass in the above formula fixes the analytic continuation of the expression and is not to be mistaken with the dimensional regulator ε. Integrals with odd power of the loop momentum in the numerator vanish and integrals in which the loop momentum in the numerator is contracted with other momenta can be brought into the form of eq. (3.35) according to the identities,

$$\begin{aligned}\int\frac{\mathrm{d}^Dk}{(2\pi)^D}\frac{k^\mu k^\nu k^\rho k^\sigma(k^2)^n}{(k^2-M^2)^r} &= \frac{g^{\mu\nu}g^{\rho\sigma}+g^{\mu\rho}g^{\nu\sigma}+g^{\mu\sigma}g^{\nu\rho}}{D(D+2)}\int\frac{\mathrm{d}^Dk}{(2\pi)^D}\frac{(k^2)^{n+2}}{(k^2-M^2)^r}\,,\\ \int\frac{\mathrm{d}^Dk}{(2\pi)^D}\frac{k^\mu k^\nu(k^2)^n}{(k^2-M^2)^r} &= \frac{g^{\mu\nu}}{D}\int\frac{\mathrm{d}^Dk}{(2\pi)^D}\frac{(k^2)^{n+1}}{(k^2-M^2)^r}, \quad n=0,1,\dots\,.\end{aligned} \tag{3.36}$$

There are two subtleties in this procedure. Firstly, after applying the Feynman parametrisation of eq. (3.34), one has to shift the momentum to obtain an integrand corresponding to the left hand side of eq. (3.35). Thus, the loop mass term M^2 is a function of the Feynman parameters x_i and the scalar products of the remaining momenta. Secondly, the singularities of the loop momentum integrals now appear as regions in the Feynman parameter space $0\le x_i\le 1$ in which the final loop mass term M^2 becomes zero. In order to isolate these divergent regions and to additionally disentangle the individual integration limits of eq. (3.34), one has to perform non-trivial transformations in the Feynman parameter space.

In the explicit case of box 13, the first Feynman parametrisation is performed on the denominators of eq. (3.32) containing the loop momentum k, with the correspondence of the denominators a_i of eq. (3.34) to the propagators depicted in the right diagram of fig. 3.5, yielding,

$$\mathcal{B}_i = \int\frac{\mathrm{d}^Dq}{(2\pi)^D}\frac{1}{q^2}\sum_{\alpha=0}^{3}\int\mathrm{d}\vec{x}_5\int\frac{\mathrm{d}^Dk'}{(2\pi)^D}\frac{\mathcal{N}_6\,g_\alpha^{(i)}\cdot(k'^2)^\alpha}{\left[k'^2-M_1^2\right]^6}\,, \tag{3.37}$$

where k' is the shifted loop momentum required to complete the square in the denominator defined in the following and M_1^2 the corresponding loop mass. The coefficients $g_\alpha^{(i)}$ are obtained by contracting the numerator of eq. (3.32) with the projectors $P_i^{\mu\nu}$, applying the momentum shift $k\to k'$ and transforming the tensorial structure according to eq. (3.36),

$$\frac{\alpha_\mathrm{s}^2}{\pi^2}g_\alpha^{(i)}\cdot(k'^2)^\alpha = F_c\,\mu_R^{2(4-D)}P_{i,\mu\nu}\cdot\tilde{\mathcal{M}}^{\mu\nu}\,, \quad \text{with} \tag{3.38}$$

$$\mathcal{M}^{\mu\nu}|_\mathrm{num} \xrightarrow{(3.41)\ (3.36)} \tilde{\mathcal{M}}^{\mu\nu} \tag{3.39}$$

They are functions of the Feynman parameters x_i, the Yukawa coupling λ_{htt} and of the scalar products of the second loop momentum q and the external momenta q_1, q_2, q_3. In topology 2, a suitable transformation of the Feynman parameters is of the form,

$$\left.\begin{aligned} x_1 &\to (1-\hat{x}_1)(1-\hat{x}_2) \\ x_2 &\to \hat{x}_2(1-\hat{x}_1) \\ x_3 &\to \hat{x}_1(1-\hat{x}_3) \\ x_4 &\to \hat{x}_1\hat{x}_3\hat{x}_4 \\ x_5 &\to \hat{x}_1\hat{x}_3\hat{x}_5(1-\hat{x}_4) \end{aligned}\right\} \Rightarrow \int \mathrm{d}\vec{x}_5 \to \underbrace{\left[\prod_{i=1}^{5}\int_0^1 \mathrm{d}\hat{x}_i\right]}_{\equiv\int \mathrm{d}\hat{\vec{x}}_5} \hat{x}_1^3\hat{x}_3^2(1-\hat{x}_1)(1-\hat{x}_4)\,, \tag{3.40}$$

so that the limits of the integrals over the new variables $\hat{x}_i$ go from 0 to 1 and, as shown in the following, the singularity of the integrand below the top quark mass threshold is described by a single variable $\hat{x}_1$. In terms of the transformed Feynman parameters the momentum shift $k \to k'$ reads,

$$\begin{aligned} k^\mu \to k'^\mu = k^\mu + q^\mu(1-\hat{x}_1) + q_2^\mu\hat{x}_2 + d^\mu\hat{x}_1\,, \quad \text{with} \\ d^\mu = -q_1^\mu\hat{x}_3(1-\hat{x}_4)\hat{x}_5 + q_2^\mu(1+\hat{x}_3\hat{x}_4-\hat{x}_2-\hat{x}_3) + q_3^\mu\hat{x}_3\hat{x}_4\,. \end{aligned} \tag{3.41}$$

The expression for the loop mass term[2] $\hat{M}_1^2$ is not given explicitly, as it is involved and it follows unambiguously from the previous steps. However, it is expedient for the second Feynman parametrisation to normalise $\hat{M}_1^2$ according to,

$$\hat{M}_1^2 = \hat{N}_1^2(-1)\hat{x}_1(1-\hat{x}_1)\,, \tag{3.42}$$

so that the form factors eq. (3.37) after the momentum integration over k read,

$$\mathcal{B}_i = \int\frac{\mathrm{d}^D q}{(2\pi)^D}\frac{1}{q^2}\int \mathrm{d}\hat{\vec{x}}_5 \sum_{\alpha=0}^{3} \frac{\hat{x}_1^3\hat{x}_3^2(1-\hat{x}_1)(1-\hat{x}_4)}{[(-1)\hat{x}_1(1-\hat{x}_1)]^{6-\alpha-D/2}} \frac{\mathcal{N}_6\,\mathcal{G}_6^\alpha\,\hat{g}_\alpha^{(i)}}{(\hat{N}_1^2)^{6-\alpha-D/2}}\,. \tag{3.43}$$

The second loop momentum integral is solved similarly by repeating the previous procedure. First, we introduce an additional Feynman parameter $\hat{x}_6$ as,

$$\mathcal{B}_i = \int \mathrm{d}\hat{\vec{x}}_5 \sum_{\alpha=0}^{3}\int_0^1 \mathrm{d}\hat{x}_6 \int\frac{\mathrm{d}^D q}{(2\pi)^D} \frac{\hat{x}_1^3\hat{x}_3^2(1-\hat{x}_1)(1-\hat{x}_4)}{[(-1)\hat{x}_1(1-\hat{x}_1)]^{6-\alpha-D/2}} \frac{\mathcal{N}_6\,\mathcal{N}_2\,\hat{x}_6^{5-\alpha-D/2}\mathcal{G}_6^\alpha\,\hat{g}_\alpha^{(i)}}{[q^2(1-\hat{x}_6)+\hat{N}_1^2\hat{x}_6]^{7-\alpha-D/2}}\,. \tag{3.44}$$

Since $\hat{N}_1^2$ is a function of q, we again need to perform a momentum shift $q \to q'$ in order to complete the square for the denominator of eq. (3.44). With the auxiliary momentum d^μ defined in eq. (3.41), the shift reads,

$$\begin{aligned} q^\mu \to q'^\mu = q^\mu - d^\mu\hat{x}_6\,, \quad \text{and} \\ q^2(1-\hat{x}_6)+\hat{N}_1^2\hat{x}_6 \to q'^2 - \hat{M}_2^2\,. \end{aligned} \tag{3.45}$$

The numerator coefficients $g_\alpha^{(i)}$ are also functions of q' of up to power 6 due to the first momentum shift eq. (3.41). Thus, they can be organised according to eq. (3.36) as,

$$\hat{g}_\alpha^{(i)} = \sum_{\beta=0}^{3} \tilde{g}_{\alpha\beta}^{(i)}\cdot(q'^2)^\beta\,, \tag{3.46}$$

where the new coefficients $\tilde{g}_{\alpha\beta}^{(i)}$ are functions of the Feynman parameters $\hat{x}_i$ and of scalar products of the external momenta $q_i\cdot q_j$. By construction, the indices α and β keep track of

[2] In the following the circumflex above M_1^2, N_1^2 and $g_\alpha^{(i)}$ means that their functional dependence was transformed according to eq. (3.40).

the loop momentum power of the numerator. In order to express the final result in terms of the dimensionless process variables ρ_i of eq. (3.6), we rewrite $\tilde{g}^{(i)}_{\alpha\beta}$ as

$$\tilde{g}^{(i)}_{\alpha\beta} = (m_t^2)^{3-\alpha-\beta}\, \hat{g}^{(i)}_{\alpha\beta}\,. \tag{3.47}$$

Applying these transformations to eq. (3.44) allows for the integration over the loop momentum q' to be performed, yielding,

$$\mathcal{B}_i = \sum_{\alpha,\beta=0}^{3} \underbrace{\int \mathrm{d}\hat{\vec{x}}_5 \int_0^1 \mathrm{d}\hat{x}_6}_{\int \mathrm{d}\hat{\vec{x}}_6} \frac{\hat{x}_1^3 \hat{x}_3^2 (1-\hat{x}_1)(1-\hat{x}_4)}{[(-1)\hat{x}_1(1-\hat{x}_1)]^{6-\alpha-D/2}} \frac{\mathcal{N}_6\, \mathcal{N}_2\, \hat{x}_6^{5-\alpha-D/2} \mathcal{G}_6^{\alpha} \mathcal{G}^{\beta}_{7-\alpha-D/2}\, \hat{g}^{(i)}_{\alpha\beta}}{(m_t^2)^{\alpha+\beta-3}\, [\hat{M}_2^2]^{7-\alpha-\beta-D}}\,. \tag{3.48}$$

For reasons which will become clear in the following, the loop mass term $\hat{M}_2^2$ is normalised as,

$$\hat{M}_2^2 = \frac{m_t^2 \hat{x}_6}{\hat{x}_1(1-\hat{x}_1)} \hat{N}_2^2\,. \tag{3.49}$$

Inserting the expressions for $\mathcal{N}_n$ according to eq. (3.34) and $\mathcal{G}_r^{\alpha}$ of eq. (3.35) leads to the final result for the form factors $\mathcal{B}_i$ in $D = 4-2\varepsilon$ dimensions,

$$\begin{aligned} \mathcal{B}_i &= \sum_{\alpha,\beta=0}^{3} \int \mathrm{d}\hat{\vec{x}}_6\, \frac{(-1)^{\alpha+\beta} \hat{x}_3^2 (1-\hat{x}_4)}{\hat{x}_1^{\beta-2-\varepsilon}(1-\hat{x}_1)^{\beta-\varepsilon}} \frac{\Gamma(3-\alpha-\beta+2\varepsilon)}{(4\pi)^{4-2\varepsilon}(m_t^2)^{2\varepsilon}} \frac{\hat{x}_6^{\beta-\varepsilon} \hat{g}^{(i)}_{\alpha\beta}}{(\hat{N}_2^2)^{3-\alpha-\beta+2\varepsilon}} \mathcal{R}_\alpha \mathcal{R}_\beta\,, \text{ with} \\ \mathcal{R}_\kappa &\equiv \frac{\Gamma(\kappa+2-\varepsilon)}{\Gamma(2-\varepsilon)}\,. \end{aligned} \tag{3.50}$$

The normalisation in eq. (3.49) was chosen such, that the final loop mass $\hat{N}_2^2$ in eq. (3.50) is expressed in terms of the process variables ρ_i introduced in eq. (3.6) and of the form,

$$\hat{N}_2^2 = 1 - \sum_{i=1}^{4} \rho_i c_i\,, \tag{3.51}$$

with the explicit coefficients c_i of the process variables found to be,

$$\begin{aligned} c_1 &= \hat{x}_1\hat{x}_3(1-\hat{x}_4)\hat{x}_5\,\{\hat{x}_2(1-\hat{x}_1)(1-\hat{x}_6)+[1-(1-\hat{x}_1)(1-\hat{x}_6)][1-\hat{x}_3(1-\hat{x}_4)]\}\,, \\ c_2 &= \hat{x}_1\hat{x}_3^2\hat{x}_4(1-\hat{x}_4)\hat{x}_5\,[1-(1-\hat{x}_1)(1-\hat{x}_6)]\,, \\ c_3 &= \hat{x}_1\hat{x}_3\hat{x}_4\,\{1-(1-\hat{x}_1)\hat{x}_2(1-\hat{x}_6)-[1-(1-\hat{x}_1)(1-\hat{x}_6)][1-\hat{x}_3(1-\hat{x}_4)]\}\,, \\ c_4 &= \hat{x}_1\hat{x}_3\hat{x}_4\,\{1-\hat{x}_3\hat{x}_4[1-(1-\hat{x}_1)(1-\hat{x}_6)]\}\,. \end{aligned} \tag{3.52}$$

The coefficients c_i take values between $0 \leq c_i \leq 0.25$, which means that the loop mass eq. (3.51) is greater than zero in the entire integration region for values of the process variables $\rho_i < 1$.[3] The singularities of the form factors can be directly isolated from eq. (3.50), but before doing so, let us conclude this technically involved calculation with some general remarks:

- The procedure transforms the two-loop momentum integral of the amplitude into a six dimensional Feynman parameter integral. After the ε poles have been completely isolated as described in the following section, these integrals are suitable for numerical integration.

[3] This corresponds to kinematic phase space points below the top quark mass threshold.

- This general framework applies directly to all diagrams of topology 1, 2 and 4, which contain 6 fermion propagators in the loops. Topologies 3 and 5 follow similar calculational strategies with modifications in the initial Feynman parametrisation. Topology 6 will be discussed separately due to its IR divergent properties.
- The Feynman parameter transformation of eq. (3.40) is applicable for all 12 diagrams of topology 2. Different transformations have to be performed in the other topologies in order to isolate the divergences. The transformations are found by trial and error and are based on experience obtained from the parametrisation of the triangle topology diagrams.
- The form factors of each diagram are described by the numerator coefficients $\hat{g}^{(i)}_{\alpha\beta}$ and the loop mass $\hat{N}_2^2$. These are unambiguously obtained from the amplitude by applying the process specific momentum shifts eqs. (3.41) and (3.45), the normalisation conditions eqs. (3.42) and (3.49) and the Feynman parameter transformation of eq. (3.40).

3.2.2. Treatment of Singularities

Before the form factors can be numerically integrated, the singularities in the dimensional regulator ε first need to be isolated. The singularities in eq. (3.50) below the virtual top mass threshold $\rho_i < 1$ have two possible origins.
The first denominator of the integrand develops end-point singularities at $\hat{x}_1 = 0$ for $\beta = 3$ and at $\hat{x}_1 = 1$ for $\beta = 1$.[4] These singularities can be isolated by end-point subtractions. The idea behind this technique is that the function is integrable, as long as the remaining integrand converges faster to zero than the singular denominator. This can be achieved by subtracting and re-adding the series expansion of the remaining integrand around the end point as,

$$\int_0^1 \frac{f(\hat{x}_1)}{\hat{x}_1^{1-\varepsilon}} \mathrm{d}\hat{x}_1 = \int_0^1 \frac{f(\hat{x}_1)-f(0)}{\hat{x}_1^{1-\varepsilon}} \mathrm{d}\hat{x}_1 + \frac{f(0)}{\varepsilon}\,, \tag{3.53}$$

$$\int_0^1 \frac{f(\hat{x}_1)}{(1-\hat{x}_1)^{1-\varepsilon}} \mathrm{d}\hat{x}_1 = \int_0^1 \frac{f(\hat{x}_1)-f(1)}{(1-\hat{x}_1)^{1-\varepsilon}} \mathrm{d}\hat{x}_1 + \frac{f(1)}{\varepsilon}\,. \tag{3.54}$$

In addition to the end-point divergences, the form factors of eq. (3.50) contain singularities due to the gamma function of the second numerator of the integrand for $\alpha+\beta = 3$. The form factors can be normalised with respect to a global gamma function prefactor which is chosen to be,

$$C_\Gamma = \frac{\Gamma(1+\varepsilon)\Gamma(1-\varepsilon)}{\Gamma(1-2\varepsilon)}\,. \tag{3.55}$$

This is achieved by using one of the defining properties of the gamma function,

$$\Gamma(z+1) = z\Gamma(z)\,, \tag{3.56}$$

to normalise all α, β summands of eq. (3.50) to an overall prefactor of $\Gamma(1+2\varepsilon)$, which is related to the prefactor C_Γ by,

$$\Gamma(1+2\varepsilon) = C_\Gamma \left[1+3\,\zeta(2)\varepsilon^2\right] + \mathcal{O}(\varepsilon^3)\,, \tag{3.57}$$

[4] At first glance one would expect singularities at $\hat{x}_1 = 1$ also for higher values of β. This is not the case, as the original amplitude is a tensor integral of rank 2 with respect to the loop momentum q. All higher rank contributions, which lead to the terms with $\beta > 1$, are due to the momentum shift eq. (3.41) and are thus accompanied by additional factors of $(1-\hat{x}_1)^\beta$ in the numerator coefficients $\hat{g}^{(i)}_{\alpha\beta}$.

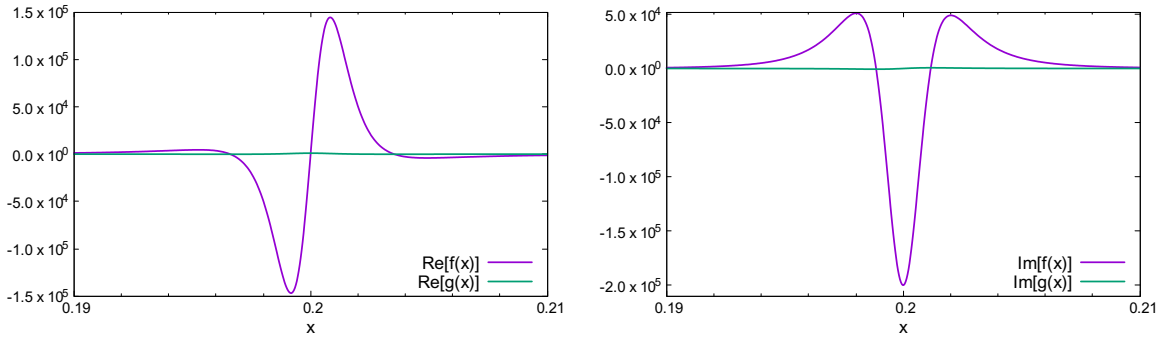

Figure 3.6: Effects of the integration by parts technique on the real (left) and imaginary (right) part of the simplified example eq. (3.60) for $\rho = 5/(1-10^{-2}\mathrm{i})$. The variation in the vicinity of the threshold reduces by several orders of magnitude.

where $\zeta(x)$ is the Riemann zeta function. This choice of normalisation will become particularly useful in the context of the cross section of the virtual corrections. At this stage, it underlines the previous statement that for $\alpha+\beta = 3$ the gamma function leads to a singularity in the form factors, since according to eq. (3.56),

$$\Gamma(2\varepsilon) = \frac{\Gamma(1+2\varepsilon)}{2\varepsilon}\,. \tag{3.58}$$

As the two conditions for the occurrence of the singularities can be fulfilled simultaneously, the form factors described here formally contain ε^{-2} poles, too. These are a remainder of the tensor reduction procedure. As such they are not cancelled by IR poles of the real corrections, but instead cancel exactly when all diagrams of the vertex corrections are summed up. After the singular behaviour has been extracted from the form factors, the expression can be expanded in a Laurent series around $\varepsilon = 0$ and the coefficients of the expansion can be integrated numerically over the six-dimensional Feynman parameter space, yielding numerically stable results for momentum space points below the top quark mass threshold.

For kinematic configurations above the virtual thresholds $\rho_i > 1$ the loop mass term eq. (3.51) leads to additional singularities within the integration region. In these configurations, the virtual top quarks can become on-shell so that the integrals develop imaginary parts. The instabilities due to threshold singularities can be treated by introducing a small imaginary part for the quark mass in a way that the constraints of micro-causality are fulfilled. This corresponds to a redefinition of the process variables eq. (3.6) to,

$$\rho_i \to \frac{\rho_i}{1-\mathrm{i}\delta}, \quad \text{with} \quad \delta \in \mathbb{R}_+\,. \tag{3.59}$$

For non-zero values of the threshold regulator δ the real and imaginary parts of the virtual integrals are well-defined and the stability of the numerical integration increases with higher values of δ. On the other hand, the final result of the numerical integration is independent of δ for sufficiently small values of δ. While the redefinition of eq. (3.59) successfully removes the threshold singularities in the real and imaginary parts of the integrands, the resulting expressions require high statistics for the Monte Carlo integration to obtain stable results. The convergence of the numerical integration can be improved by reducing the exponent of the loop mass term in the denominator through integration by parts (IBP) techniques. For the sake of argument let us consider a simple function $f(x)$ similar to the integrands of eq. (3.50) and its partially integrated form $g(x)$,

$$f(x) = \frac{x}{(1-\rho x)^3} \xrightarrow{\text{IBP}} g(x) = \frac{1}{2\rho(1-\rho)^2} - \frac{1}{2\rho(1-\rho x)^2}\,. \tag{3.60}$$

	Re	Δ_{int}	Im	Δ_{int}
$f(x)$	$0.31243(14)\cdot10^{-1}$	$\pm0.66\cdot10^{-7}$	$-0.781(18)\cdot10^{-3}$	$\pm0.69\cdot10^{-7}$
$g(x)$	$0.3124316(14)\cdot10^{-1}$	$\pm0.57\cdot10^{-9}$	$-0.78122(08)\cdot10^{-3}$	$\pm0.46\cdot10^{-9}$

Table 3.1: Numerical results of the `vegas` integration and the integration error Δ_{int} of eq. (3.60) with 10^7 sampling points.

For $\rho = 5$ the function $f(x)$ possesses a singularity at $x = 0.2$. Shifting the function according to eq. (3.59) with $\delta = 10^{-2}$ leads to non-divergent expressions for the real and imaginary part of $f(x)$ with rapid oscillations in the vicinity of the original pole as shown in fig. 3.6. The variation of the partially integrated form $g(x)$ is in comparison minuscule. This effect is also confirmed in the explicit numerical integration. For a `vegas` [103] integration setup $N_1 = 10$ iterations in for the grid determination and $N_2 = 5$ iterations for the evaluation of the integral with $N = 10^7$ sampling points in each iteration, the numerical results for the integration of $f(x)$ and $g(x)$ listed in table 3.1 agree within numerical uncertainties. While the stability of the integration of $f(x)$ suffers from the large numerical cancellations near the threshold, the error Δ_{int} of the integration of $g(x)$ is reduced by two orders of magnitude.
The effects illustrated by this example also occur in the actual form factors, however the calculations are much more involved. The loop mass terms are often quadratic polynomials in the Feynman parameter with respect to which the integration by parts is performed. Furthermore, the coefficients of these polynomials are functions of the process variables and the remaining Feynman parameters, which means that the partially integrated form can lead to additional thresholds. For these reasons the final expressions for the form factors above the threshold only yield stable numerical results for high `vegas` statistics, which poses the computational bottle neck of the entire calculation. Explicitly, the integration routine needs to be called with $N = 10^9$ sampling points and the threshold regulator set to $\delta = 10^{-2}$ in order to reach an integration error of $\Delta_{\text{int}} \leq 1\%$.

3.2.3. Infrared Divergent Diagrams

While the previously described techniques are sufficient to obtain numerically integrable expressions for all diagrams of topologies $1-5$, additional complications arise in topology 6. In order to elaborate this, let us consider box 45 of appendix B depicted in fig. 3.7. The reduction of the loop integrals according to the procedure of section 3.2.1 is performed by parametrising the fermionic propagators in the first step as shown in fig. 3.7 right. The resulting loop mass term N_1^2 is subsequently parametrised with the gluon propagators as,

$$\int_0^1 \mathrm{d}x_4 \int_0^{1-x_4} \mathrm{d}x_5 \int_0^{1-x_4-x_5} \mathrm{d}x_6 \, \frac{x_4^{3-\alpha-N/2}}{[q^2(1-x_4-x_5-x_6)+N_1^2 x_4+(q+q_1)^2 x_5+(q-q_2)^2 x_6]^{7-\alpha-N/2}} \,. \tag{3.61}$$

Figure 3.7: Process definitions for a sample IR divergent diagram. Left: momentum assignment of the propagators. Right: Denominator assignment for the Feynman parametrisation of eq. (3.34).

Together with the Feynman parameter transformations,

$$\begin{aligned} &x_1 \to (1-\hat{x}_1)\,, \qquad x_2 \to \hat{x}_1(1-\hat{x}_2)\,, \qquad x_3 \to \hat{x}_1\hat{x}_2\hat{x}_3\,, \\ &x_4 \to \hat{x}_4\hat{x}_5\,, \qquad x_5 \to (1-\hat{x}_5)\,, \qquad x_6 \to (1-\hat{x}_4)\hat{x}_5\hat{x}_6 \end{aligned} \tag{3.62}$$

and the momentum shifts,

$$k^\mu \to k'^\mu = k^\mu - q^\mu(1-\hat{x}_1) + q_1^\mu \hat{x}_1\hat{x}_2 - q_2^\mu \hat{x}_1(1-\hat{x}_2) + q_3^\mu \hat{x}_1\hat{x}_2\hat{x}_3\,, \tag{3.63}$$

$$q^\mu \to q'^\mu = q^\mu - q_1^\mu[1-\hat{x}_5(1-\hat{x}_2\hat{x}_4)] + q_2^\mu \hat{x}_5[\hat{x}_6+\hat{x}_4(1-\hat{x}_2-\hat{x}_6)] - q_3^\mu \hat{x}_2\hat{x}_3\hat{x}_4\hat{x}_5\,, \tag{3.64}$$

this leads to form factors of similar structure as in topology 2. In order to keep the notation as simple as possible, we restrain the explicit form factors to the terms of relevance for this discussion and collect all additional factors in a prefactor $G_\eta^{(i)}$,

$$\mathcal{B}_i = \int \mathrm{d}\hat{\vec{x}}_6\, G_\eta^{(i)}\, \frac{\hat{x}_1^{1+\varepsilon}(1-\hat{x}_1)^{1+\varepsilon}\, \hat{x}_4^{1+\eta+\varepsilon}\hat{x}_5^{-\varepsilon}}{(\hat{N}_2^2)^{3+2\varepsilon}}\,, \quad \text{with } \eta \in \mathbb{N}_0\,. \tag{3.65}$$

The index η keeps track of the power of $\hat{x}_4$ in the numerator, which will be required in the following. The corresponding prefactors $G_\eta^{(i)}$ are polynomials of the Feynman parameters and process variables and also involve gamma functions from the reduction procedure, which means that they lead to UV divergences of up to $\mathcal{O}(1/\varepsilon^2)$. For this reason, the IR structure of the amplitude has to be determined up to $\mathcal{O}(\varepsilon^2)$ to consistently include all finite and divergent contributions of the matrix element. In contrast to topologies 1−5, the loop mass term $\hat{N}_2^2$ cannot be completely cast into the form of eq. (3.51), but instead reads

$$\hat{N}_2^2 = \hat{x}_4 - \sum_{i=1}^{4} \rho_i c_i\,, \quad \text{with} \tag{3.66}$$

$$\begin{aligned} c_1 &= \hat{x}_1\{\hat{x}_1\hat{x}_2(1-\hat{x}_2)\hat{x}_4 + (1-\hat{x}_1)[1-\hat{x}_5(1-\hat{x}_2\hat{x}_4)][(1-\hat{x}_4)\hat{x}_6 + (1-\hat{x}_2)\hat{x}_4]\}\,, \\ c_2 &= \hat{x}_1\hat{x}_2\hat{x}_3\hat{x}_4\{1-\hat{x}_1\hat{x}_2 - (1-\hat{x}_1)[1-\hat{x}_5(1-\hat{x}_2\hat{x}_4)]\}\,, \\ c_3 &= \hat{x}_1\hat{x}_2\hat{x}_3\hat{x}_4\{\hat{x}_1(1-\hat{x}_2) + (1-\hat{x}_1)\hat{x}_5[(1-\hat{x}_4)\hat{x}_6 + (1-\hat{x}_2)\hat{x}_4]\}\,, \\ c_4 &= \hat{x}_1\hat{x}_2\hat{x}_3\hat{x}_4[1-\hat{x}_1\hat{x}_2\hat{x}_3 - (1-\hat{x}_1)\hat{x}_2\hat{x}_3\hat{x}_4\hat{x}_5]\,. \end{aligned} \tag{3.67}$$

The mathematical structure of eq. (3.66) is a consequence of the IR divergence of the diagram due to the virtual gluon exchange between the initial state gluons. The IR poles have to be isolated before the form factors can be treated according to section 3.2.2. This is achieved by analytic integration with respect to the Feynman parameter $\hat{x}_4$, in terms of which the loop mass term eq. (3.66) is a second degree polynomial,

$$\hat{N}_2^2 = \omega_2\hat{x}_4^2 + \omega_1\hat{x}_4 + \omega_0\,, \quad \text{with} \tag{3.68}$$

$$\omega_0 = -\rho_1\hat{x}_1(1-\hat{x}_1)(1-\hat{x}_5)\hat{x}_6\,, \tag{3.69}$$

$$\begin{aligned} \omega_1 = 1 &- \rho_1\hat{x}_1\{\hat{x}_1\hat{x}_2(1-\hat{x}_2) + (1-\hat{x}_1)[(1-\hat{x}_5)(1-\hat{x}_2-\hat{x}_6) + \hat{x}_2\hat{x}_5\hat{x}_6]\} \\ &- \rho_2\hat{x}_1\hat{x}_2\hat{x}_3[1-\hat{x}_1\hat{x}_2 - (1-\hat{x}_1)(1-\hat{x}_5)] - \rho_3\hat{x}_1\hat{x}_2\hat{x}_3(\hat{x}_1(1-\hat{x}_2) + (1-\hat{x}_1)\hat{x}_5\hat{x}_6) \\ &- \rho_4\hat{x}_1\hat{x}_2\hat{x}_3(1-\hat{x}_1\hat{x}_2\hat{x}_3)\,, \end{aligned} \tag{3.70}$$

$$\begin{aligned} \omega_2 = &-\rho_1\hat{x}_1(1-\hat{x}_1)\hat{x}_2\hat{x}_5(1-\hat{x}_2-\hat{x}_6) + \rho_2\hat{x}_1(1-\hat{x}_1)\hat{x}_2^2\hat{x}_3\hat{x}_5 \\ &- \rho_3\hat{x}_1(1-\hat{x}_1)\hat{x}_2\hat{x}_3\hat{x}_5(1-\hat{x}_2-\hat{x}_6) + \rho_4\hat{x}_1(1-\hat{x}_1)\hat{x}_2^2\hat{x}_3^2\hat{x}_5\,. \end{aligned} \tag{3.71}$$

In eq. (3.65) one can see that the divergences arise solely in the roots of $\hat{N}_2^2$ and eq. (3.68) implies that this corresponds to the simultaneous limit of $\omega_0 \to 0$ and $\hat{x}_4 \to 0$. Thus, by

subtracting this limit as

$$\begin{aligned}
\mathcal{B}_i &= \mathcal{I}_1+\mathcal{I}_2\,, \quad \text{with} \\
\mathcal{I}_1 &= \int \mathrm{d}\hat{\vec{x}}_6\, \frac{\hat{x}_1^{1+\varepsilon}(1-\hat{x}_1)^{1+\varepsilon}\,\hat{x}_4^{1+\eta+\varepsilon}}{\hat{x}_5^{\varepsilon}} \left[\frac{G_\eta^{(i)}}{(\hat{N}_2^2)^{3+2\varepsilon}} - \frac{G_\eta^{(i)}|_{\hat{x}_4=0}}{[\omega_0+\omega_1\hat{x}_4]^{3+2\varepsilon}}\right] \\
\mathcal{I}_2 &= \int \mathrm{d}\hat{\vec{x}}_6\, \frac{\hat{x}_1^{1+\varepsilon}(1-\hat{x}_1)^{1+\varepsilon}\,G_\eta^{(i)}|_{\hat{x}_4=0}}{\hat{x}_5^{\varepsilon}\,\omega_0^{3+2\varepsilon}} \frac{\hat{x}_4^{1+\eta+\epsilon}}{[1+\frac{\omega_1}{\omega_0}\hat{x}_4]^{3+2\varepsilon}}\,,
\end{aligned} \tag{3.72}$$

the integral $\mathcal{I}_1$ is by construction finite and $\mathcal{I}_2$ can be expressed in terms of hypergeometric functions,

$$F(a,b;c;z) = \frac{\Gamma(c)}{\Gamma(b)\Gamma(c-b)} \int_0^1 \mathrm{d}t\, t^{b-1}(1-t)^{c-b-1}(1-zt)^{-a}\,, \quad \text{as} \tag{3.73}$$

$$\mathcal{I}_2 = \frac{\Gamma(2+\eta+\varepsilon)}{\Gamma(3+\eta+\varepsilon)} \int \mathrm{d}\hat{\vec{x}}_6|_{\hat{x}_4}\, \frac{\hat{x}_1^{1+\varepsilon}(1-\hat{x}_1)^{1+\varepsilon}\,G_\eta^{(i)}|_{\hat{x}_4=0}}{\hat{x}_5^{\varepsilon}\,\omega_0^{3+2\varepsilon}} F(3+2\varepsilon, 2+\eta+\varepsilon; 3+\eta+\varepsilon; -\frac{\omega_1}{\omega_0})\,. \tag{3.74}$$

The notation $\mathrm{d}\hat{\vec{x}}_6|_{\hat{x}_4}$ is an abbreviation for the five dimensional differential in which $\mathrm{d}\hat{x}_4$ is omitted. The divergences of $\mathcal{I}_2$ can now be isolated by making use of the properties of hypergeometric functions [104],

$$F(a,0;c;z) = 1\,, \tag{3.75}$$

$$\begin{aligned}
F(a,b;c;z) = {}& \frac{\Gamma(c)\Gamma(b-a)}{\Gamma(b)\Gamma(c-a)}(-z)^{-a}F(a,1-c+a;1-b+a;z^{-1}) \\
&+ \frac{\Gamma(c)\Gamma(a-b)}{\Gamma(a)\Gamma(c-b)}(-z)^{-b}F(b,1-c+b;1-a+b;z^{-1})\,,
\end{aligned} \tag{3.76}$$

leading to the form of $\mathcal{I}_2$ in which singularities only occur for $\eta = 0$,

$$\begin{aligned}
\mathcal{I}_2 &= \frac{\Gamma(\eta-1-\varepsilon)}{\Gamma(\eta+1-\varepsilon)}\,\mathcal{I}_3 + \frac{\Gamma(2+\eta+\varepsilon)\Gamma(1+\varepsilon-\eta)}{\Gamma(3+2\varepsilon)}\,\mathcal{I}_4\,, \quad \text{with} \\
\mathcal{I}_3 &= \int \mathrm{d}\hat{\vec{x}}_6|_{\hat{x}_4}\, \hat{x}_1^{1+\varepsilon}(1-\hat{x}_1)^{1+\varepsilon}\,\hat{x}_5^{-\varepsilon} G_\eta^{(i)}|_{\hat{x}_4=0} \frac{F(3+2\varepsilon, 1+\varepsilon-\eta; 2+\varepsilon-\eta; -\frac{\omega_0}{\omega_1})}{\omega_1^{3+2\varepsilon}} \quad \text{and} \\
\mathcal{I}_4 &= \int \mathrm{d}\hat{\vec{x}}_6|_{\hat{x}_4}\, \hat{x}_1^{1+\varepsilon}(1-\hat{x}_1)^{1+\varepsilon}\,\hat{x}_5^{-\varepsilon}\, G_\eta^{(i)}|_{\hat{x}_4=0}\, \omega_0^{\eta-1-\varepsilon}\, \omega_1^{-\eta-2-\varepsilon}\,.
\end{aligned} \tag{3.77}$$

The expressions $\mathcal{I}_3$ and $\mathcal{I}_4$ have a well-defined pole structure and can be expanded in a Laurent series around $\varepsilon = 0$. The first integral $\mathcal{I}_3$ is finite and yields explicitly,

$$\begin{aligned}
\frac{\Gamma(-1-\varepsilon)}{\Gamma(1-\varepsilon)}\,\mathcal{I}_3 &= \int \mathrm{d}\hat{\vec{x}}_6 \frac{\hat{x}_1(1-\hat{x}_1)G_0^{(i)}|_{\hat{x}_4=0}}{(\omega_1+\omega_0\hat{x}_4)^3} \left[1+\varepsilon\log\Omega+\frac{\varepsilon^2}{2}\log^2\Omega\right]\,, \quad \text{with} \\
\Omega &= \frac{\hat{x}_1(1-\hat{x}_1)\hat{x}_4}{\hat{x}_5(\omega_1+\omega_0\hat{x}_4)^2}\,,
\end{aligned} \tag{3.78}$$

while $\mathcal{I}_4$ contains divergences due to the end points of ω_0 according to eq. (3.69),

$$\frac{\Gamma(2+\varepsilon)\Gamma(1+\varepsilon)}{\Gamma(3+2\varepsilon)}\,\mathcal{I}_4 = \int \mathrm{d}\hat{\vec{x}}_6|_{\hat{x}_4}\, \frac{(-\rho_1)^{-1-\varepsilon}\hat{x}_5^{-\varepsilon}}{(1-\hat{x}_5)^{1+\varepsilon}\hat{x}_6^{1+\varepsilon}}\,\tilde{G}_0^{(i)}\,, \quad \text{with} \quad \tilde{G}_0^{(i)} = \frac{G_0^{(i)}|_{\hat{x}_4=0}}{\omega_1^{2+\varepsilon}}. \tag{3.79}$$

The end point subtraction for $\mathcal{I}_4$ has to be performed simultaneously for two parameters according to

$$\begin{aligned}\int_0^1 \frac{f(x,y)}{x^{1+\varepsilon}(1-y)^{1+\varepsilon}}\,\mathrm{d}x\mathrm{d}y = \int_0^1 \frac{f(x,y)-f(0,y)-f(x,1)+f(0,1)}{x^{1+\varepsilon}(1-y)^{1+\varepsilon}}\,\mathrm{d}x\mathrm{d}y+\frac{f(0,1)}{\varepsilon^2}\\ -\frac{1}{\varepsilon}\left[\int_0^1 \frac{f(0,y)-f(0,1)}{(1-y)^{1+\varepsilon}}\,\mathrm{d}y+\int_0^1 \frac{f(x,1)-f(0,1)}{x^{1+\varepsilon}}\,\mathrm{d}x\right].\end{aligned} \tag{3.80}$$

Once the end points of $\hat{x}_5$ and $\hat{x}_6$ in eq. (3.79) are subtracted, the IR singularities are fully isolated as ε^{-1} and ε^{-2} poles and and the integral $\mathcal{I}_4$ can also be expanded in a Laurent series around $\varepsilon = 0$. Together with the Laurent expansion of the remaining matrix element term $G_\eta^{(i)}$, which also contains ε^{-1} and ε^{-2} poles of similar structure as the example of box 13 discussed in section 3.2.2, this calculation leads to expressions for the matrix element with fully regulated IR and UV divergences suitable for numerical integration. The form factors also contain ε^{-3} poles which are a remainder of the tensor reduction and cancel exactly when all diagrams of topology 6 are summed up.

3.2.4. Finite Virtual Corrections

The previously presented techniques are sufficient to isolate the UV and IR poles and to avoid instabilities due to threshold singularities in the form factors. These involved calculations yield well-defined expressions for the full matrix element of the virtual two-loop diagrams $\mathcal{M}_{\text{virt}}$. In order to obtain the finite virtual NLO corrections $\Delta\sigma_{\text{virt}}$, the UV and IR poles of the form factors now need to be cancelled. For the UV divergences this is achieved through renormalisation of the physical parameters involved in the LO process, which are the strong coupling constant α_s and the top quark mass m_t. In analogy to the LO and virtual matrix elements, the counterterm matrix element $\mathcal{M}^{ab}_{\text{CT}}$ can be written in terms of form factors,

$$\begin{aligned}\mathcal{M}^{ab}_{\text{CT}} &= \delta m_t \frac{\partial \mathcal{M}^{ab}_{\text{LO}}}{\partial m_t}+\delta\alpha_{\text{s}}\frac{\partial \mathcal{M}^{ab}_{\text{LO}}}{\partial \alpha_{\text{s}}}\\ \mathcal{M}^{ab}_{\text{CT}} &= \frac{\alpha_{\text{s}}^2}{\pi^2}\left[(\mathcal{A}^{\text{CT}}_\Delta+\mathcal{A}^{\text{CT}}_1)T_1^{\mu\nu}+\mathcal{A}^{\text{CT}}_2 T_2^{\mu\nu}\right]\delta_{ab}\,\epsilon^a_\mu(q_1)\,\epsilon^b_\nu(q_2)\,.\end{aligned} \tag{3.81}$$

The top quark mass counterterm δm_t previously defined in the on-shell scheme eq. (2.28) reads explicitly,

$$\delta m_t = -\Gamma(1+\varepsilon)\left(\frac{4\pi\mu_R^2}{m_t^2}\right)^{\varepsilon} m_t\left[\frac{1}{\varepsilon}+\frac{4}{3}\right]\frac{\alpha_s}{\pi}\,. \tag{3.82}$$

and the definition of the counterterm for the strong coupling δg_s in the $\overline{\text{MS}}$ scheme was obtained in eq. (2.24)

$$\delta\alpha_{\text{s}}^{(5),\overline{\text{MS}}} = \frac{\alpha_{\text{s}}^2}{4\pi}\left[\left(11-\frac{2}{3}N_F-\frac{2}{3}\right)\left(-\Delta+\log\frac{\mu_R^2}{\mu^2}\right)-\frac{2}{3}\log\frac{m_t^2}{\mu_R^2}\right]. \tag{3.83}$$

with the number of active quark flavours N_F set to $N_F = 5$, and the top quark decoupled from the running of α_{s}. After the UV poles have been cancelled, the renormalised form factors $\tilde{\mathcal{B}}_n$ given by the sum of the form factor contributions represented in fig. 3.4 and the counterterm form factors,

$$\tilde{\mathcal{B}}_n = \mathcal{A}^{\text{CT}}_n+\sum_{\text{diags}}\mathcal{B}_n \tag{3.84}$$

still contain IR divergences. These are cancelled on the cross section level by the corresponding IR poles of the real corrections in the context of the Kinoshita-Lee-Nauenberg theorem [58,59].

Numerical NLO QCD calculations often employ subtraction techniques to obtain separately finite expressions for the virtual and real corrections. In this calculation, a suitable subtraction mechanism is provided by the results in the heavy quark mass limit (HQL) of [15], as due to the QCD factorisation the relative IR divergent structure of the HQL matrix elements and of the matrix elements with full quark mass dependence is equal,

$$\left.\frac{\tilde{\mathcal{B}}_n}{\mathcal{A}_n}\right|_{\text{div}} = \left.\frac{\tilde{\mathcal{B}}_n^{\text{HQL}}}{\mathcal{A}_n^{\text{HQL}}}\right|_{\text{div}} \Rightarrow \mathcal{C}_n := \frac{\tilde{\mathcal{B}}_n}{\mathcal{A}_n} - \frac{\tilde{\mathcal{B}}_n^{\text{HQL}}}{\mathcal{A}_n^{\text{HQL}}} \sim \mathcal{O}(\varepsilon^0)\,. \tag{3.85}$$

In terms of the relative form factors $\mathcal{C}_n$ of eq. (3.85) and the LO form factors, eqs. (3.19), (3.22) and (3.23), the differential virtual corrections $d\sigma_{\text{virt}}$ can thus be organised as,

$$d\sigma_{\text{virt}} = d\sigma_{\text{virt}}^{\text{fin}} + d\sigma_{\text{HQL}}\,, \quad \text{with} \tag{3.86}$$

$$d\sigma_{\text{virt}}^{\text{fin}} = \frac{\alpha_s^3(\mu_R^2)}{16\pi^3\hat{s}}\text{Re}\left[|\mathcal{A}_\Delta|^2\,\mathcal{C}_\Delta + |\mathcal{A}_1|^2\,\mathcal{C}_1 + |\mathcal{A}_2|^2\,\mathcal{C}_2 + (\mathcal{A}_\Delta^*\mathcal{A}_1)(\mathcal{C}_\Delta+\mathcal{C}_1)\right] \quad \text{and} \tag{3.87}$$

$$\begin{aligned} d\sigma_{\text{HQL}} = {} & \frac{\alpha_s^3(\mu_R^2)}{16\pi^3\hat{s}}\text{Re}\left[|\mathcal{A}_\Delta|^2\,\frac{\tilde{\mathcal{B}}_\Delta^{\text{HQL}}}{\mathcal{A}_\Delta^{\text{HQL}}} + |\mathcal{A}_1|^2\,\frac{\tilde{\mathcal{B}}_1^{\text{HQL}}}{\mathcal{A}_1^{\text{HQL}}} + |\mathcal{A}_2|^2\,\frac{\tilde{\mathcal{B}}_2^{\text{HQL}}}{\mathcal{A}_2^{\text{HQL}}} + (\mathcal{A}_\Delta^*\mathcal{A}_1)\Big(\frac{\tilde{\mathcal{B}}_\Delta^{\text{HQL}}}{\mathcal{A}_\Delta^{\text{HQL}}} + \frac{\tilde{\mathcal{B}}_1^{\text{HQL}}}{\mathcal{A}_1^{\text{HQL}}}\Big)\right] \\ & - \frac{2\varepsilon\,\alpha_s^3(\mu_R^2)}{16\pi^3\hat{s}}\text{Re}\left[(\mathcal{A}_\Delta^*\mathcal{A}_2)\Big(\frac{\tilde{\mathcal{B}}_\Delta^{\text{HQL}}}{\mathcal{A}_\Delta^{\text{HQL}}} + \frac{\tilde{\mathcal{B}}_2^{\text{HQL}}}{\mathcal{A}_2^{\text{HQL}}}\Big) + (\mathcal{A}_1^*\mathcal{A}_2)\Big(\frac{\tilde{\mathcal{B}}_1^{\text{HQL}}}{\mathcal{A}_1^{\text{HQL}}} + \frac{\tilde{\mathcal{B}}_2^{\text{HQL}}}{\mathcal{A}_2^{\text{HQL}}}\Big)\right]. \end{aligned} \tag{3.88}$$

The divergent parts of $d\sigma_{\text{HQL}}$ cancel exactly against the corresponding terms in the real corrections after phase space integration. However, by construction in eq. (3.85), the auxiliary cross section also involves IR finite terms which correspond to the virtual corrections in the HQL. By this convenient choice, the virtual two-loop corrections $\Delta\sigma_{\text{virt}}$ of eq. (3.1) can be expressed as a direct sum of the HQL corrections C_{HQL} given in [15] and of the corrections exclusively due to the finite mass effects of the two-loop diagrams C_{MASS},

$$\begin{aligned} \Delta\sigma_{\text{virt}} &= \frac{\alpha_s(\mu_R^2)}{\pi}\int_{\tau_0}^1 \text{d}\tau\,\frac{d\mathcal{L}^{gg}}{d\tau}\,\hat{\sigma}_{\text{LO}}(\hat{s}=\tau s)\,[C_{\text{MASS}}+C_{\text{HQL}}]\,, \quad \text{with} \\ C_{\text{MASS}} &= 2\text{Re}\frac{\int_{\hat{t}_-}^{\hat{t}_+}\text{d}\hat{t}\left[|\mathcal{A}_\Delta|^2\,\mathcal{C}_\Delta + |\mathcal{A}_1|^2\,\mathcal{C}_1 + |\mathcal{A}_2|^2\,\mathcal{C}_2 + (\mathcal{A}_\Delta^*\mathcal{A}_1)(\mathcal{C}_\Delta+\mathcal{C}_1)\right]}{\int_{\hat{t}_-}^{\hat{t}_+}\text{d}\hat{t}\,[|\mathcal{A}_\Delta+\mathcal{A}_1|^2+|\mathcal{A}_2|^2]}\,. \end{aligned} \tag{3.89}$$

3.3. Real Corrections

The final missing components of the NLO calculation are the contributions due to an unresolved real emission. These corrections consist of one-loop diagrams with an additional massless parton in the final state, meaning that the amplitudes involve three-, four- and five-point one-loop tensor integrals formally of up to rank four, as can be inferred from fig. 3.1 $(3a)-(6a)$ and $(3b)-(6b)$. The calculation of these corrections including finite top quark mass effects was performed in the `MadLoop` framework [105] and used in the analysis of [81]. As the main topic of this thesis was the calculation of the virtual two-loop corrections, the explicit expressions for the real corrections still need to be implemented. However, at this stage we can already discuss the general structure of the corrections, which follows from the HQL result of [15]. Upon integration of the spin and color averaged squared matrix elements over the D dimensional three-particle phase space,

$$\text{dPS}_3 = \mu_R^{4-D}\frac{d^{D-1}q_3}{(2\pi)^{D-1}2q_3^0}\frac{d^{D-1}q_4}{(2\pi)^{D-1}2q_4^0}\frac{d^{D-1}q_5}{(2\pi)^{D-1}2q_5^0}(2\pi)^D\delta_D(q_3+q_4+q_5-q_1-q_2)\,, \tag{3.90}$$

the IR divergences cancel exactly against the IR divergent subtraction term of the virtual corrections obtained from the phase space integration of eq. (3.88). The partonic real corrections can be expressed as,

$$\hat{\sigma}_{ij} = \hat{\sigma}_{\mathrm{LO}} \frac{\alpha_{\mathrm{s}}(\mu_R^2)}{\pi} D_{ij}(z)\theta(1-z)\,, \tag{3.91}$$

where the real correction coefficients D_{ij} of the gluon-gluon, quark-gluon and quark-antiquark initial states read respectively,

$$\begin{aligned} D_{gg}(z) &= d_{gg}(z) - \frac{z}{\varepsilon}\frac{\Gamma(1-\varepsilon)}{\Gamma(1-2\varepsilon)}\left(\frac{4\pi\mu_R^2}{\mu_F^2}\right)^{\varepsilon} P_{gg}(z) + 6[1+z^4+(1-z)^4]\left[\frac{\log(1-z)}{1-z}\right]_+\,, \\ D_{gq}(z) &= d_{gq}(z) - \frac{z}{2\varepsilon}\frac{\Gamma(1-\varepsilon)}{\Gamma(1-2\varepsilon)}\left(\frac{4\pi\mu_R^2}{\mu_F^2}\right)^{\varepsilon} P_{gq}(z)\,, \\ D_{q\bar{q}}(z) &= d_{q\bar{q}}(z)\,, \end{aligned} \tag{3.92}$$

with the plus-distribution,

$$[f(x)]_+ = f(x) - \delta(1-x)\int_0^1 \mathrm{d}x\, f(x)\,. \tag{3.93}$$

The expressions $d_{ij}(z)$ are the still to be calculated finite contributions of the real corrections, which are known in the HQL,

$$d_{gg}(z) \xrightarrow{\text{HQL}} -\frac{11}{2}(1-z)\,, \quad d_{gq}(z) \xrightarrow{\text{HQL}} \frac{2}{3}z^2-(1-z)^2\,, \quad d_{q\bar{q}}(z) \xrightarrow{\text{HQL}} \frac{32}{27}(1-z)^3\,, \tag{3.94}$$

and the coefficients of the regularised Altarelli-Parisi splitting functions $P_{ij}(z)$ [106],

$$P_{gg}(z) = 6\left\{\left[\frac{1}{1-z}\right]_+ + \frac{1}{z} - 2 + z(1-z)\right\} + \delta(1-z)\frac{33-2N_F}{6}\,, \tag{3.95}$$

$$P_{gq}(z) = \frac{4}{3}\frac{1+(1-z)^2}{z}\,, \tag{3.96}$$

contain residual collinear divergences which are cancelled by replacing the bare gluon densities $f_g^B(x)$ by the renormalised gluon densities $f_g^R(x)$. In the $\overline{\mathrm{MS}}$ factorisation scheme, up to $\mathcal{O}(\alpha_{\mathrm{s}})$ these are given by the relation [66],

$$f_g^B(x,\mu_R) = f_g^R(x,\mu_F) + \frac{\alpha_{\mathrm{s}}}{2\pi}\left(\frac{4\pi\mu_R^2}{\mu_F^2}\right)^{\varepsilon}\frac{1}{\varepsilon}\frac{\Gamma(1-\varepsilon)}{\Gamma(1-2\varepsilon)}\left\{P_{gg}\otimes f_g^R(x,\mu_R) + P_{gq}\otimes f_q^R(x,\mu_R)\right\} \tag{3.97}$$

where the operator $\otimes$ depicts the convolution of the Altarelli-Parisi splitting functions with the renormalised parton densities,

$$f\otimes g(x,\mu) = \int_x^1 \frac{\mathrm{d}z}{z} f(z,\mu)\, g(x/z,\mu)\,. \tag{3.98}$$

Thus, the finite real corrections $\Delta\sigma_{ij}$ contributing to eq. (3.1) are obtained in analogy to the HQL result of [15] as,

$$\Delta\sigma_{gg} = \frac{\alpha_{\mathrm{s}}(\mu_R^2)}{\pi}\int_{\tau_0}^1 \mathrm{d}\tau \frac{d\mathcal{L}^{gg}}{d\tau}\int_{\tau_0/\tau}^1 \frac{dz}{z}\,\hat{\sigma}_{\mathrm{LO}}(\hat{s}=z\tau s)C_{gg}(z)\,, \tag{3.99}$$

$$\Delta\sigma_{gq} = \frac{\alpha_{\mathrm{s}}(\mu_R^2)}{\pi}\int_{\tau_0}^1 \mathrm{d}\tau \sum_{q,\bar{q}} \frac{d\mathcal{L}^{gq}}{d\tau}\int_{\tau_0/\tau}^1 \frac{dz}{z}\,\hat{\sigma}_{\mathrm{LO}}(\hat{s}=z\tau s)C_{gq}(z)\,, \tag{3.100}$$

$$\Delta\sigma_{q\bar{q}} = \frac{\alpha_{\mathrm{s}}(\mu_R^2)}{\pi}\int_{\tau_0}^1 \mathrm{d}\tau \sum_{q} \frac{d\mathcal{L}^{q\bar{q}}}{d\tau}\int_{\tau_0/\tau}^1 \frac{dz}{z}\,\hat{\sigma}_{\mathrm{LO}}(\hat{s}=z\tau s)\, C_{q\bar{q}}(z)\,, \tag{3.101}$$

with the real correction coefficients $C_{gg}(z)$, $C_{gq}(z)$ and $C_{q\bar{q}}(z)$ given by,

$$C_{gg}(z) = d_{gg}(z) - zP_{gg}(z)\log\frac{\mu_F^2}{\tau s} + 6[1+z^4+(1-z)^4]\left[\frac{\log(1-z)}{1-z}\right]_+ , \tag{3.102}$$

$$C_{gq}(z) = d_{gq}(z) - \frac{z}{2}P_{gq}(z)\log\frac{\mu_F^2}{\tau s(1-z)^2} , \tag{3.103}$$

$$C_{q\bar{q}}(z) = d_{q\bar{q}}(z) . \tag{3.104}$$

Once the finite contributions $d_{ij}(z)$ of the real corrections have been determined, the last ingredient of this technically involved calculation can be implemented in the numerical framework, allowing for the calculation of the NLO QCD corrections to Higgs boson pair production with full top quark mass dependence.

CHAPTER 4

NLO Corrections including Dimension-6 Operators

The discussion throughout the previous chapters was limited to the Higgs boson pair production within the SM. This process is, however, also interesting in the context of NP searches, especially since up to now the LHC has not provided direct discovery of BSM physics. Even though the measured properties of the Higgs boson are so far in good agreement with the SM predictions, further more precise studies of its couplings may reveal hints for NP. Various BSM models allow for scenarios in which the Higgs boson self-couplings deviate significantly from the SM value, while the remaining properties of the Higgs boson are fairly SM-like [49]. In addition to the coupling modifications, BSM models can further affect cross section predictions due to contributions from Feynman diagrams containing novel particles and couplings. Examples for such contributions to Higgs boson pair production can be obtained in BSM theories with an extended Higgs spectrum where already at LO the virtual Higgs boson in the triangle topology diagram can be (one of) the additional Higgs bosons of the model, or in composite Higgs models which give rise to direct couplings of two fermions to two Higgs bosons.

The absence of a discovery of new physical states suggests that the scale of NP is well separated from the electroweak scale, which encourages a description within the Effective Field Theory (EFT) framework. The EFT description is based on the idea, that the heavy degrees of freedom of a BSM model can be integrated out, giving rise to effective, local operators of the SM fields. These higher dimensional operators modify the SM couplings and introduce novel couplings not present in the SM. The matching of the Wilson coefficients of the EFT operators to experimental data allows for rather model-independent limits, which can be translated into constraints on parameters of specific NP models.

The EFT approach to Higgs boson pair production in gluon fusion is of interest, since it provides model independent predictions for deviations of the measurable signal from the SM prediction. Conversely, future experimental results can be used to set limits for the allowed EFT coupling values, which narrow down the parameter space of specific NP models. In order to provide reliable estimates for these limits, the EFT analysis has to include higher order corrections to the Higgs pair production process. Prior to this project, the results of which were published in [48], the Higgs pair production process was already studied in the EFT framework including approximate NLO QCD corrections in [49]. The strategy to ac-

count for higher order corrections in this analysis was to calculate the LO amplitude including dimension-6 EFT operators and to multiply the resulting cross section with the overall K-factor, given by the ratio of the SM result for the NLO QCD cross section divided by the LO cross section in the heavy top quark limit [15]. In this study we investigate the validity of this approximation by including the dimension-6 contributions directly at the NLO amplitude level in the heavy top quark limit. These two approaches lead to different results, as the individual contributions to Higgs pair production are affected differently by the NLO QCD corrections.

The following chapter presents the details of this project. After the introduction of the EFT framework and the heavy quark limit in section 4.1 and section 4.2, the implementation of the process is presented in section 4.3 and the results of the calculation are discussed in section 4.4.

4.1. Effective Field Theory

The influence of BSM physics realised at some high scale on SM observables can be parametrised in a rather model-independent way by introducing higher-dimensional operators. When the Higgs boson is, in analogy to the SM, embedded within a weak doublet, the leading BSM effects originate mostly from dimension-6 operators. Although in certain phase space regions the dimension-8 operators can become equally important, the investigation of these kinematic regions is challenging. Therefore, the contributions of dimension-8 operators are neglected in this project. The dimension-6 operators relevant for Higgs boson pair production without CP-violating effects in the Strongly-Interacting-Light Higgs (SILH) operator basis [107] are given by,

$$\begin{aligned}\Delta\mathcal{L}_6^{\text{SILH}} \supset\ & \bar{c}_g \frac{g_s^2}{m_W^2} H^\dagger H G^a_{\mu\nu} G^{a\mu\nu} + \frac{\bar{c}_H}{2v^2}\partial_\mu(H^\dagger H)\partial^\mu(H^\dagger H) \\ & + \frac{\bar{c}_u}{v^2} y_t (H^\dagger H \bar{q}_L H^c t_R + h.c.) - \frac{\bar{c}_6}{6v^2}\frac{3m_h^2}{v^2}(H^\dagger H)^3 \,,\end{aligned} \tag{4.1}$$

where v is the Higgs field vacuum expectation value $v \simeq 246\,\text{GeV}$, $m_h = 125\,\text{GeV}$ the Higgs boson mass, $m_W = 80.38\,\text{GeV}$ the mass of the W boson, y_t the top quark Yukawa coupling, g_s the strong coupling and $G^a_{\mu\nu}$ the gluon field strength tensor. The first operator describes the effective contact interactions of gluons with one and two Higgs bosons, while the remaining three operators modify the top Yukawa coupling and the trilinear Higgs self-couplings. Additionally, the first operator in the second line of eq. (4.1) introduces a novel coupling of two top quarks to two Higgs bosons. The coefficients of the operators $\bar{c}_H$, $\bar{c}_u$, $\bar{c}_6$ and $\bar{c}_g$ parametrise the deviation from the SM and are bounded by experimental findings [107].
An alternative parametrisation of the dimension-6 operators can be obtained when the electroweak group $\text{SU}(2)_L \otimes U(1)_Y$ is non-linearly realised and the physical Higgs boson is a generic CP-even scalar, which is a singlet of the custodial symmetry and need not necessarily be embedded in a weak doublet. The dimension-6 operators of the non-linearly realised EFT Lagrangian [108] relevant for Higgs pair production read

$$\Delta\mathcal{L}_{\text{non-lin}} \supset -m_t \bar{t}t\left(c_t\frac{h}{v} + c_{tt}\frac{h^2}{2v^2}\right) - \frac{c_3}{6}\left(\frac{3m_h^2}{v}\right)h^3 + \frac{\alpha_\text{s}}{\pi}G^{a\mu\nu}G^a_{\mu\nu}\left(c_g\frac{h}{v} + c_{gg}\frac{h^2}{2v^2}\right), \tag{4.2}$$

with $\alpha_\text{s} = g_s^2/(4\pi)$. The coefficients of the non-linear EFT Lagrangian c_g, c_{gg}, c_t, c_{tt} and c_3 in the SM limit of the EFT description read

$$c_t \to 1\,, \quad c_{tt} \to 0\,, \quad c_3 \to 1\,, \quad c_g \to 0\,, \quad c_{gg} \to 0\,. \tag{4.3}$$

In contrast to the SILH parametrisation, where the coefficients need to be small, the non-linear Lagrangian is valid for arbitrary values of the couplings c_i and they are only restricted by experiment [49]. Furthermore, the coefficients of both parametrisation can be set into relation through,

$$c_t = 1-\frac{\bar{c}_H}{2}-\bar{c}_u\,, \quad c_{tt} = -\frac{1}{2}(\bar{c}_H+3\bar{c}_u)\,, \quad c_3 = 1-\frac{3}{2}\bar{c}_H+\bar{c}_6\,, \quad c_g = c_{gg} = \bar{c}_g\left(\frac{2\pi v}{m_W}\right)^2. \quad (4.4)$$

In the following the results will be given in the non-linear parametrisation.[1]

4.2. Heavy Top Quark Limit

In analogy to the SM (and supersymmetric) calculation of [15], the NLO QCD corrections in the EFT framework can be obtained in the heavy top quark limit. These corrections are calculated by explicit expansion of the two-loop amplitude in the heavy quark mass according to the general algorithm of [109,110] or in an equivalent approach by applying the low-energy theorem for Higgs physics [111–113]. In the low-energy limit, the Higgs field operator acts like a constant field and the NLO corrected interaction of Higgs fields with gluon fields is generated from the top quark contribution to the unrenormalised transverse gluon-polarisation at zero-momentum transfer $\Pi^t_{gg}(0)$ [15,113]. At two-loop order, this yields

$$\Pi^t_{gg}(0) = \frac{\alpha_s}{\pi}\Gamma(1+\varepsilon)\left[\frac{4\pi\mu^2}{(m_t^0)^2}\right]^\varepsilon\left\{\frac{1}{6\varepsilon}+\frac{\alpha_s}{\pi}\Gamma(1+\varepsilon)\left[\frac{4\pi\mu^2}{(m_t^0)^2}\right]^\varepsilon\frac{1}{16\varepsilon}\right\}+\mathcal{O}(\varepsilon^0,\,\alpha_s^3) \quad (4.5)$$

and the Higgs field couplings to gluons are obtained from the Higgs field dependence of the bare top quark mass m_t^0 in the low-energy limit,

$$m_t^0 \to m_t^0\left(1+c_t\frac{h}{v}\right). \quad (4.6)$$

After renormalisation and by consistently including the EFT contributions from the couplings of two gluons to one and two Higgs fields described by the parameters c_g and c_{gg} respectively, as well as the novel coupling of two top quarks to two Higgs bosons described by c_{tt}, the effective Lagrangian for the couplings of Higgs bosons to gluons reads

$$\mathcal{L}_{\text{eff}} = \frac{\alpha_s}{12\pi}G^{a\mu\nu}G^a_{\mu\nu}\left\{\frac{h}{v}\left[c_t\left(1+\frac{11\alpha_s}{4\pi}\right)+12c_g\right]+\frac{h^2}{2v^2}\left[(c_{tt}-c_t^2)\left(1+\frac{11\alpha_s}{4\pi}\right)+12c_{gg}\right]\right\}. \quad (4.7)$$

In the SM limit given by eq. (4.3), the effective Lagrangian agrees with the corresponding SM result of [15]. The factor $(1+11\alpha_s/(4\pi))$ was obtained by consistently deriving the effective Lagrangian from the transverse gluon-polarisation at two-loop order and thus it describes the matching of the effective theory to the full theory at NLO QCD. The Feynman rules for the effective couplings obtained from eq. (4.7) are summarised in fig. 4.1.

The validity of the heavy top quark limit for the calculation of the NLO QCD corrections to Higgs boson pair production was already discussed for the SM case in section 2.3.4. The analysis of the finite top quark mass effects performed in [88,91,92] estimated the uncertainty on the K-factor to be of $\mathcal{O}(10\%)$ at NLO. The application of the heavy quark mass limit in BSM models can, however, lead to much larger uncertainties than in the SM, as was shown for the minimal composite Higgs model in [47,114], where the LO result with full mass dependence deviates by up to 50% from the result of the heavy top quark approximation. But since the NLO corrections are dominated by soft and collinear gluon effects, the K-factor uncertainty in EFT can be expected to be of order $10-20\%$.

[1] In the publication to this project [48], the results in the SILH parametrisation are included in the appendix.

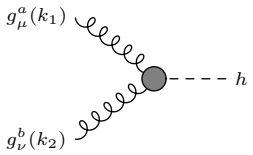

$$= -\mathrm{i}\delta^{ab}\tfrac{\alpha_\mathrm{s}}{3\pi v^2}[(k_1\cdot k_2)g^{\mu\nu}-k_2^\mu k_1^\nu][c_t(1+\tfrac{11\alpha_\mathrm{s}}{4\pi})+12c_g]$$

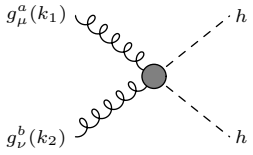

$$= -\mathrm{i}\delta^{ab}\tfrac{\alpha_\mathrm{s}}{3\pi v^2}[(k_1\cdot k_2)g^{\mu\nu}-k_2^\mu k_1^\nu][(c_{tt}-c_t^2)(1+\tfrac{11\alpha_\mathrm{s}}{4\pi})+12c_{gg}]$$

Figure 4.1: Feynman rules for the couplings of two gluons to one and two Higgs boson in the heavy top quark limit. The expressions contain corrections from the matching to the exact theory at NLO QCD as well as contributions from the EFT dimension-6 operators.

4.3. Details of the Calculation

The calculation of the NLO QCD corrections in the EFT framework follows the same strategy as the discussion of chapter 3. However, since the results are obtained in the heavy top quark limit, it is straightforward to perform the calculation using the conventions of [15]. Generic contributions to the LO process are depicted in fig. 4.2. The LO partonic cross section can be written as

$$\hat{\sigma}_\mathrm{LO}^\mathrm{EFT}(\hat{s}) = \frac{G_F^2\alpha_\mathrm{s}^2(\mu_R)}{512(2\pi)^3}\int_{\hat{t}_-}^{\hat{t}_+}\mathrm{d}\hat{t}\Big[|\mathcal{A}_1^\mathrm{EFT}|^2+|\mathcal{A}_2^\mathrm{EFT}|^2\Big]\,,\quad\text{with} \tag{4.8}$$

$$\mathcal{A}_1^\mathrm{EFT} = C_\Delta c_3(c_t\,F_\Delta+8c_g)+c_{tt}F_\Delta+8c_{gg}+c_t^2\,F_\Box\,, \tag{4.9}$$

$$\mathcal{A}_2^\mathrm{EFT} = c_t^2\,G_\Box\,. \tag{4.10}$$

The form factors $\mathcal{A}_1^\mathrm{EFT}$ and $\mathcal{A}_2^\mathrm{EFT}$ are expressed in terms of the EFT coefficients c_i as well as the coupling coefficient

$$C_\Delta = 3m_h^2/(\hat{s}-m_h^2+\mathrm{i}m_h\Gamma_h) \tag{4.11}$$

and the SM form factors F_Δ, $F_\Box$ and $G_\Box$, which are given by the SM expressions of [46] and contain the full top quark mass dependence. The spin zero form factor $\mathcal{A}_1^\mathrm{EFT}$ receives contributions from all LO diagrams and the individual terms in eq. (4.9) correspond, respectively, to the diagrams represented in fig. 4.2, while only the box topology diagrams contribute to the spin two form factor $\mathcal{A}_2^\mathrm{EFT}$.

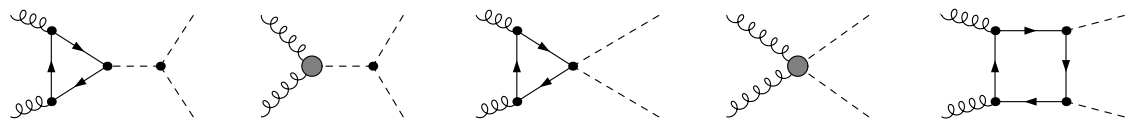

Figure 4.2: Generic contributions to Higgs boson pair production in gluon fusion at LO including dimension-6 operators.

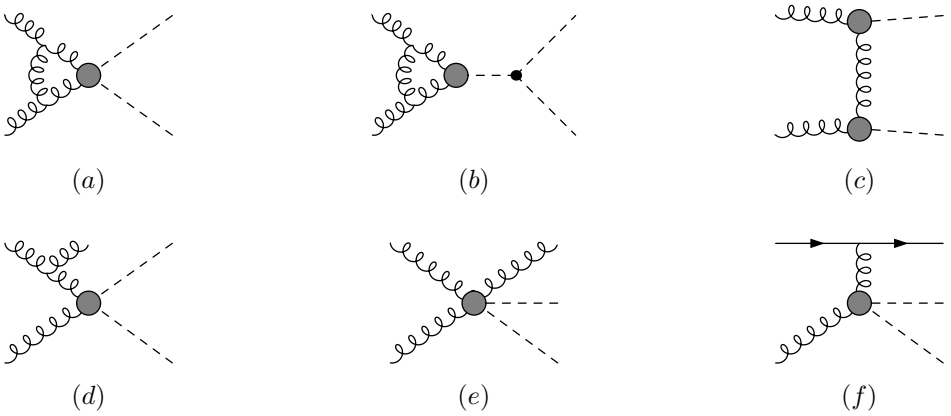

Figure 4.3: Sample contributions for the virtual (upper) and real (lower) corrections to Higgs boson pair production at NLO in the heavy quark limit.

The partonic differential cross section is a function of the partonic Mandelstam variables $\hat{s}$, $\hat{t}$, and $\hat{u}$ and the phase space integration is expressed in terms of the momentum transfer $\hat{t}$, as defined previously in section 3.1.4,

$$\hat{s} = \tau s\,, \quad \hat{t} = m_h^2 - \frac{\hat{s}(1-\beta\cos\theta)}{2}\,, \quad \hat{u} = 2m_h^2 - \hat{s} - \hat{t}\,, \quad \hat{t}_\pm = m_h^2 - \frac{\hat{s}(1\mp\beta)}{2}\,, \quad \text{with} \\ \beta = \sqrt{1-4m_h^2/\hat{s}}\,. \tag{4.12}$$

For the calculation of the NLO QCD corrections we use the effective couplings of fig. 4.1. The corrections consist of real and virtual contributions, with sample diagrams shown in fig. 4.3. The calculation is performed in dimensional regularisation in $D = 4-2\varepsilon$ dimensions, as the NLO amplitudes develop ultraviolet (UV) and infrared (IR) divergences. The UV singularities of the virtual corrections are cancelled by renormalisation of the strong coupling constant α_s in the $\overline{\text{MS}}$ scheme with five active flavours according to eq. (2.24). The IR divergences cancel in the sum of the real and virtual corrections and remaining collinear initial state singularities are absorbed by the definition of the NLO parton densities, which are also defined in the $\overline{\text{MS}}$ scheme with five active flavours. The finite hadronic NLO cross section can be organised as

$$\sigma_{\text{NLO}}^{\text{EFT}}(pp \to hh+X) = \sigma_{\text{LO}}^{\text{EFT}} + \Delta\sigma_{\text{virt}}^{\text{EFT}} + \Delta\sigma_{gg}^{\text{EFT}} + \Delta\sigma_{gq}^{\text{EFT}} + \Delta\sigma_{q\bar{q}}^{\text{EFT}}\,. \tag{4.13}$$

The individual contributions are obtained in analogy to the SM calculation of [15], as also discussed in sections 3.2.4 and 3.3, yielding

$$\sigma_{\text{LO}}^{\text{EFT}} = \int_{\tau_0}^1 \mathrm{d}\tau \frac{d\mathcal{L}^{gg}}{d\tau}\, \hat{\sigma}_{\text{LO}}^{\text{EFT}}(\hat{s}=\tau s)\,, \tag{4.14}$$

$$\Delta\sigma_{\text{virt}}^{\text{EFT}} = \frac{\alpha_s(\mu_R)}{\pi} \int_{\tau_0}^1 \mathrm{d}\tau \frac{d\mathcal{L}^{gg}}{d\tau}\, \hat{\sigma}_{\text{LO}}^{\text{EFT}}(\hat{s}=\tau s)\, C_{\text{virt}}^{\text{EFT}}\,, \tag{4.15}$$

$$\Delta\sigma_{gg}^{\text{EFT}} = \frac{\alpha_s(\mu_R)}{\pi} \int_{\tau_0}^1 \mathrm{d}\tau \frac{d\mathcal{L}^{gg}}{d\tau} \int_{\tau_0/\tau}^1 \frac{\mathrm{d}z}{z}\, \hat{\sigma}_{\text{LO}}^{\text{EFT}}(\hat{s}=z\tau s)\, C_{gg}^{\text{EFT}}(z)\,, \tag{4.16}$$

$$\Delta\sigma_{gq}^{\text{EFT}} = \frac{\alpha_s(\mu_R)}{\pi} \sum_{q\bar{q}} \int_{\tau_0}^1 \mathrm{d}\tau \frac{d\mathcal{L}^{gg}}{d\tau} \int_{\tau_0/\tau}^1 \frac{\mathrm{d}z}{z}\, \hat{\sigma}_{\text{LO}}^{\text{EFT}}(\hat{s}=z\tau s)\, C_{gq}^{\text{EFT}}(z)\,, \tag{4.17}$$

$$\Delta\sigma_{q\bar{q}}^{\text{EFT}} = \frac{\alpha_s(\mu_R)}{\pi} \sum_{q} \int_{\tau_0}^1 \mathrm{d}\tau \frac{d\mathcal{L}^{gg}}{d\tau} \int_{\tau_0/\tau}^1 \frac{\mathrm{d}z}{z}\, \hat{\sigma}_{\text{LO}}^{\text{EFT}}(\hat{s}=z\tau s)\, C_{q\bar{q}}^{\text{EFT}}(z)\,, \tag{4.18}$$

where μ_R denotes the renormalisation scale, $\sqrt{s}$ is the hadronic centre-of-mass energy and $\tau_0 = 4m_h^2/s$. With the factorisation scale of the parton-parton luminosities $d\mathcal{L}^{ij}/d\tau$ denoted by μ_F and the definitions of the Altarelli-Parisi splitting functions $P_{ij}(z)$ given in section 3.3, the coefficients of the real corrections read

$$C_{gg}^{\text{EFT}}(z) = -z\,P_{gg}(z)\log\frac{\mu_F^2}{\tau s} - \frac{11}{2}(1-z)^3 + 6[1+z^4+(1-z)^4]\Big(\frac{\log(1-z)}{1-z}\Big)_+\,, \tag{4.19}$$

$$C_{gq}^{\text{EFT}}(z) = -\frac{z}{2}\,P_{gq}(z)\log\frac{\mu_F^2}{\tau s(1-z)^2} + \frac{2}{3}z^2 - (1-z)^2\,, \tag{4.20}$$

$$C_{q\bar{q}}^{\text{EFT}}(z) = \frac{32}{27}(1-z)^3\,. \tag{4.21}$$

These expression agree exactly with the corresponding SM coefficients due to QCD factorisation. The virtual corrections, on the other hand, are altered in comparison to the SM case because of the EFT coefficients and due to the novel effective vertices not present in the SM. The coefficient of the virtual corrections $C_{\text{virt}}^{\text{EFT}}$ is found as

$$\begin{aligned} C_{\text{virt}}^{\text{EFT}} = {} & \left[\pi^2 + \frac{33-2N_F}{6}\log\frac{\mu_R^2}{\hat{s}} + \frac{11}{2}\right] - 44\,\text{Re}\left\{\frac{\int_{\hat{t}_-}^{\hat{t}_+}\mathrm{d}\hat{t}\,\mathcal{A}_1^{\text{EFT}}[C_\Delta^* c_g + c_{gg}]}{\int_{\hat{t}_-}^{\hat{t}_+}\mathrm{d}\hat{t}[|\mathcal{A}_1^{\text{EFT}}|^2 + |\mathcal{A}_2^{\text{EFT}}|^2]}\right\} \\ & + \frac{4(c_t+12c_g)^2}{9}\,\text{Re}\left\{\frac{\int_{\hat{t}_-}^{\hat{t}_+}\mathrm{d}\hat{t}\Big[\mathcal{A}_1^{\text{EFT}} - \mathcal{A}_2^{\text{EFT}}[\frac{p_T^2}{2\hat{t}\hat{u}}(\hat{s}-2m_h^2)]\Big]}{\int_{\hat{t}_-}^{\hat{t}_+}\mathrm{d}\hat{t}[|\mathcal{A}_1^{\text{EFT}}|^2 + |\mathcal{A}_2^{\text{EFT}}|^2]}\right\}, \quad \text{with} \\ p_T^2 = {} & \frac{(\hat{t}-m_h^2)(\hat{u}-m_h^2)}{\hat{s}} - m_h^2\,. \end{aligned} \tag{4.22}$$

The first line of eq. (4.22) corresponds to the contributions from the diagrams of fig. 4.3 (a) and (b), where the term in the first bracket is the universal NLO coefficient known from the SM heavy quark limit corrections and the second term is due to the novel EFT couplings of two gluons to one or two Higgs bosons. The term in the second line of eq. (4.22) originates from the diagram fig. 4.3 (c) and in the SM limit it agrees with the heavy quark limit contributions from the reducible double-triangle diagrams of fig. 3.4 (b).

4.4. Analysis and Results

The results of the calculation presented in the previous section were implemented in the Fortran program `HPAIR` [115]. For the analysis we have chosen the centre-of-mass energy $\sqrt{s} = 14\,\text{TeV}$ and set the masses of the Higgs boson, top and bottom quark respectively to $m_h = 125\,\text{GeV}$, $m_t = 173.2\,\text{GeV}$ and $m_b = 4.75\,\text{GeV}$. We have used the MSTW08 [116–118] parton densities for the LO and NLO cross section with the value of the strong coupling at LO and NLO set to $\alpha_s^{\text{LO}} = 0.13939$ and $\alpha_s^{\text{NLO}} = 0.12018$.

In order to determine the impact of the new couplings on the QCD corrections, we calculate the EFT K-factor, which is defined as the ratio of the NLO and LO hadronic cross sections,

$$K = \frac{\sigma_{\text{NLO}}^{\text{EFT}}}{\sigma_{\text{LO}}^{\text{EFT}}}\,, \tag{4.23}$$

where the parton densities and the strong coupling in $\sigma_{\text{NLO}}^{\text{EFT}}$ and $\sigma_{\text{LO}}^{\text{EFT}}$ are taken at the appropriate order. Deviations of the K-factor from the SM value are mainly due to the virtual corrections, as the EFT coefficients are involved non-trivially in the virtual correction factor eq. (4.22). Additionally, the weights of the τ integration in the real corrections are shifted due to the modified LO cross section. We investigate the effects of the dimension-6 operators on

the K-factor by varying individual parameters while fixing the remaining EFT parameters to their SM value according to eq. (4.3). To examine the validity of the approximate inclusion of the NLO corrections used in [49], we also determine the maximal relative deviation of the SM and EFT K-factors

$$\delta_{\max}^{c_i} = \frac{\max|K^{c_i} - K^{\mathrm{SM}}|}{K^{\mathrm{SM}}} \tag{4.24}$$

for the variations of the individual coefficients $c_i = c_g$, c_{gg}, c_t, c_{tt}, c_3.

Figure 4.4 (upper) shows the variation of the effective coupling of two gluons to one Higgs boson c_g away from its SM value $c_g = 0$ in the range $-0.15 \leq c_g \leq 0.15$. Since this coupling also affects signal strengths for single Higgs boson production, it is rather strictly constrained by experimental data under certain assumptions [49, 119]. The variation range exceeds these constraints for illustrative purposes. The K-factor is flat in the entire variation range, which can be explained by the fact that the coefficient c_g enters the EFT form factors through diagrams with an s-channel Higgs propagator, which are numerically suppressed.
In fig. 4.4 (lower) we have set $c_g = 0$ and varied c_{gg} away from its SM value $c_{gg} = 0$ in the range $-0.15 \leq c_{gg} \leq 0.15$ [49]. The maximal deviation of the K-factor is found for $c_{gg} = -0.15$ where the K-factor reaches a plateau. In this region, the relative K-factor deviation amounts to $\delta_{\max}^{c_{gg}} = 5.4\%$. While the impact on the K-factor is rather small, the impact on the total cross section is much larger. At NLO the EFT cross section can be enhanced considerably compared to the SM cross section. We find

$$\frac{\max|\sigma^{c_{gg}} - \sigma^{\mathrm{SM}}|}{\sigma^{\mathrm{SM}}} = 5.8 \tag{4.25}$$

within the variation range of c_{gg} allowed by experimental constraints. This significant deviation from the SM predictions confirms the potential of the Higgs boson pair production process for indirect BSM searches.

The variation of the novel contact interaction between two top quarks and two Higgs bosons c_{tt} is shown in fig. 4.5 within the range $-1.5 \leq c_{tt} \leq 1.5$ [49]. The K-factor yields a maximal deviation of $\delta_{\max}^{c_{tt}} = 3.2\%$ for $c_{tt} \approx 0.7$ where the individual terms of the LO cross section interfere destructively. The maximal deviation is reached at a much higher value of the coefficient c_{tt} compared to the previous variations of c_g and c_{gg}. This can be explained by the different normalisations of these couplings within the Feynman rules of fig. 4.1. Since the value of the trilinear Higgs self-coupling is so far practically unconstrained by experiment and the value of the coupling in BSM models can differ significantly from the SM prediction, we perform the variation of the coefficient c_3 in the wide range of $-10 \leq c_3 \leq 10$ [49] while setting the remaining EFT couplings to their SM values. The effect of the c_3 variation is small and leads to a maximal K-factor deviation of $\delta_{\max}^{c_3} = 2.1\%$ in the region $5 \lesssim c_3 \lesssim 10$. The minor impact of this coefficient on the K-factor can again be explained by the fact, that the coefficient only contributes to diagrams with an s-channel Higgs propagator, which suppresses its effect.

In addition to the variations presented in figs. 4.4 to 4.6, we also investigated the impact of the Yukawa coupling modifying EFT parameter c_t in the still allowed range $0.65 \leq c_t \leq 1.15$ [49], as well as the effects of these variations for a very high centre-of-mass energy of $\sqrt{s} = 100\,\mathrm{TeV}$. For such high energies the EFT framework still retains its validity due to the peaking of the parton density functions of quarks and gluons at low energy fractions, if we assume that NP sets in somewhere above $\Lambda_{\mathrm{NP}} > 10\,\mathrm{TeV}$. These variations lead to K-factor deviations of a few per cent, which underlines the dominance of the soft and collinear gluon effects in the NLO QCD corrections, as these factorise from the LO cross section.

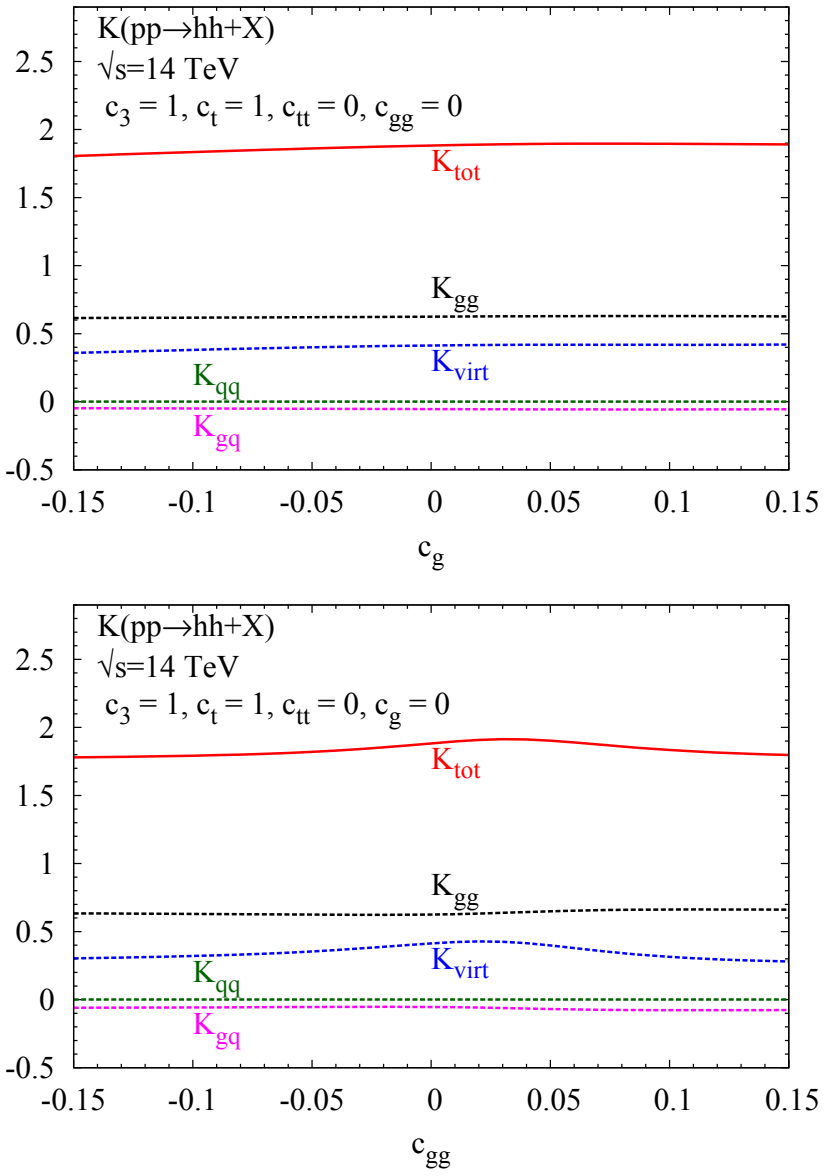

Figure 4.4: Upper: K-factors of the NLO QCD corrected cross section for Higgs boson pair production in gluon fusion at $\sqrt{s} = 14\,\text{TeV}$ as a function of the EFT coupling of two gluons to one Higgs boson c_g, while the remaining EFT parameters are set to their SM limits of eq. (4.3). The dashed lines describe the contributions of the individual QCD correction terms of eq. (4.13). Lower: same setup for the variation of the EFT coupling of two gluons to two Higgs bosons c_{gg}. The figures are already published in [48].

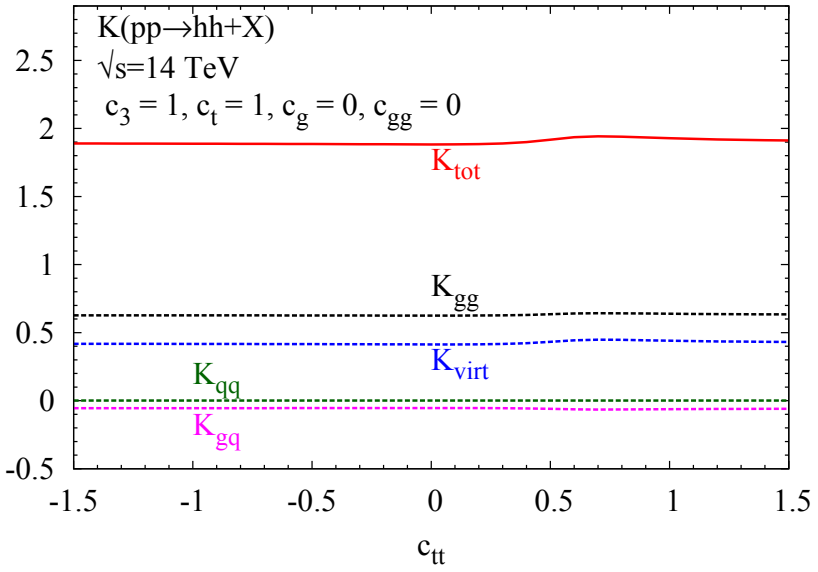

Figure 4.5: Same as fig. 4.4, but with the SM values for the coefficients $c_g = c_{gg} = 0$, $c_t = c_3 = 1$ and the coefficient for the interaction between two top quarks and two Higgs bosons c_{tt} is varied over its experimentally allowed range.

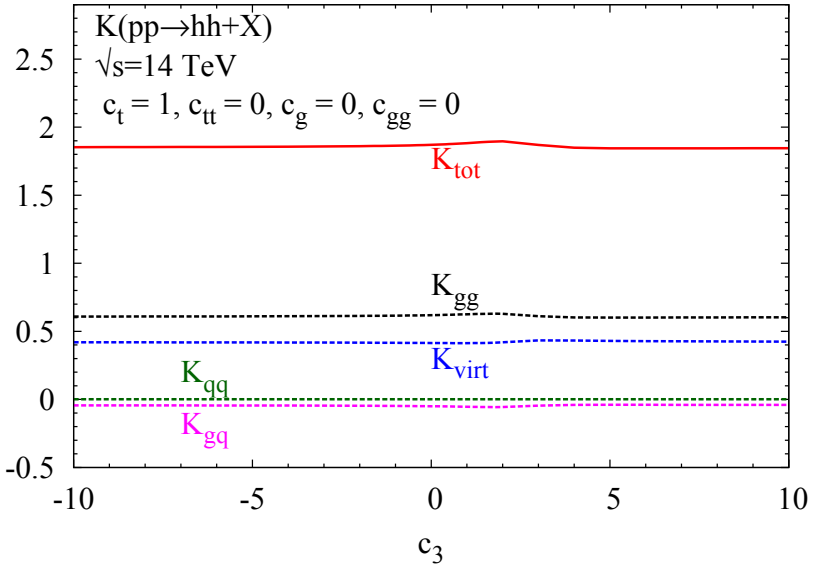

Figure 4.6: Same as fig. 4.4, but with the SM values for the coefficients $c_g = c_{gg} = c_{tt} = 0$, $c_t = 1$ and the coefficient for the modification of the trilinear Higgs self-coupling c_3 is varied over its experimentally allowed range.

CHAPTER 5

Conclusion and Outlook

In this thesis two projects involving the NLO QCD corrections to Higgs boson pair production were performed. Chapter 4 describes the calculation of the NLO QCD correction to Higgs boson pair production in the EFT framework in the heavy top quark mass limit. The considered dimension-6 EFT operators not only modify the SM Higgs couplings, but also induce novel couplings not present in the SM and can lead to significant deviations from the SM prediction of the Higgs pair production cross section.

The calculation of the NLO QCD corrections within the SM with full top quark mass dependence was discussed in chapter 3. Here the most crucial step of the calculation has been performed by the implementation of the two-loop amplitude of the virtual corrections. This implementation is an elaborate task, as there is no systematic algorithm for the calculation of two-loop four point functions with massive external and internal particles. For each of the 47 contributing box topology diagrams a proper Feynman parametrisation had to be found, which allows for the isolation of the UV and IR poles and numerical integration. Due to the enclosed top quark loop, which consists of up to 6 fermionic propagators, the calculation also demands for careful bookkeeping in order to correctly reduce the two-loop momentum tensor integrals to scalar six-dimensional Feynman parameter integrals. For these reasons a semi-flexible `FORM` and `Mathematica` procedure had to be developed, which follows the calculational strategy described in section 3.2 and is capable of reducing the variety of terms occurring in the virtual amplitude.
Having already found a suitable description of all diagrams below the virtual top quark mass threshold, the final challenge of this calculation is given by the treatment of the threshold singularities. While these divergences can be formally treated by introducing a small regulator for the imaginary part of the propagator quark mass, the numerical integration of the Feynman parameters becomes unstable due to large cancellations in the vicinity of the threshold. The numerical stability of the integrals can be improved by partial integration of the Feynman integrals. Since for each diagram there are several ways to perform the partial integration, the individual possibilities are currently being carefully investigated, in order to find the optimal choice which minimises the calculational time of the integrals. Once this stage of the project is finished, the obtained results can be used to perform the integration over the phase space, yielding the final result for the virtual correction factor C_{MASS} of eq. (3.89). The outlook of this project in the near future is the development of a numerical program package

for the calculation of the total and differential cross section of Higgs pair production with NLO accuracy, in which the finite top quark mass effects are fully included.

In the long term, this calculation triggers a wide range of exciting phenomenological investigations. Especially the improvement in the calculation of differential distributions can yield interesting consequences for the measurement prospects of the trilinear Higgs self-coupling at the LHC. The results can also be combined with the calculation performed within the EFT framework presented in chapter 4 to further improve the EFT predictions for Higgs boson pair production.

APPENDIX A

Formulary

A.1. One Loop Tensor Integral Reduction

A.1.1. Three-Point Tensor Integrals

In the calculation of the leading order form factors, we encounter tensor one loop integrals of up to rank two,

$$\mathcal{A}_{i,\Delta} \sim C_{\{0,\mu,\mu\nu\}}(p_1,p_2) = (2\pi\mu)^{4-D}\int\frac{\mathrm{d}^D q}{\mathrm{i}\pi^2}\frac{\{1,q_\mu,q_\mu q_\nu\}}{[q^2-m_t^2][(q+p_1)^2-m_t^2][(q+p_2)^2-m_t^2]}\,, \tag{A.1}$$

which can be reduced to scalar one loop integrals in order to simplify the numerical evaluation. Following the strategy described in [96], the tensor integral coefficients,

$$C^\mu(p_1,p_2) = p_1^\mu C_1(p_1,p_2)+p_2^\mu C_2(p_1,p_2) \tag{A.2}$$

$$\begin{aligned} C^{\mu\nu}(p_1,p_2) = {}& g^{\mu\nu}C_{00}(p_1,p_2)+p_1^\mu p_1^\nu C_{11}(p_1,p_2)\\ &+(p_1^\mu p_2^\nu+p_2^\mu p_1^\nu)C_{12}(p_1,p_2)+p_2^\mu p_2^\nu C_{22}(p_1,p_2), \end{aligned} \tag{A.3}$$

can be expressed in terms of scalar two- and three-point one loop integrals B_0, C_0 as,

$$C_{00}(p_1,p_2) = \frac{1}{2(D-2)}(B_0(p_2-p_1)+2m_t^2C_0(p_1,p_2)+\sum_{i=1}^{2}p_i^2C_i(p_1,p_2)), \tag{A.4}$$

$$C_{ij}(p_1,p_2) = \sum_{n=1}^{2}\frac{1}{2}\Delta_{in}^{-1}(p_1,p_2)(R_{nj}(p_1,p_2)-2C_{00}(p_1,p_2)\delta_{nj}), \tag{A.5}$$

$$R_{nj}(p_1,p_2) = B_1^{(n)}(p_1,p_2)(1-\delta_{nj})-\tilde{B}_j(p_1,p_2)-p_n^2C_j(p_1,p_2), \tag{A.6}$$

$$C_i(p_1,p_2) = \sum_{n=1}^{2}\frac{1}{2}\Delta_{in}^{-1}(p_1,p_2)(B_0^{(n)}(p_1,p_2)-B_0(p_2-p_1)), \tag{A.7}$$

with Δ_{in}^{-1} being the inverse of the Gram matrix,

$$\Delta_{in} = p_i\cdot p_n, \tag{A.8}$$

and

$$B^{(1)}_{\{0,1\}}(p_1,p_2) = B_{\{0,1\}}(p_2), \tag{A.9}$$

$$B^{(2)}_{\{0,1\}}(p_1,p_2) = B_{\{0,1\}}(p_1), \tag{A.10}$$

$$\tilde{B}_1(p_1,p_2) = -B_1(p_2-p_1)-B_0(p_2-p_1), \tag{A.11}$$

$$\tilde{B}_2(p_1,p_2) = B_1(p_2-p_1), \tag{A.12}$$

$$B_1(p_1) = -\frac{1}{2}B_0(p_1). \tag{A.13}$$

A.1.2. Four-Point Tensor Integrals

Using the abbreviation,

$$\langle f(q,p_i)\rangle = (2\pi\mu)^{4-D}\int\frac{\mathrm{d}^Dq}{\mathrm{i}\pi^2}\frac{f(q,p_i)}{[q^2-m_t^2][(q+p_1)^2-m_t^2][(q+p_2)^2-m_t^2][(q+p_3)^2-m_t^2]} \tag{A.14}$$

the following numerator structures need to be implemented for the calculation

$$\begin{aligned}\langle q^2q^2\rangle &= g^{\mu\nu}C^{(0)}_{\mu\nu}(p_1,p_2,p_3)-2p_1^\mu C^{(0)}_\mu(p_1,p_2,p_3)\\ &\quad+(p_1^2+m_t^2)C^{(0)}_0(p_1,p_2,p_3)+m_t^4D_0(p_1,p_2,p_3)\,,\end{aligned} \tag{A.15}$$

$$\begin{aligned}\langle q^2(qp_i)(qp_j)\rangle &= p_i^\mu p_j^\nu C^{(0)}_{\mu\nu}(p_1,p_2,p_3)-\big((p_1p_i)p_j^\mu+(p_1p_j)p_i^\mu+\frac{m_t^2}{2}p_i^\mu\big)C^{(0)}_\mu(p_1,p_2,p_3)\\ &\quad+\frac{m_t^2}{2}p_i^\mu C^{(j)}_\mu(p_1,p_2,p_3)+\big((p_1p_i)(p_1p_j)+\frac{m_t^2(p_1p_i)}{2}+\frac{m_t^2p_j^2}{4}\big)\times\\ &\quad\times C^{(0)}_0(p_1,p_2,p_3)-\frac{m_t^2p_j^2}{4}C^{(i)}_0(p_1,p_2,p_3)+\frac{m_t^2p_i^2p_j^2}{4}D_0(p_1,p_2,p_3)\,,\end{aligned} \tag{A.16}$$

$$\begin{aligned}\langle q^2(qp_i)\rangle &= p_i^\mu C^{(0)}_\mu(p_1,p_2,p_3)-\big(p_1p_i+\frac{m_t^2}{2}\big)C^{(0)}_0(p_1,p_2,p_3)\\ &\quad+\frac{m_t^2}{2}C^{(i)}_0(p_1,p_2,p_3)-\frac{m_t^2p_i^2}{2}D_0(p_1,p_2,p_3)\,,\end{aligned} \tag{A.17}$$

$$\begin{aligned}\langle(qp_i)(qp_j)(qp_k)\rangle &= \frac{1}{2}\Big\{p_i^\mu p_j^\nu\big(C^{(k)}_{\mu\nu}(p_1,p_2,p_3)-C^{(0)}_{\mu\nu}(p_1,p_2,p_3)\big)-\frac{p_k^2}{2}p_i^\mu C^{(j)}_\mu(p_1,p_2,p_3)\\ &\quad+\big((p_1p_i)p_j^\mu+(p_1p_j)p_i^\mu+\frac{p_k^2}{2}p_i^\mu\big)C^{(0)}_\mu(p_1,p_2,p_3)\\ &\quad-\big((p_1p_i)(p_1p_j)+\frac{(p_1p_i)p_k^2}{2}+\frac{p_j^2p_k^2}{4}\big)C^{(0)}_0(p_1,p_2,p_3)\\ &\quad+\frac{p_j^2p_k^2}{4}C^{(i)}_0(p_1,p_2,p_3)-\frac{p_i^2p_j^2p_k^2}{4}D_0(p_1,p_2,p_3)\Big\}\,,\end{aligned} \tag{A.18}$$

$$\langle q^2\rangle = C^{(0)}_0(p_1,p_2,p_3)+m_t^2D_0(p_1,p_2,p_3), \tag{A.19}$$

$$\begin{aligned}\langle(qp_i)(qp_j)\rangle &= \frac{1}{2}\Big\{p_i^\mu\big(C^{(j)}_\mu(p_1,p_2,p_3)-C^{(0)}_\mu(p_1,p_2,p_3)\big)\\ &\quad+\big(p_1p_i+\frac{p_j^2}{2}\big)C^{(0)}_0(p_1,p_2,p_3)-\frac{p_j^2}{2}C^{(i)}_0(p_1,p_2,p_3)\\ &\quad+\frac{p_i^2p_j^2}{2}D_0(p_1,p_2,p_3)\Big\}\,,\end{aligned} \tag{A.20}$$

$$\langle qp_i\rangle = \frac{1}{2}\Big\{C^{(i)}_0(p_1,p_2,p_3)-C^{(0)}_0(p_1,p_2,p_3)-p_i^2D_0(p_1,p_2,p_3)\Big\}\,, \tag{A.21}$$

where the superscript of the loop functions keeps track of which denominator term drops out,

$$C^{(0)}_{\{0,\mu,\mu\nu\}}(p_1,p_2,p_3) = C_{\{0,\mu,\mu\nu\}}(p_2-p_1,p_3-p_1), \tag{A.22}$$

$$C^{(1)}_{\{0,\mu,\mu\nu\}}(p_1,p_2,p_3) = C_{\{0,\mu,\mu\nu\}}(p_2,p_3), \tag{A.23}$$

$$C^{(2)}_{\{0,\mu,\mu\nu\}}(p_1,p_2,p_3) = C_{\{0,\mu,\mu\nu\}}(p_1,p_3), \tag{A.24}$$

$$C^{(3)}_{\{0,\mu,\mu\nu\}}(p_1,p_2,p_3) = C_{\{0,\mu,\mu\nu\}}(p_1,p_2). \tag{A.25}$$

The resulting three-point tensor integrals can eventually be reduced to scalar integrals using the identities of appendix A.1.1.

APPENDIX B

Two-Loop Diagrams

Triangle Topology

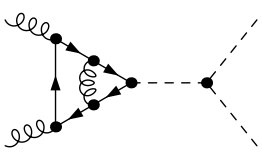

Triangle 1

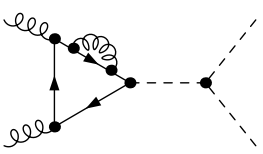

Triangle 4

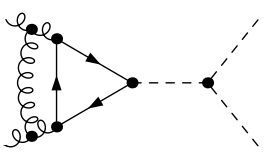

Triangle 7

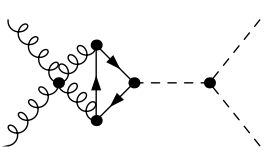

Triangle 8

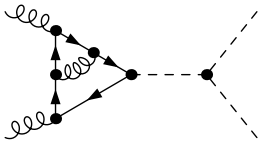

Triangle 2

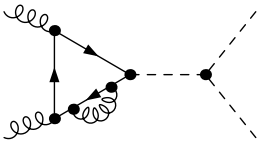

Triangle 5

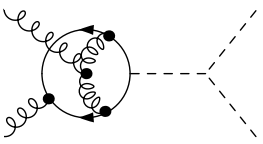

Triangle 9

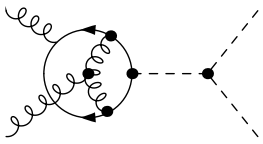

Triangle 10

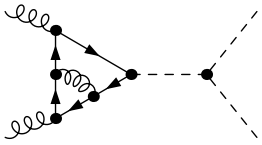

Triangle 3

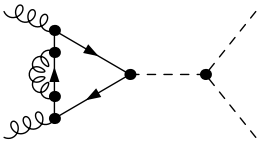

Triangle 6

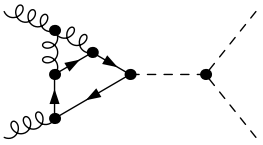

Triangle 11

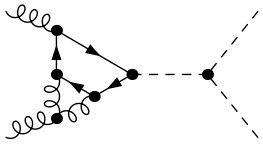

Triangle 12

Double Triangle Topology

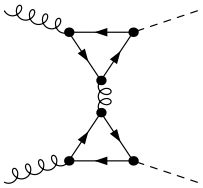

Double Triangle 1

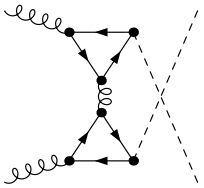

Double Triangle 2

Topology 1:

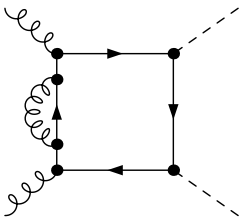
Box 1

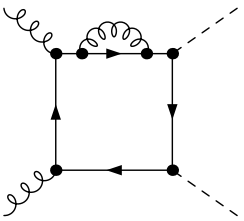
Box 2

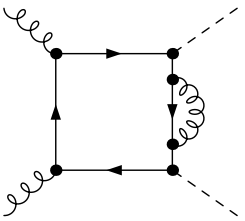
Box 3

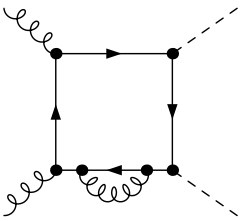
Box 4

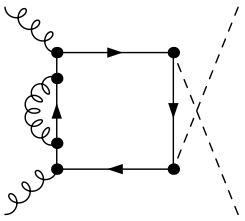
Box 5

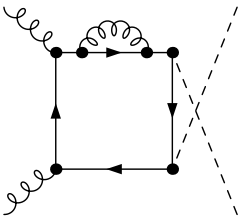
Box 6

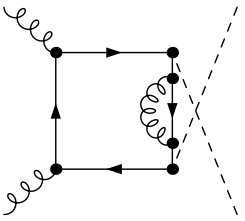
Box 7

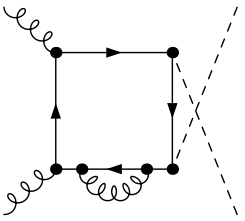
Box 8

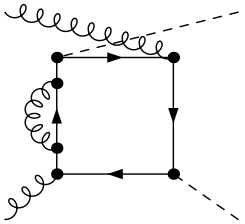
Box 9

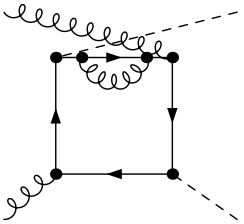
Box 10

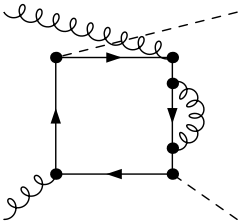
Box 11

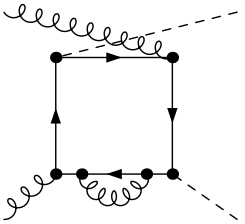
Box 12

Topology 2:

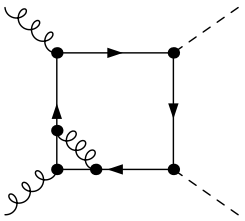
Box 13

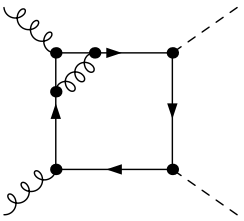
Box 14

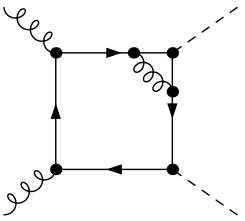
Box 15

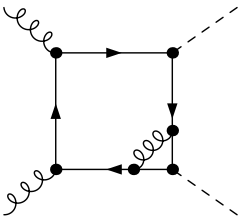
Box 16

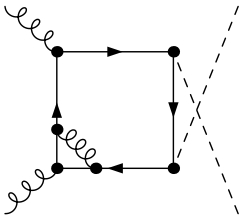
Box 17

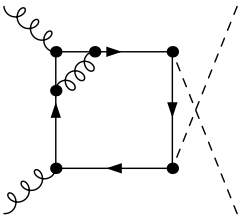
Box 18

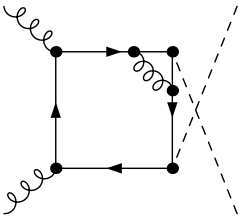
Box 19

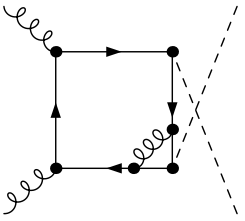
Box 20

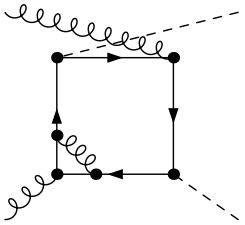
Box 21

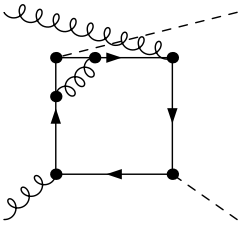
Box 22

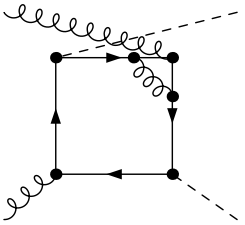
Box 23

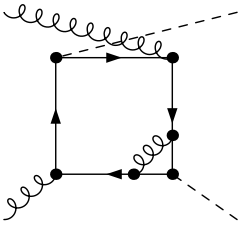
Box 24

Topology 3:

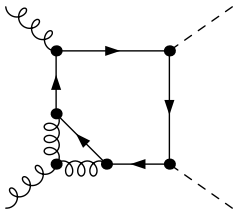
Box 25

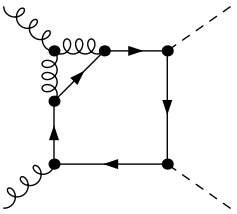
Box 26

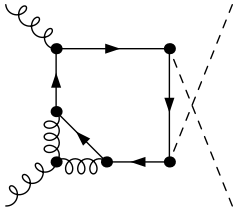
Box 27

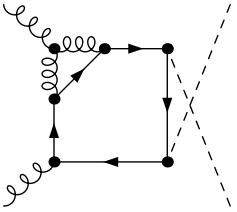
Box 28

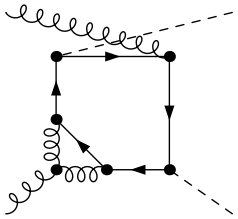
Box 29

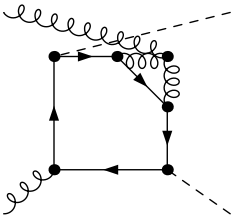
Box 30

Topology 4:

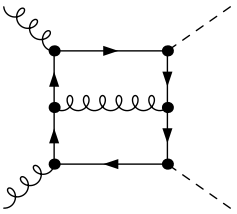
Box 31

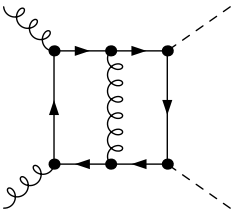
Box 32

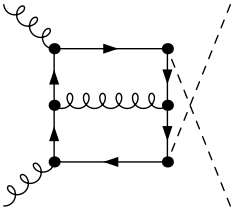
Box 33

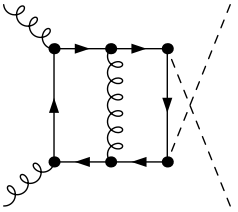
Box 34

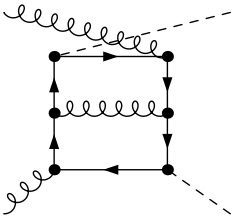
Box 35

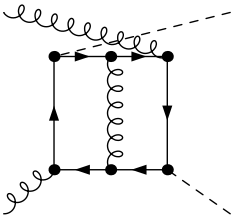
Box 36

Topology 5:

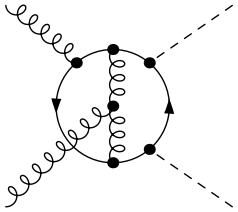
Box 37

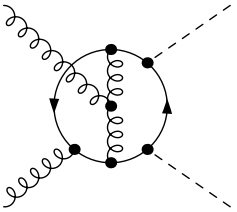
Box 38

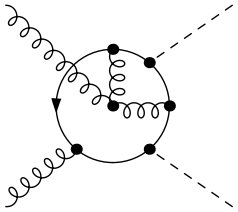
Box 39

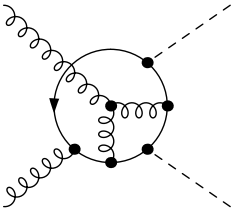
Box 40

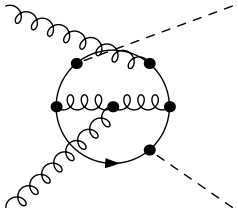
Box 41

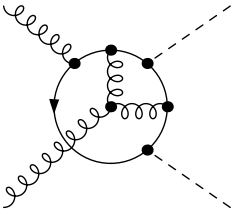
Box 42

Topology 6:

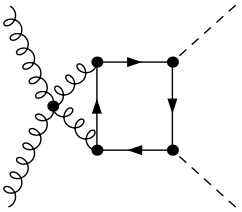
Box 43

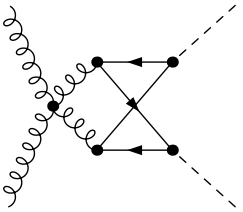
Box 44

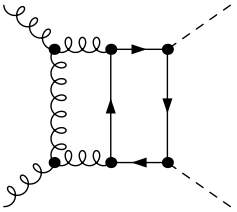
Box 45

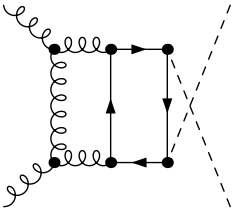
Box 46

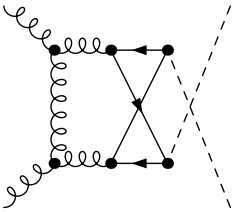
Box 47

References

[1] P. Higgs, *Broken symmetries, massless particles and gauge fields*. Physics Letters **12** (1964) no. 2, 132 – 133.

[2] P. W. Higgs, *Broken Symmetries and the Masses of Gauge Bosons.* Phys. Rev. Lett. **13** (Oct, 1964) 508–509.

[3] P. W. Higgs, *Spontaneous Symmetry Breakdown without Massless Bosons.* Phys. Rev. **145** (May, 1966) 1156–1163.

[4] F. Englert and R. Brout, *Broken Symmetry and the Mass of Gauge Vector Mesons.* Phys. Rev. Lett. **13** (Aug, 1964) 321–323.

[5] T. W. B. Kibble, *Symmetry Breaking in Non-Abelian Gauge Theories.* Phys. Rev. **155** (Mar, 1967) 1554–1561.

[6] G. S. Guralnik, C. R. Hagen, and T. W. B. Kibble, *Global Conservation Laws and Massless Particles*Phys. Rev. Lett. **13** (Nov, 1964) 585–587.

[7] S. L. Glashow, *Partial-symmetries of weak interactions*. Nuclear Physics **22** (1961) no. 4, 579 – 588.

[8] S. Weinberg, *A Model of Leptons*Phys. Rev. Lett. **19** (Nov, 1967) 1264–1266.

[9] A. Salam, *Weak and Electromagnetic Interactions*. Conf. Proc. **C680519** (1968) 367–377.

[10] **ATLAS** Collaboration, G. Aad *et al.*, *Observation of a new particle in the search for the Standard Model Higgs boson with the ATLAS detector at the LHC*. Phys. Lett. **B716** (2012) 1–29, `arXiv:1207.7214 [hep-ex]`.

[11] **CMS** Collaboration, S. Chatrchyan *et al.*, *Observation of a new boson at a mass of 125 GeV with the CMS experiment at the LHC*. Phys. Lett. **B716** (2012) 30–61, `arXiv:1207.7235 [hep-ex]`.

[12] **ATLAS, CMS** Collaboration, *Measurements of the Higgs boson production and decay rates and constraints on its couplings from a combined ATLAS and CMS analysis of the LHC pp collision data at $\sqrt{s}$ = 7 and 8 TeV* Tech. Rep. ATLAS-CONF-2015-044, CERN, Geneva, Sep, 2015. `http://cds.cern.ch/record/2052552`.

[13] **CMS** Collaboration, S. Chatrchyan *et al.*, *Study of the Mass and Spin-Parity of the Higgs Boson Candidate Via Its Decays to Z Boson Pairs*. Phys. Rev. Lett. **110** (2013) no. 8, 081803, `arXiv:1212.6639 [hep-ex]`.

[14] **ATLAS** Collaboration, G. Aad *et al.*, *Evidence for the spin-0 nature of the Higgs boson using ATLAS data*. Phys. Lett. **B726** (2013) 120–144, `arXiv:1307.1432 [hep-ex]`.

[15] S. Dawson, S. Dittmaier, and M. Spira, *Neutral Higgs-boson pair production at hadron colliders: QCD corrections.* Phys. Rev. D **58** (Nov, 1998) 115012.

[16] A. Djouadi, W. Kilian, M. Muhlleitner, and P. M. Zerwas, *Testing Higgs selfcouplings at e^+ e^- linear colliders*. Eur. Phys. J. **C10** (1999) 27–43, arXiv:hep-ph/9903229 [hep-ph].

[17] A. Djouadi, W. Kilian, M. Muhlleitner, and P. M. Zerwas, *Production of neutral Higgs boson pairs at LHC*. Eur. Phys. J. **C10** (1999) 45–49, arXiv:hep-ph/9904287 [hep-ph].

[18] M. M. Muhlleitner, *Higgs particles in the standard model and supersymmetric theories*. PhD thesis, Hamburg U., 2000. arXiv:hep-ph/0008127 [hep-ph].

[19] G. Cynolter, E. Lendvai, and G. Pocsik, *Resonance production of three neutral supersymmetric Higgs bosons at LHC*. Acta Phys. Polon. **B31** (2000) 1749–1757, arXiv:hep-ph/0003008 [hep-ph].

[20] **CLIC Physics Working Group** Collaboration, E. Accomando *et al.*, *Physics at the CLIC multi-TeV linear collider*. arXiv:hep-ph/0412251 [hep-ph].

[21] T. Plehn and M. Rauch, *Quartic Higgs coupling at hadron colliders*Phys. Rev. D **72** (Sep, 2005) 053008.

[22] T. Plehn and M. Rauch, *The quartic higgs coupling at hadron colliders*. Phys. Rev. **D72** (2005) 053008, arXiv:hep-ph/0507321 [hep-ph].

[23] T. Binoth, S. Karg, N. Kauer, and R. Ruckl, *Multi-Higgs boson production in the Standard Model and beyond*. Phys. Rev. **D74** (2006) 113008, arXiv:hep-ph/0608057 [hep-ph].

[24] U. Baur, T. Plehn, and D. L. Rainwater, *Determining the Higgs boson selfcoupling at hadron colliders*. Phys. Rev. **D67** (2003) 033003, arXiv:hep-ph/0211224 [hep-ph].

[25] U. Baur, T. Plehn, and D. L. Rainwater, *Measuring the Higgs boson self coupling at the LHC and finite top mass matrix elements*. Phys. Rev. Lett. **89** (2002) 151801, arXiv:hep-ph/0206024 [hep-ph].

[26] U. Baur, T. Plehn, and D. L. Rainwater, *Examining the Higgs boson potential at lepton and hadron colliders: A Comparative analysis*. Phys. Rev. **D68** (2003) 033001, arXiv:hep-ph/0304015 [hep-ph].

[27] U. Baur, T. Plehn, and D. L. Rainwater, *Probing the Higgs selfcoupling at hadron colliders using rare decays*. Phys. Rev. **D69** (2004) 053004, arXiv:hep-ph/0310056 [hep-ph].

[28] M. J. Dolan, C. Englert, and M. Spannowsky, *Higgs self-coupling measurements at the LHC*. JHEP **10** (2012) 112, arXiv:1206.5001 [hep-ph].

[29] A. Papaefstathiou, L. L. Yang, and J. Zurita, *Higgs boson pair production at the LHC in the $b\bar{b}W^+W^-$ channel*. Phys. Rev. **D87** (2013) no. 1, 011301, arXiv:1209.1489 [hep-ph].

[30] J. Baglio, A. Djouadi, R. Gröber, M. Mühlleitner, J. Quevillon, and M. Spira, *The measurement of the Higgs self-coupling at the LHC: theoretical status*. Journal of High Energy Physics **2013** (2013) no. 4, 1–40.

[31] F. Goertz, A. Papaefstathiou, L. L. Yang, and J. Zurita, *Higgs Boson self-coupling measurements using ratios of cross sections*. JHEP **06** (2013) 016, arXiv:1301.3492 [hep-ph].

[32] W. Yao, *Studies of measuring Higgs self-coupling with $HH \to b\bar{b}\gamma\gamma$ at the future hadron colliders*. arXiv:1308.6302 [hep-ph].

[33] A. J. Barr, M. J. Dolan, C. Englert, and M. Spannowsky, *Di-Higgs final states augMT2ed – selecting hh events at the high luminosity LHC*. Phys. Lett. **B728** (2014) 308–313, arXiv:1309.6318 [hep-ph].

[34] M. J. Dolan, C. Englert, N. Greiner, and M. Spannowsky, *Further on up the road: hhjj production at the LHC*. Phys. Rev. Lett. **112** (2014) 101802, arXiv:1310.1084 [hep-ph].

[35] V. Barger, L. L. Everett, C. B. Jackson, and G. Shaughnessy, *Higgs-Pair Production and Measurement of the Triscalar Coupling at LHC(8,14)*. Phys. Lett. **B728** (2014) 433–436, arXiv:1311.2931 [hep-ph].

[36] D. E. Ferreira de Lima, A. Papaefstathiou, and M. Spannowsky, *Standard model Higgs boson pair production in the ($b\bar{b}$)($b\bar{b}$) final state*. JHEP **08** (2014) 030, arXiv:1404.7139 [hep-ph].

[37] C. Englert, F. Krauss, M. Spannowsky, and J. Thompson, *Di-Higgs phenomenology in $t\bar{t}hh$: The forgotten channel*. Phys. Lett. **B743** (2015) 93–97, arXiv:1409.8074 [hep-ph].

[38] D. Wardrope, E. Jansen, N. Konstantinidis, B. Cooper, R. Falla, and N. Norjoharuddeen, *Non-resonant Higgs-pair production in the $b\bar{b}$ $b\bar{b}$ final state at the LHC*. Eur. Phys. J. **C75** (2015) no. 5, 219, arXiv:1410.2794 [hep-ph].

[39] Q. Li, Z. Li, Q.-S. Yan, and X. Zhao, *Probe Higgs boson pair production via the 3l2j+$\not{E}$ mode*. Phys. Rev. **D92** (2015) no. 1, 014015, arXiv:1503.07611 [hep-ph].

[40] C.-T. Lu, J. Chang, K. Cheung, and J. S. Lee, *An exploratory study of Higgs-boson pair production*. JHEP **08** (2015) 133, arXiv:1505.00957 [hep-ph].

[41] M. J. Dolan, C. Englert, N. Greiner, K. Nordstrom, and M. Spannowsky, *hhjj production at the LHC*. Eur. Phys. J. **C75** (2015) no. 8, 387, arXiv:1506.08008 [hep-ph].

[42] Q.-H. Cao, Y. Liu, and B. Yan, *Measuring Trilinear Higgs Coupling in WHH and ZHH Productions at the HL-LHC*. arXiv:1511.03311 [hep-ph].

[43] J. K. Behr, D. Bortoletto, J. A. Frost, N. P. Hartland, C. Issever, and J. Rojo, *Boosting Higgs pair production in the $b\bar{b}b\bar{b}$ final state with multivariate techniques*. arXiv:1512.08928 [hep-ph].

[44] F. Maltoni, E. Vryonidou, and M. Zaro, *Top-quark mass effects in double and triple Higgs production in gluon-gluon fusion at NLO*. JHEP **11** (2014) 079, arXiv:1408.6542 [hep-ph].

[45] E. W. N. Glover and J. J. van der Bij, *Higgs boson pair production via gluon fusion*. Nucl. Phys. **B309** (1988) 282.

[46] T. Plehn, M. Spira, and P. M. Zerwas, *Pair production of neutral Higgs particles in gluon-gluon collisions*. Nucl. Phys. **B479** (1996) 46–64, arXiv:hep-ph/9603205 [hep-ph]. [Erratum: Nucl. Phys.B531,655(1998)].

[47] M. Gillioz, R. Grober, C. Grojean, M. Muhlleitner, and E. Salvioni, *Higgs Low-Energy Theorem (and its corrections) in Composite Models*. JHEP **10** (2012) 004, arXiv:1206.7120 [hep-ph].

[48] R. Grober, M. Muhlleitner, M. Spira, and J. Streicher, *NLO QCD corrections to Higgs pair production including dimension-6 operators*. Journal of High Energy Physics **2015** (2015) no. 9, 1–15.

[49] A. Azatov, R. Contino, G. Panico, and M. Son, *Effective field theory analysis of double Higgs boson production via gluon fusion*. Phys. Rev. **D92** (2015) no. 3, 035001, arXiv:1502.00539 [hep-ph].

[50] M. Gell-Mann, *A schematic model of baryons and mesons*. Physics Letters **8** (1964) no. 3, 214 – 215.

[51] G. Zweig, *An SU_3 model for strong interaction symmetry and its breaking. oai:cds.cern.ch:352337; Part I.*

[52] D. J. Gross and F. Wilczek, *Ultraviolet Behavior of Non-Abelian Gauge Theories*Phys. Rev. Lett. **30** (Jun, 1973) 1343–1346.

[53] H. D. Politzer, *Reliable Perturbative Results for Strong Interactions?*Phys. Rev. Lett. **30** (Jun, 1973) 1346–1349.

[54] A. Salam and J. C. Ward, *Electromagnetic and weak interactions*. Phys. Lett. **13** (1964) 168–171.

[55] J. C. Collins, D. E. Soper, and G. F. Sterman, *Factorization of Hard Processes in QCD*. Adv. Ser. Direct. High Energy Phys. **5** (1989) 1–91, arXiv:hep-ph/0409313 [hep-ph].

[56] R. P. Feynman, *Space-Time Approach to Quantum Electrodynamics*Phys. Rev. **76** (Sep, 1949) 769–789.

[57] H. M. Georgi, S. L. Glashow, M. E. Machacek, and D. V. Nanopoulos, *Higgs Bosons from Two-Gluon Annihilation in Proton-Proton Collisions*Phys. Rev. Lett. **40** (Mar, 1978) 692–694.

[58] T. Kinoshita, *Mass singularities of Feynman amplitudes*. Journal of Mathematical Physics **3** (1962) no. 4, 650–677.

[59] T. D. Lee and M. Nauenberg, *Degenerate systems and mass singularities.* Phys. Rev. **133** (Mar, 1964) B1549–B1562.

[60] G. 't Hooft and M. Veltman, *Regularization and renormalization of gauge fields.* Nuclear Physics B **44** (1972) no. 1, 189 – 213.

[61] G. Passarino and M. J. G. Veltman, *One Loop Corrections for e^+ e^- Annihilation Into μ^+ μ^- in the Weinberg Model*. Nucl. Phys. **B160** (1979) 151–207.

[62] J. Collins, F. Wilczek, and A. Zee, *Low-energy manifestations of heavy particles: Application to the neutral current*Phys. Rev. D **18** (Jul, 1978) 242–247.

[63] W. J. Marciano, *Flavor thresholds and Λ in the modified minimal-subtraction scheme*Phys. Rev. D **29** (Feb, 1984) 580–582.

[64] P. Nason, S. Dawson, and R. K. Ellis, *The Total Cross-Section for the Production of Heavy Quarks in Hadronic Collisions*. Nucl. Phys. **B303** (1988) 607–633.

[65] A. Denner, *Techniques for calculation of electroweak radiative corrections at the one loop level and results for W physics at LEP-200*. Fortsch. Phys. **41** (1993) 307–420, arXiv:0709.1075 [hep-ph].

[66] S. Catani and M. H. Seymour, *A General algorithm for calculating jet cross-sections in NLO QCD*. Nucl. Phys. **B485** (1997) 291–419, arXiv:hep-ph/9605323 [hep-ph]. [Erratum: Nucl. Phys.B510,503(1998)].

[67] S. Catani and M. H. Seymour, *The Dipole formalism for the calculation of QCD jet cross-sections at next-to-leading order*. Phys. Lett. **B378** (1996) 287–301, arXiv:hep-ph/9602277 [hep-ph].

[68] S. Catani, S. Dittmaier, M. H. Seymour, and Z. Trocsanyi, *The Dipole formalism for next-to-leading order QCD calculations with massive partons*. Nucl. Phys. **B627** (2002) 189–265, arXiv:hep-ph/0201036 [hep-ph].

[69] S. Frixione, Z. Kunszt, and A. Signer, *Three jet cross-sections to next-to-leading order*. Nucl. Phys. **B467** (1996) 399–442, arXiv:hep-ph/9512328 [hep-ph].

[70] D. A. Kosower, *Antenna factorization of gauge theory amplitudes*. Phys. Rev. **D57** (1998) 5410–5416, arXiv:hep-ph/9710213 [hep-ph].

[71] A. Gehrmann-De Ridder and M. Ritzmann, *NLO Antenna Subtraction with Massive Fermions*. JHEP **07** (2009) 041, arXiv:0904.3297 [hep-ph].

[72] **ATLAS, CMS** Collaboration, G. Aad *et al.*, *Combined Measurement of the Higgs Boson Mass in pp Collisions at $\sqrt{s} = 7$ and 8 TeV with the ATLAS and CMS Experiments*. Phys. Rev. Lett. **114** (2015) 191803, arXiv:1503.07589 [hep-ex].

[73] O. J. P. Eboli, G. C. Marques, S. F. Novaes, and A. A. Natale, *Twin Higgs boson production*. Phys. Lett. **B197** (1987) 269–272.

[74] D. A. Dicus, C. Kao, and S. S. D. Willenbrock, *Higgs boson pair production from gluon fusion*. Phys. Lett. **B203** (1988) 457–461.

[75] W.-Y. Keung, *Double Higgs From $W-W$ Fusion*. Mod. Phys. Lett. **A2** (1987) 765.

[76] D. A. Dicus, K. J. Kallianpur, and S. S. D. Willenbrock, *Higgs Boson Pair Production in the Effective W Approximation*. Phys. Lett. **B200** (1988) 187–192.

[77] K. J. Kallianpur, *Pair Production of Higgs Bosons via Heavy Quark Annihilation*. Phys. Lett. **B215** (1988) 392–396.

[78] A. Dobrovolskaya and V. Novikov, *On heavy Higgs boson production*. Z. Phys. **C52** (1991) 427–436.

[79] A. Abbasabadi, W. W. Repko, D. A. Dicus, and R. Vega, *Comparison of Exact and Effective Gauge Boson Calculations for Gauge Boson Fusion Processes*. Phys. Rev. **D38** (1988) 2770.

[80] M. Moretti, S. Moretti, F. Piccinini, R. Pittau, and A. D. Polosa, *Higgs boson self-couplings at the LHC as a probe of extended Higgs sectors*. JHEP **02** (2005) 024, arXiv:hep-ph/0410334 [hep-ph].

[81] R. Frederix, S. Frixione, V. Hirschi, F. Maltoni, O. Mattelaer, P. Torrielli, E. Vryonidou, and M. Zaro, *Higgs pair production at the LHC with NLO and parton-shower effects*. Physics Letters B **732** (2014) 142 – 149.

[82] V. D. Barger, T. Han, and R. J. N. Phillips, *Double Higgs Boson Bremsstrahlung From W and Z Bosons at Supercolliders*. Phys. Rev. **D38** (1988) 2766.

[83] J. Baglio, A. Djouadi, and J. Quevillon, *Prospects for Higgs physics at energies up to 100 TeV*. arXiv:1511.07853 [hep-ph].

[84] **LHC Higgs Cross Section Working Group** Collaboration, J. R. Andersen *et al.*, *Handbook of LHC Higgs Cross Sections: 3. Higgs Properties*. arXiv:1307.1347 [hep-ph].

[85] J. M. Butterworth, A. R. Davison, M. Rubin, and G. P. Salam, *Jet substructure as a new Higgs search channel at the LHC*. Phys. Rev. Lett. **100** (2008) 242001, arXiv:0802.2470 [hep-ph].

[86] D. de Florian and J. Mazzitelli, *Two-loop virtual corrections to Higgs pair production.* Phys. Lett. **B724** (2013) 306–309, arXiv:1305.5206 [hep-ph].

[87] D. de Florian and J. Mazzitelli, *Higgs Boson Pair Production at Next-to-Next-to-Leading Order in QCD.* Phys. Rev. Lett. **111** (2013) 201801, arXiv:1309.6594 [hep-ph].

[88] J. Grigo, K. Melnikov, and M. Steinhauser, *Virtual corrections to Higgs boson pair production in the large top quark mass limit.* Nucl. Phys. **B888** (2014) 17–29, arXiv:1408.2422 [hep-ph].

[89] D. Y. Shao, C. S. Li, H. T. Li, and J. Wang, *Threshold resummation effects in Higgs boson pair production at the LHC.* JHEP **07** (2013) 169, arXiv:1301.1245 [hep-ph].

[90] D. de Florian and J. Mazzitelli, *Higgs pair production at next-to-next-to-leading logarithmic accuracy at the LHC.* JHEP **09** (2015) 053, arXiv:1505.07122 [hep-ph].

[91] J. Grigo, J. Hoff, K. Melnikov, and M. Steinhauser, *On the Higgs boson pair production at the LHC.* Nucl. Phys. **B875** (2013) 1–17, arXiv:1305.7340 [hep-ph].

[92] J. Grigo, J. Hoff, and M. Steinhauser, *Higgs boson pair production: top quark mass effects at NLO and NNLO.* Nucl. Phys. **B900** (2015) 412–430, arXiv:1508.00909 [hep-ph].

[93] S. Borowka, N. Greiner, G. Heinrich, S. P. Jones, M. Kerner, J. Schlenk, U. Schubert, and T. Zirke, *Higgs boson pair production in gluon fusion at NLO with full top-quark mass dependence.* arXiv:1604.06447 [hep-ph].

[94] G. Cullen *et al.*, *GOSAM-2.0: a tool for automated one-loop calculations within the Standard Model and beyond.* Eur. Phys. J. **C74** (2014) no. 8, 3001, arXiv:1404.7096 [hep-ph].

[95] S. Borowka, G. Heinrich, S. P. Jones, M. Kerner, J. Schlenk, and T. Zirke, *SecDec-3.0: numerical evaluation of multi-scale integrals beyond one loop.* Comput. Phys. Commun. **196** (2015) 470–491, arXiv:1502.06595 [hep-ph].

[96] A. Denner and S. Dittmaier, *Reduction of one loop tensor five point integrals.* Nucl. Phys. **B658** (2003) 175–202, arXiv:hep-ph/0212259 [hep-ph].

[97] T. Hahn, *Generating Feynman diagrams and amplitudes with FeynArts 3.* Comput. Phys. Commun. **140** (2001) 418–431, arXiv:hep-ph/0012260 [hep-ph].

[98] M. Spira, A. Djouadi, D. Graudenz, and P. M. Zerwas, *Higgs boson production at the LHC.* Nucl. Phys. **B453** (1995) 17–82, arXiv:hep-ph/9504378 [hep-ph].

[99] M. Spira, *HIGLU: A program for the calculation of the total Higgs production cross-section at hadron colliders via gluon fusion including QCD corrections.* arXiv:hep-ph/9510347 [hep-ph].

[100] G. Degrassi, P. P. Giardino, and R. Gröber, *On the two-loop virtual QCD corrections to Higgs boson pair production in the Standard Model.* arXiv:1603.00385 [hep-ph].

[101] J. A. M. Vermaseren, *New features of FORM.* arXiv:math-ph/0010025 [math-ph].

[102] Wolfram Research Inc., *Mathematica 10.0*, 2014. http://www.wolfram.com.

[103] G. P. Lepage, *A new algorithm for adaptive multidimensional integration.* Journal of Computational Physics **27** (1978) no. 2, 192 – 203.

[104] A. P. Sexton, *Conference Proceedings*, ch. Abramowitz and Stegun – A Resource for Mathematical Document Analysis, pp. 159–168. Springer Berlin Heidelberg, Berlin, Heidelberg, 2012.

[105] V. Hirschi, R. Frederix, S. Frixione, M. Vittoria Garzelli, F. Maltoni, and R. Pittau, *Automation of one-loop QCD computations*. Journal of High Energy Physics **2011** (2011) no. 5, 1–65.

[106] G. Altarelli and G. Parisi, *Asymptotic freedom in parton language*. Nuclear Physics B **126** (1977) no. 2, 298 – 318.

[107] G. F. Giudice, C. Grojean, A. Pomarol, and R. Rattazzi, *The Strongly-Interacting Light Higgs*. JHEP **06** (2007) 045, arXiv:hep-ph/0703164 [hep-ph].

[108] R. Contino, C. Grojean, M. Moretti, F. Piccinini, and R. Rattazzi, *Strong Double Higgs Production at the LHC*. JHEP **05** (2010) 089, arXiv:1002.1011 [hep-ph].

[109] V. A. Smirnov, *Asymptotic expansions of Feynman diagrams on the mass shell in momenta and masses*. Phys. Lett. **B394** (1997) 205–210, arXiv:hep-th/9608151 [hep-th].

[110] S. G. Gorishnii, *Construction of Operator Expansions and Effective Theories in the Ms Scheme*. Nucl. Phys. **B319** (1989) 633–666.

[111] J. R. Ellis, M. K. Gaillard, and D. V. Nanopoulos, *A Phenomenological Profile of the Higgs Boson*. Nucl. Phys. **B106** (1976) 292.

[112] M. A. Shifman, A. I. Vainshtein, M. B. Voloshin, and V. I. Zakharov, *Low-Energy Theorems for Higgs Boson Couplings to Photons*. Sov. J. Nucl. Phys. **30** (1979) 711–716. [Yad. Fiz.30,1368(1979)].

[113] B. A. Kniehl and M. Spira, *Low-energy theorems in Higgs physics*. Z. Phys. **C69** (1995) 77–88, arXiv:hep-ph/9505225 [hep-ph].

[114] R. Grober and M. Muhlleitner, *Composite Higgs Boson Pair Production at the LHC*. JHEP **06** (2011) 020, arXiv:1012.1562 [hep-ph].

[115] M. Spira, HPAIR. http://tiger.web.psi.ch/proglist.html.

[116] A. D. Martin, W. J. Stirling, R. S. Thorne, and G. Watt, *Parton distributions for the LHC*. Eur. Phys. J. **C63** (2009) 189–285, arXiv:0901.0002 [hep-ph].

[117] A. D. Martin, W. J. Stirling, R. S. Thorne, and G. Watt, *Uncertainties on alpha(S) in global PDF analyses and implications for predicted hadronic cross sections*. Eur. Phys. J. **C64** (2009) 653–680, arXiv:0905.3531 [hep-ph].

[118] A. D. Martin, W. J. Stirling, R. S. Thorne, and G. Watt, *Heavy-quark mass dependence in global PDF analyses and 3- and 4-flavour parton distributions*. Eur. Phys. J. **C70** (2010) 51–72, arXiv:1007.2624 [hep-ph].

[119] **CMS Collaboration** Collaboration, *Precise determination of the mass of the Higgs boson and studies of the compatibility of its couplings with the standard model* Tech. Rep. CMS-PAS-HIG-14-009, CERN, Geneva, 2014. http://cds.cern.ch/record/1728249.

Danksagung

An erster Stelle möchte ich mich bei meiner “Doktormutter” Prof. Margarete Mühlleitner für die Gelegenheit bedanken, meine Dissertation auf diesem herausfordernden und hochaktuellen Themengebiet anfertigen zu können. Unseren regelmäßigen Gesprächen konnte ich stets neue Anregungen abgewinnen und gerade während der Fertigstellung dieser Arbeit haben mir die unzähligen Korrekturvorschläge, sowie ihr gelassener Umgang mit meinem chaotischen Zeitmanagement sehr weiter geholfen.

Herrn Dr. Michael Spira danke ich für die Übernahme des Korreferats und dafür dass er mir häufig mit Rat und Tat zur Seite stand, wenn mich die wundersame Welt der Zweischleifenrechnungen verwirrt hat.

Bei Julien Baglio und Francisco Campanario möchte ich mich für den hilfreichen Austausch und für das Korrekturlesen meiner Arbeit bedanken.

Dem gesamten ITP möchte ich meinen Dank aussprechen für die produktive aber gleichzeitig entspannte Atmosphäre – im Speziellen war es mir eine Freunde, die letzten drei Jahre das Büro mit Hanna Ziesche teilen zu können und dass unsere gelegentlichen Gespräche über dem Bildschirmrand den Arbeitsalltag aufgelockert haben. Bei Alexander Wlotzka möchte ich mich für den Austausch über die Freuden und Frusten des Doktorandendaseins bedanken und dafür dass er auf Reisen auch zu später Stunde immer zielsicher den Heimweg findet.

Zu guter letzt gilt mein Dank meinen Eltern, die mich stets ermutigt haben meinen eigenen Weg zu finden und immer für mich da sind, wenn ich sie brauche.